

Stellingen

behorende bij het proefschrift

Towards in vivo parameter estimation for a musculoskeletal model of the human shoulder.

1.

Voor segmentatie van spieren in tomografische beelden is een contour gebaseerde segmentatiemethode het meest geschikt (dit proefschrift).

2.

Om de kwaliteit van een complex spier-skelet model, zoals het Delftse Schoudermodel, te kunnen analyseren zijn meerdere parametersets nodig (dit proefschrift).

3.

Om verificatie van meetresultaten achteraf mogelijk te maken zou van ieder kadaver dat gebruikt wordt in een dissectie experiment eerst MRI opnamen gemaakt moeten worden (dit proefschrift).

4.

Zolang de parameters van het spier-skelet model realistisch blijven is het beter om ze aan te passen door het fitten van de resultaten van het model op gemeten data (dit proefschrift).

5.

Sinds de gemeenten zorgdragen voor de uitvoering van de Wet Voorzieningen Gehandicapten kunnen deze voorzieningen niet meer landelijk getoetst worden.

6.

Multidisciplinaire samenwerking is essentieel voor het te verwachten succes van de DIOC's.

7.

Het feit dat in de figuren uit de medische literatuur zelden een krachterspel compleet, correct en eenduidig wordt weergegeven duidt op een gebrek aan mechanisch inzicht in de medische wetenschap.

8.

Elke informatieleverancier moet haar informatie tenminste ook door middel van het Internet toegankelijk maken.

9.

Op basis van de evolutietheorie worden meer verschijnselen verklaard dan op basis van een wetenschappelijk bewijs mogelijk zou zijn.

10.

Fietsen op een ligfiets vergt minder inspanning dan fietsen op een traditionele fiets.

11.

Gratis toegang tot internet en email leiden tot vervuiling en misbruik van het Internet.

12.

Gratis lokaal telefoneren is beter dan gratis Internet.

13.

Zeuren helpt.



728-08

3419

3419g

TR 3419

Towards in vivo parameter estimation for a musculoskeletal model of the human shoulder.

Proefschrift

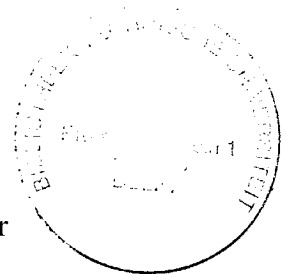
ter verkrijging van de graad van doctor
aan de Technische Universiteit Delft,
op gezag van de Rector Magnificus prof. ir. K.F. Wakker,
in het openbaar te verdedigen ten overstaan van een commissie,
door het College voor Promoties aangewezen,

op maandag 22 november 1999 te 16.00 uur

door

Bartholomeus Leonardus KAPTEIN

werktuigkundig ingenieur,
geboren te Breezand.



Dit proefschrift is goedgekeurd door de promotoren:

Prof. dr. ir. H.G. Stassen
Prof. dr. F.C.T. van der Helm

Toegevoegd promotor:

Dr. ir. J.J. Gerbrands

Samenstelling promotiecommissie:

Rector Magnificus,	voorzitter
Prof. dr. ir. H.G. Stassen,	Technische Universiteit Delft, promotor
Prof. dr. F.C.T. van der Helm	Technische Universiteit Delft, promotor
Dr. ir. J.J. Gerbrands	Technische Universiteit Delft, toegevoegd promotor
Prof. dr. T.M.G.J. van Eijden	Universiteit van Amsterdam
Prof. dr. I.T. Young	Technische Universiteit Delft
Prof. dr. J.A.N. Verhaar	Erasmus Universiteit Rotterdam
Prof. dr. A. Huson	Technische Universiteit Eindhoven

Towards in vivo parameter estimation for a musculoskeletal model of the human shoulder

Kaptein, Barholomeus Leonardus

Thesis Delft University of Technology - with ref - with Summary in Dutch

Printed by Universal Press, Veenendaal

Cover: MRI image of the author

ISBN 90-3700175-0

Copyright © 1999 by B.L. Kaptein

All rights reserved. No part of this thesis may be reproduced or transmitted in any form or by any means, electronic, mechanical, photocopying, any information storage and retrieval system, or other, without written permission from the copyright owner.

Contents

• Chapter 1	Introduction.	1
• Chapter 2	Image analysis of MRI images. Interactive contour detection.	13
• Chapter 3	Different parameter sets for the Delft Shoulder Model.	27
• Chapter 4	Parameters for a model of the human shoulder.	45
• Chapter 5	Estimating muscle attachment contours by transforming geometrical bone models.	69
• Chapter 6	Adapting the Delft Shoulder Model on the basis of measured movements.	81
• Chapter 7	Concluding remarks.	99
•	References.	105
• Appendix A	Coordinate systems and definitions of rotations.	115
• Appendix B	Muscle moment arms.	119
• Appendix C	Muscle attachment data.	125
• Appendix D	Muscle attachments.	127
•	Summary	137
•	Samenvatting	141
•	Acknowledgements	145
•	Curriculum Vitae	147



Chapter 1: Introduction.

1.1 General Perspective

The incidence of shoulder complaints in the total Dutch population is estimated between 70 and 260 per thousand a year [Windt 1997]. Due to the poor ergonomic design of computer workstations and because people work with them longer and longer, the incidence of shoulder problems will grow in the near future. The functioning of the shoulder is very important in performing the Activities of Daily Living (ADL) like combing your hair, cleaning yourself, or toilet visits. With the aging of the population, the total amount of shoulder disorders will grow in the near future. Therefore, developing adequate treatment of such shoulder disorders is important.

Despite this growing importance of treatment of shoulder disorders, and the growing interest in the human shoulder, many questions about the shoulder are still unanswered. One of the striking examples is the relative lack of success of total shoulder replacement compared to the replacement of other joints like the hip or knee. After surgery, the pain is reduced adequately, but the functioning of the shoulder is not restored properly.

1.2 Historical Perspective

In the past, the upper extremity was included in the subjects of research of the Man-Machine Systems and Control Group of the Laboratory for Measurement and Control at the Faculty of Design, Engineering and Production of the Delft University of Technology. Their research started with a project focused on improving the results of a gleno-humeral arthrodesis. A gleno-humeral arthrodesis is an orthopaedic intervention fixating the humerus to the scapula in order to partially restore the arm function of patients suffering from paralysis of the muscles of the arm. After this intervention, the arm can be moved in relation to the thorax by means of the muscles of the shoulder girdle. Pronk analysed the human shoulder [Pronk 1991a] and also developed an adjustable external fixator to adjust the individual orientation of the humerus with respect to the scapula [Nieuwenhuis 1989]; [Pronk 1991a]. The elbow function of the paralyzed arm can be achieved by means of an orthosis [Cool 1989].

Pronk concluded that a functional analysis of the human shoulder was needed, and for this, a biomechanical model of the human shoulder was developed [Pronk 1991a]; [Helm 1991b]; [Helm 1994a]. This model was based on an extensive cadaver study [Veeger 1991a]; [Helm 1992]. The model can be used to evaluate surgical interventions like transposition of muscles, glenohumeral arthrodesis and the

insertion of an endoprosthesis [Helm 1994d]; [Leest 1996].

To validate this model in varying conditions, other research at the Man Machine Systems and Control Group focused on fast goal-directed arm movements [Happee 1995]. Shoulder instability is one of the problems. Atraumatic recurrent dislocation of the glenohumeral joint is one of the effects of an unstable shoulder. Stability of the shoulder was investigated by Rozendaal [Rozendaal 1997]. Validation of the shoulder model and analysis of motion and loading of the shoulder was done by de Groot [Groot 1998b]. Because control of arm movements proved to be very important, research on neuro-muscular control by means of neural net models was done by Stroeve [Stroeve 1998]. Brouwn focused his research on experimental modelling of position control under external disturbances [Brouwn 2000].

The shoulder research project is executed in close cooperation with the Orthopaedic Department of the Leiden University Medical Centre, where the clinical part of the research takes place. Meskers studied the quantitative assessment of shoulder functions in a clinical setting [Meskers 1998b]. At the Department of Human Movement Science at the Free University of Amsterdam the focus is on ergonomics and wheelchair propulsion [Veeger 1991b]. These three research groups from Delft, Leiden and Amsterdam are united in the Dutch Shoulder Group.

1.3 Problem definition

The shoulder model has shown to be valid and useful for medical practice. The problem is the discrepancy between the general model and the individual patient. The model is based on parameters of a cadaver, but simulations have to be done using input motions of healthy subjects, or patients. This discrepancy between model and subject decreases the quality of the simulation results of the model, which makes correct interpretation and medical intervention on the basis of these simulation results more difficult.

The contribution of the research reported in this thesis is focused on the parameters of the shoulder model. The goal of this research is to investigate the discrepancy between model and subject and to adapt the shoulder model to the individual subject.

1.4 The shoulder

Bones. The shoulder mechanism is the musculo-skeletal complex composed of the thorax, the clavicle, the scapula and the humerus (Figure 1.1). The thorax is considered to be the base of the mechanism. The clavicle is connected to the thorax at the Sterno-Clavicular (SC) joint. The scapula is connected to the clavicle at the Acromio-Clavicular (AC) joint. The scapula slides over the Scapulo-Thoracic gliding plane at the back of the thorax. This makes the constellation of thorax,

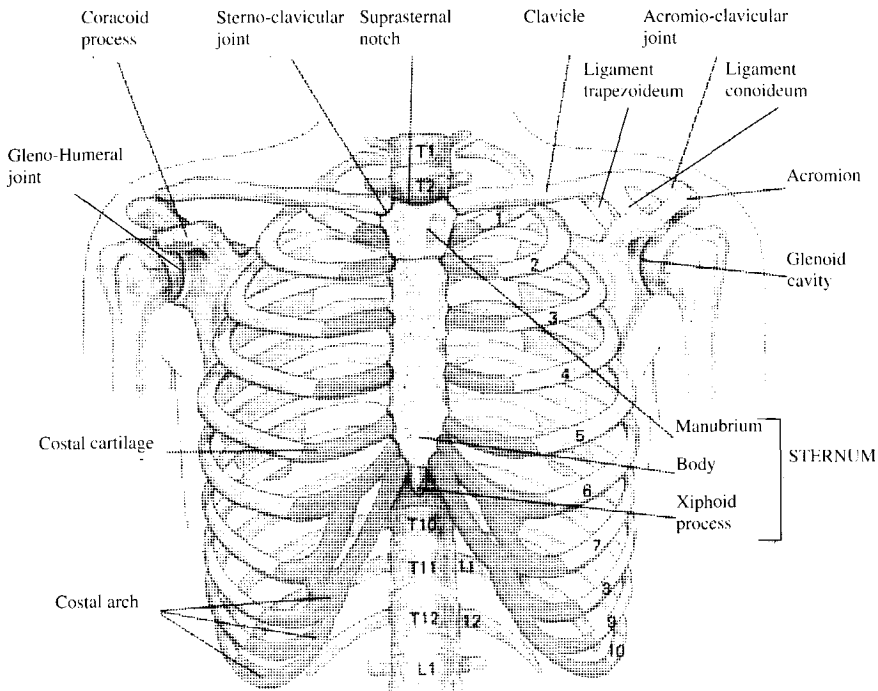


Figure 1.1: Bones of the shoulder [Guyton 1985].

clavicle and scapula, known as the shoulder girdle, act like a closed chain mechanism. The shoulder girdle provides a stable, yet movable base for the humerus, which is connected to the scapula at the Gleno-Humeral (GH) joint. This joint is, in a narrow sense, also known as the shoulder joint.

Ligaments. The movements of the bones of the shoulder girdle are restricted by ligaments: The conoid and the trapezoid ligaments tightly connect the scapula and the clavicle, whereas the costoclavicular and sternoclavicular ligaments form an additional connection between the clavicle and the thorax.

Muscles. The shoulder movements are performed by the muscles of the shoulder. Figure 1.2 gives an overview of all of these muscles. Except for generating movements, the muscles are also necessary for the shoulder joint stability [Helm 1994a]; [Rozendaal 1997]. The cavity of the GH-joint (glenoid) is relatively small in comparison with the humeral head. It is necessary that the GH-joint reaction force is directed inside this cavity to prevent GH-joint dislocation (Figure 1.3). This stabilization is done by active steering of the muscle forces. The coordination of the muscle forces in order to move the arm without dislocating the GH-joint is very complicated. The shoulder contains seven bi-articular muscles and two tri-articular muscles. Contractions of these muscles will affect a combination of joints. For the

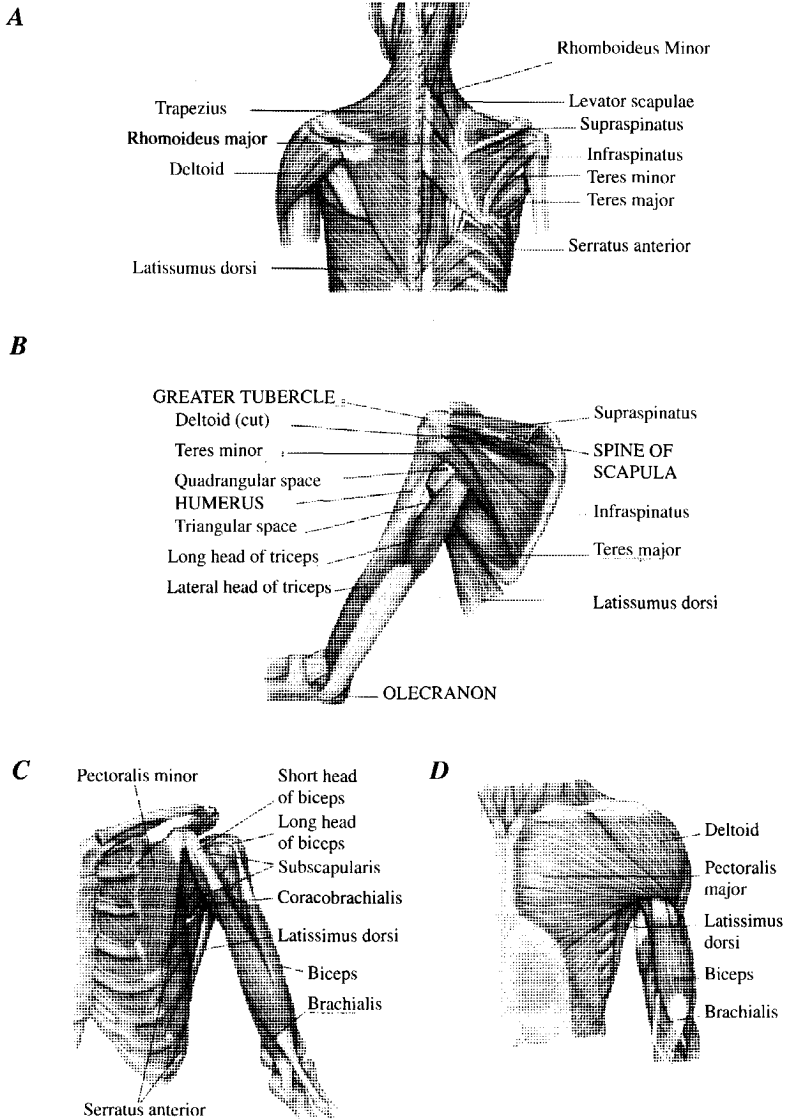


Figure 1.2: Muscles of the shoulder [Guyton 1985].

A: Posterior view.

B: Anterior view of the muscles of the scapula.

C: Anterior view of the inner muscles of the shoulder.

D: Anterior view of the surface muscles of the shoulder.

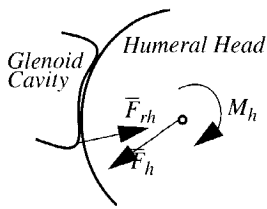


Figure 1.3: Resultant force vector \bar{F}_h should point to the glenoid cavity, otherwise it cannot be neutralized by the joint reaction force \bar{F}_{rh} and the joint will dislocate [Helm 1994a].

coordination of a single joint, the activity of other muscles is needed in order to compensate for the so-called parasite moments.

Movements. The human arm has a large range of motion. This is made possible by the shape of the glenohumeral joint and the movements of the scapula with respect to the thorax. About one third of the arm elevation originates from the scapular rotations relative to the thorax in the sterno-clavicular joint and the acromio-clavicular joint. Two thirds of the arm elevation originates from gleno-humeral rotations between the scapula and the humerus. The ratio of the humeral elevation over the scapular rotations with respect to the thorax is called the scapulo-humeral rhythm [Inman 1944]. A 3-D quantitative description of this rhythm has been given by de Groot [Groot 1997a].

1.4.1 The Delft Shoulder Model

The Delft Shoulder Model is a multi-body computer model describing the relationships between movements and external forces acting on the arm and the internal forces and movements of the muscles. The model is built using the software package SPACAR [Werff 1977]; [Jonker 1988] and runs on a Unix workstation.

Model Input. The model is fed by movements of the bones and external loads acting on these bones. For this, the 3-D rotations of the scapula, humerus and clavicle are measured. This is done by digitizing the bony landmarks on these bones and by calculating the 3-D rotations of the bones from the locations of these bony landmarks. For digitizing, we used a palpation technique; we measured the 3-D locations of points by means of a digitizing apparatus called the palpator [Pronk 1991b]. This palpation technique is necessary because the scapula moves underneath the skin. Thus its location cannot be measured by means of external markers. Recently, the mechanical palpator is replaced by a magnetic tracking device called Flock-Of-Birds (FOB) [Meskers 1998a]; [Meskers 1999]. This device measures in 3-D orientation and position of receivers fixed on the human body. For the scapula, a specially designed scapula locator has been used to palpate the bony landmarks on the scapula. The use of the FOB device reduces the time of experiments significantly and is thus more suitable for measuring patients.

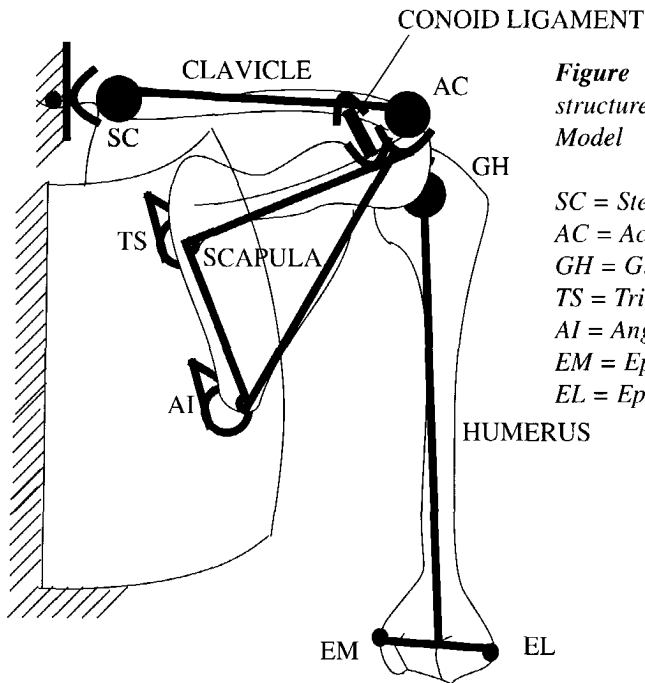


Figure 1.4: Kinematic structure of the Dutch Shoulder Model

SC = Sterno-Clavicular joint
 AC = Acromio-Clavicular joint
 GH = Gleno-Humeral joint
 TS = Trigonum Spinae
 AI = Angulus Inferior
 EM = Epicondile Medialis
 EL = Epicondile Lateralis

External loads are measured using force transducers. For experiments, also dead weight is used to apply forces on the arm. Except for these external loads, the arm is loaded by its own weight.

Model Structure. The model consists of four rigid bodies, modelling the thorax, clavicle, scapula, and humerus (Figure 1.4). Recently, an elbow and forearm joint have been added to the model, but these will not be considered in this thesis.

The four rigid bodies are connected by ideal ball-and-socket joints, modelling the rotational joints of the shoulder. The points Trigonum Spinae (TS) and Angulum Inferior (AI) of the scapula are connected to the thorax by specially designed surface joints. These joints provide a constant distance between the points and the surface of the thorax, which is modelled as an ellipsoid.

The muscles of the human shoulder are modelled by truss elements. Each truss element represents one muscle line of action. Because a muscle with surface shaped attachments has more than one degree of freedom, a muscle can be modelled by a maximum of six muscle lines of action [Helm 1991a]. Some muscles are curved around a bone, like for example the Deltoid muscle. For these muscles, curved truss elements were designed. These elements make it possible to model muscle lines of action around simple geometric objects like spheres, cylinders, and ellipsoids.

Only one of the ligaments of the shoulder is modelled in the shoulder model: the conoid ligament. It connects the clavicle and the scapula and is modelled as a rigid truss element. This element restricts the rotations of the AC joint.

Model Parameters. The parameters of the model were obtained by means of a cadaver study [Veeger 1991a]; [Helm 1992]. Seven cadavers were dissected, and from the resulting data sets of fourteen shoulders, one more or less medium data set was chosen for the parameters of the shoulder model. The following parameters were measured:

- The location of origin and insertion of all muscles.
- The shape and position of bony contours determining the muscle path.
- Muscle architecture.
- The location of the attachments of the costo-clavicular, conoid and trapezoid ligaments.
- The location of the joint rotation centres of the sterno-clavicular, acromio-clavicular and gleno-humeral joints.
- Articular surfaces.
- The shape and position of the scapulo-thoracic gliding plane.
- The position of well-defined bony landmarks.
- Muscle mass.
- Muscle cross-sectional area

Kinematic analysis. The kinematic structure of the model consists of a number of rigid bodies, connected by joints. When we assume that the thorax is fixed to the world, the Degrees Of Freedom (DOFs) for the shoulder model can be described as follows:

The clavicle is connected by a rotational joint to the thorax, thus, three DOFs can be defined for the clavicle. The scapula is connected by a rotational joint to the clavicle, adding three DOFs to the mechanism. In the rotational joints, translations are neglected. Motion constraints reduce the number of DOFs. The clavicle and the scapula are connected by a rigid truss element (the conoid ligament), reducing the number of DOFs by one. The two surface joints between the scapula and the thorax also reduce the number of DOFs in the mechanism by two. So, in the shoulder model, the shoulder girdle has three DOFs. The humerus adds three DOFs because it is connected to the scapula by a rotational joint, so there are six DOFs in total.

Using six coordinates, the complete position of the system is defined. These six coordinates can be chosen freely as long as they are independent. They are called Generalized Coordinates (GCs). During the kinematic analysis, a new position of the mechanism is calculated given the six GCs. The kinematics of the system can be described by a non-linear function of these GCs. In the shoulder model, this non-linear function is approximated for each position of the model. Figure 1.5 shows a block diagram of the structure of the shoulder model.

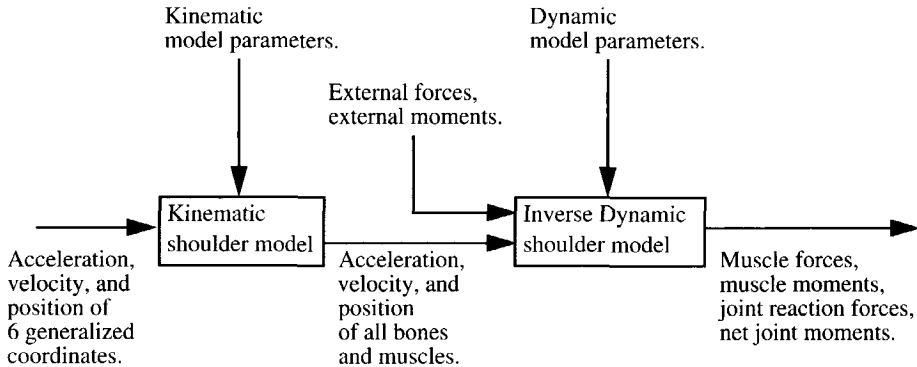


Figure 1.5: Block diagram of the shoulder model. Input variables are the 6 generalized coordinates, and for the inverse dynamic simulations the external forces and moments. Output variables are the acceleration, velocity and position of all bones and muscles, and for the dynamic simulations the muscle forces, muscle moments, net joint moments, and joint reaction forces.

Inverse Dynamic analysis. The dynamic structure of the model consists of the inertia of the bodies and the external and internal forces. In inverse dynamics, the driving forces are calculated given the acceleration, velocity, and position of the system and the external load acting on the system. For this, the six motion equations are reduced to six algebraic equations.

The driving forces are generated by the truss elements of the system (muscles). Because the system is overdetermined, meaning that there are more truss elements than DOFs, the forces for the truss elements are calculated using an optimization procedure. For this optimization procedure, different criteria can be used: Minimization of the quadratic muscle stresses is a commonly used criterion. In this optimization some boundary conditions must be met such as; the glenohumeral joint reaction force should point to the glenoid cavity (See Figure 1.3), and the reaction forces between thorax and scapula should be positive.

Forward Dynamic analysis. In forward dynamic analysis, the neural inputs for the muscles are input to the system. These are used to calculate the driving forces of the system. Using these driving forces and the prescribed external forces, we integrate the equations of motion to calculate each state of the system. Because of the difficulties in optimizing the input for the muscle elements to generate the desired motion, this analysis method is seldom used for large-scale systems (Figure 1.6).

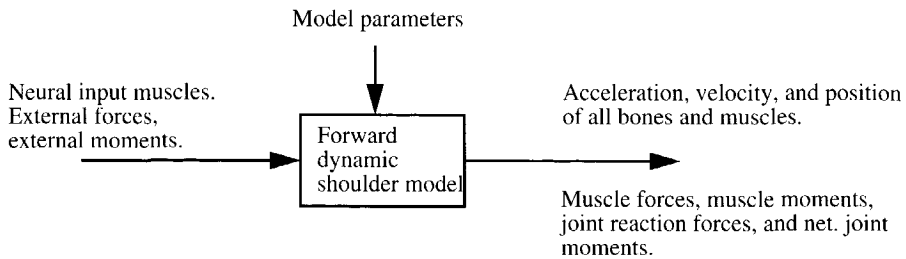


Figure 1.6: Block diagram of a forward dynamic shoulder model. Inputs are: neural input muscles, external forces and external moments. Outputs are: acceleration, velocity and position of all bones and muscles. Muscle forces, muscle moments, joint reaction forces, and net. joint moments.

1.5 Goal of this study

One of the problems of working with the Delft Shoulder Model is that there is a discrepancy between the morphology of the model and the morphology of the person whose movements are simulated. The model is based on parameters obtained from cadavers of mostly elderly persons, whereas for model simulations, younger people or patients are used.

This discrepancy between the general model and the individual subject is the reason why the model cannot simulate the same motions as were measured from the subject. This is because motions in the model are restricted by the motion constraints as explained earlier in this chapter. Also muscle moment arms can differ between subjects, resulting in different muscle forces.

Except for the kinematic differences between model and subject, there are also dynamic differences, such as the muscle cross-sectional area and inertia of the different body segments.

To improve the agreement between the simulation results of the model and the measurements from a subject, it is necessary to base the model on the morphology of that particular subject. This is important in, for example, a medical intervention restoring some shoulder function for which purpose tendons of the shoulder are to be displaced. Adapting the shoulder model to an individual subject involves measuring the geometric structures of that individual subject *in vivo*. For measuring geometric structures of a person in a non-invasive way, medical imaging techniques are suitable. Especially Magnetic Resonance Imaging (MRI) is non-invasive, believed to be not harmful and very suitable to make an image of the soft tissues of the inner body.

The general goal of this study is to individualize the Delft Shoulder Model to a given subject using medical imaging techniques. An important boundary condition is that this individualization is to be used in a medical setting, which means that the method needs to be fast, harmless for the patient, and with minimal user interaction.

1.6 Literature

When MRI techniques became more widely available in medical practice, biomechanical researchers started to use MRI images for obtaining data of the inner body. The main reason for this is that MRI images provide good contrast for soft tissue like muscles [Berquist 1987]. Another reason is that MRI is believed to be non-harmful to the human body, in contrast to Computer Tomography (CT), which is based on the harmful roentgen radiation.

MRI has been used to estimate inertial properties of segments [Martin 1989]; [Mungiole 1990]. It is also possible to obtain muscle cross-sectional areas from MRI images [Fukunaga 1992]. Obtaining muscle lines of action from MRI images is more difficult. Problems exist with the interpretation of the images and with the definition of the correct muscle line of action. Bassett worked with cross-sections of cadaver specimens. He obtained muscle volume, cross-sectional areas, muscle centroid lines, and muscle moment vectors of these specimens in a position of 90 degrees abduction and 90 degrees external rotation [Bassett 1990]. A weak point of the data of Bassett is that they are not suitable for a biomechanical model because the moment arms are only defined at one particular position. Using this method in an MRI setup is impossible because of the limited space inside an MRI tube, restricting arm positions to 0 and 180 degree elevation.

For other parts of the human body these direct methods of obtaining muscle moment arms from muscle centroid lines have also been used. Rugg has obtained moment arms for the ankle *in vivo* [Rugg 1990], Spoor did the same for the knee *in vitro* [Spoor 1992].

Koolstra developed a method for defining muscle lines of action from parallel cross-sections for the masticatory muscles *in vivo* [Koolstra 1990].

In the CHARM project, a model of the human shoulder is built using the Visible Human data set [NLM 1995]. For this project, muscle contours were detected semi-automatically from the cryo-sections [Gingins 1996a]; [Gingins 1996b]; [Kalra 1995]. From this short literature overview we can conclude that MRI can be used for obtaining model parameters for a biomechanical model. Until now, automatic or semi-automatic methods for obtaining parameters for biomechanical models have not been presented.

1.7 Layout of the thesis

The thesis is composed of 5 articles, i.e. Chapters 2 to 6, concluded with a general discussion about the research.

In Chapter 2, an interactive contour detection tool is described. This tool was developed especially for working with MRI images made for this project. At the start of the project, the focus was on developing automatic model based contour detection algorithms. Because the quality of the MRI images did not improve as much as we hoped five years ago automatic contour detection of muscle contours in MRI images was not possible. For working with MRI and CT images, an interactive approach was more valuable and we developed an interactive contour detection tool to this end. This tool has proven to be of value to the shoulder project, and has shown its use for other contour detection problems.

Because of the problems encountered in using automatic contour detection, the idea of complete automatic transformation from MRI image to model parameters was abandoned. We decided to change the focus of the research towards transforming or adapting the shoulder model. Using the existing model as a base, less data from MRI images are necessary to individualize the model. The main question becomes: What parts of the model need to be adapted?

In Chapter 3, a sensitivity analysis of the shoulder model is made. To this end, we have used three parameter sets from three cadavers in the shoulder model.

The three parameter sets make it possible to compare the muscle moment arms for different subjects. Because the same method is used to calculate and estimate these moment arms for the different data sets, a good comparison is possible.

To investigate what parameters can be extracted using MRI and how accurately these parameters can be extracted, in Chapter 4 we present a comparison between an MRI study and a cadaver study. For this comparison, we scanned a cadaver and the same cadaver was used for a dissecting experiment.

Because human interaction with an expert is necessary to detect muscle contours in an MRI image, it is not possible to build a model of the human shoulder using only data from MRI images. Expert knowledge is necessary. This makes the MRI data less useful for building a biomechanical model of the human shoulder.

In Chapter 5, the idea of using model knowledge for building an individualized model of the human shoulder is the subject of further investigation. The hypothesis is that muscle attachment locations and shapes correlate with the shape of the bone they are attached to. If this hypothesis holds, it is possible to predict the location of muscle attachments from the shape of the bones. To validate this hypothesis, geometric models of the bones of three human cadavers were built. Corresponding muscle attachments, measured by means of a cadaver study, were mapped onto these bones. After geometric transformation of the bones, the muscle attachments of the different cadavers with each other were compared.

In Chapter 6, a simpler form of model individualisation is studied. In this chapter, part of the kinematic structure is adapted based on the measured kinematic possibilities of the individual subject. This is done to reduce the difference in kinematic structure between the subject and the model. Reducing this difference results in a better conformity between the movements of the shoulder model and the measured movements.

Finally in Chapter 7, concluding remarks, conclusions and recommendations for further research are presented.

Chapter 2:

Image analysis of MRI images.

Interactive contour detection.

Abstract. An interactive contour detection tool is presented that can be used to detect 3-D objects in tomographic images. Human interaction is necessary because in most cases, automatic segmentation of these types of images is not possible. For contour detection, a model-based contour detection algorithm is used. This algorithm is based on dynamic programming techniques to minimize a cost function. The model, necessary for this contour detection method, is interactively supplied by a human operator. Also contour correction and contour propagation techniques are implemented in the method. The method has successfully been used for extracting muscle contours from MRI images of the human shoulder and for extracting bone contours from CT images of shoulder bones.

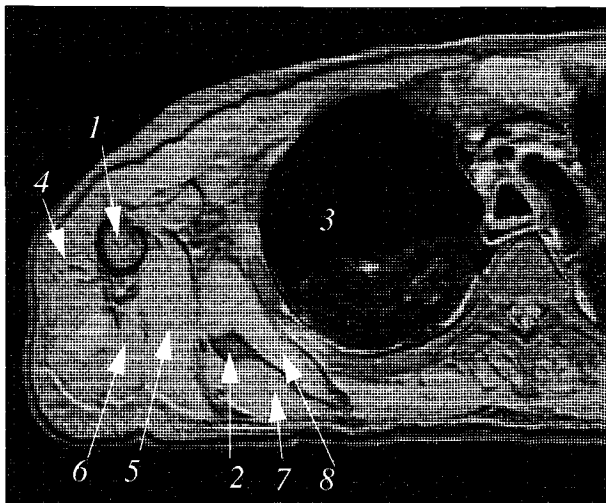
2.1 Introduction

Medical image data provides a good source of information for building a biomechanical model. If we look at an MRI image, Figure 2.1, all bone and muscle structures seem to be visible. The images only need to be segmented and classified. The problem of building biomechanical models from tomographic images is not the scope of this paper, however. This paper focuses on the segmentation and classification of the musculo skeletal structures in tomographic MRI images.

In biomechanical research, and especially in building a model of the human shoulder, the amount of data from an MRI experiment is huge and the muscular structures that need to be segmented have complex three- dimensional shapes. To

Figure 2.1: Example of a transverse MRI image slice of the human shoulder.

- 1: Humerus
- 2: Scapula
- 3: Lung
- 4: Deltoid muscle
- 5: Teres Major muscle
- 6: Teres Minor muscle
- 7: Infraspinatus muscle
- 8: Subscapularis muscle



distinguish between muscle and bone is not enough: Each muscle must be annotated separately. Because all muscles consist of the same tissue, the only way to distinguish one muscle from another is by detecting the very thin fascia and fat layer that is between the muscles. Because this layer is very thin, it is hardly visible in MRI images.

Even when one uses the cryosections of the visible human data set [NLM 1995], of which the resolution is high, in distinguishing one muscle from another one often relies on their texture, fibre orientation, or purely on anatomical knowledge [Gingins 1996a].

For muscular structures, no automatic segmentation algorithms are available. In research where muscular structures from MRI or CT images need to be segmented, contours are drawn manually [Koolstra 1990]; [Fukunaga 1992]. In the CHARM project, a model of the human shoulder has been built using the Visible Human data set [NLM 1995]. Contours of the high resolution cryosections were drawn manually. Snakes were used to refine these contours [Kass 1987]; [Terzopoulos 1991], but user intervention was necessary to validate and correct the contours [Gingins 1996a]; [Gingins 1996b]; [Kalra 1995]. In other medical applications manual contour detection is common practice as well [Montgomery 1993].

Until now, the problem of segmenting and classifying medical images automatically has not been solved [Höhne 1992]; [Schiemann 1997]. Only for specific classes of images and for specific objectives, successful applications have been developed [Schiemann 1997]. Automatic segmentation is mainly used for images of the heart and brain.

Because medical images cannot be segmented automatically yet, semi-automatic, or interactive segmentation procedures have been developed: Udupa presented a method based on region filling, where the user can isolate certain subregions [Udupa 1982]. This method is especially useful in the case of overlapping objects present in the image. Schieman presented a method based on morphological operations on 3-D data [Schiemann 1992]; [Höhne 1992]. One of the possibilities of this method is that the operator can erode a 3-D data set in order to break the thin connections between the different objects. The next step is to remove the unwanted objects. Another approach of interactively correcting a pre segmented image is the method presented by Higgens [Higgens 1993]. In this method, a 3-D watershed algorithm segments an image into different regions. The operator indicates the regions of interest. Together these regions build up the object of interest.

These existing methods are based on regions. An example of a contour-based approach is the work of Porrill [Porrill 1994]. In his method, a human operator is needed to draw initial contours, which were refined by an active contour model.

The intervention of the operator takes place at two moments: Before the segmentation, to generate a region of interest and after the segmentation, to correct the segmentation results.

According to Olabbarriaga [Olabbarriaga 1997] there are three possible situations in which user intervention is useful to improve the segmentation process:

- At the beginning of the segmentation process, by providing initial parameters, such as a seed point, some points in the contour, a threshold level, a region of interest, etc.
- At the end of the segmentation process to confirm the final result or to correct remaining errors by manual editing.
- During the segmentation process, by adjusting parameters or supplying additional information.

A combination of these approaches is most desirable.

In this paper, an interactive segmentation procedure especially designed for segmentation of MRI images of the human shoulder is presented. This segmentation procedure is contour based and intervention of the operator takes place before, during and after the segmentation.

2.2 Method

Image segmentation techniques are used to distinguish between the objects of interest and the background. This latter group is also referred to as the background. Segmentation techniques can be divided into region-based methods, contour-based methods, and a combination of the two. In the region based methods, regions are detected with more or less uniform properties. An example of such a technique is thresholding: A simple technique that divides the image into pixels with an intensity higher than a certain threshold, and pixels with an intensity lower than a certain threshold. Contour-based methods detect the contour around the object of interest. A simple example of a combination of the two techniques is the following: The gradient of an image is calculated, and this gradient image is thresholded in order to find the pixels with a high gradient. A challenge in this technique is to find closed contours.

In our case the muscles that need to be segmented all have the same properties, as a result of which region-based methods do not work well. A contour-based method was chosen as a base for the interactive segmentation procedure. The muscle contours are not easy to detect in the MRI images however, which makes it necessary to use a model-based contour detection method. The model is used to add the information that is not available in the images and to provide the contour detection method with information on the location and shape of the contour.

Examples of model-based contour detection methods are the deformable models, or snake models, as introduced by Kass e.a. [Kass 1987]. In these models, a closed contour is modelled as a flexible rod. We deform this rod by means of forces exerted by edge points in the image, in order to minimize an energy criterion. The energy consists of the internal bending energy and an external potential energy. This idea

was improved by Cohen e.a. [Cohen 1991] and extended to three dimensions [Terzopoulos 1987]; [Terzopoulos 1991]; [Cohen 1992]. Another extension of these methods is the active-shape model. In this model, more specific information about the shape of a structure is added [Terzopoulos 1991].

In other examples of model-based contour detection methods the model provides an initial contour and a region in which the real contour is to be found. The contour detection method uses a cost criterion to calculate a contour that is closed, smooth, and connected. The costs are extracted from the image by means of a local gradient filter. Because dynamic programming is used in finding the optimal solution, this method does not require a lot of computation time [Gerbrands 1988]. Nowadays, this method is often used to refine contour estimates obtained from model information about the approximate location of the contour. Several applications of this technique for medical images have been described [Thedens 1991]; [Thedens 1995]; [Philip 1994]; [Geest 1994].

For interactive contour detection, the idea of a magnetic mouse, as mentioned by Orange, seems to be very suitable for medical images [Orange 1994]. In the method of Orange, an operator points with a mouse pointer at an edge in the image. The contour is drawn instantaneously in the image when the operator moves the mouse pointer along the edge. The contour is not drawn exactly where the mouse points, but is calculated by a minimum cost segmentation algorithm. Moving the mouse pointer back along the found contour partly removes the contour. In this way, the human operator intervenes the segmentation process at all three possible intervention moments:

- At the beginning of the segmentation process, by pointing at the location where the contour is to be found.
- During the segmentation process, by moving the mouse pointer along the edge.
- After the segmentation process, by moving the mouse pointer back when the segmentation process results in a contour that is wrong according to the human operator.

The advantage of this method is that the human operator has full control on where the contour is to be detected without the need of being precise. Another advantage is that by using such a semi-automatic method, the resulting contour is more objective than a contour drawn by hand.

A disadvantage of this method is that when the contour is being drawn, every movement of the mouse or other pointing device is used by the system. This makes the method sensitive for hardware errors, like a badly functioning mouse, and human errors, like unintended hand movements. Because of this, the operator will be more stressed when working with the system. However, this method also makes it possible to make corrections after a contour has been completed.

2.3 Description of the proposed method

Contour Drawing. The procedure proposed in this paper is very much like the procedure described by Orange. The main difference is that the mouse positions are not used constantly as input for the contour detection, but only when the mouse button is pressed. This makes the method more user friendly, because for the user, it is more convenient to press a mouse button when the mouse pointer is at the desired location than to move a mouse along a predefined path without leaving this path. So, the contour-drawing process consists of the following actions:

1. The operator moves the mouse to the desired position on the edge of the object of interest.
2. When the mouse is at the desired position the operator presses the left mouse button defining a target point. When a target point is defined, a Region Of Interest (ROI) is defined by a rectangular area between the last point of the contour and the target point. When the target point is the first point of the contour, first a second point is defined using step 1 and 2. (Note that the target point needn't to be on the edge, although it is important that the edge of the object is within the ROI)
3. The contour detection method calculates a contour with minimal costs in the ROI and draws this contour on the image.
4. The operator checks the contour drawn and if he is satisfied, continues to the next part of the contour by acting according to step 1.
5. If the operator is not satisfied, he presses the right mouse button, deleting the last part of the drawn contour. Then he continues with step 1 to find the contour part again.
6. When the contour is completed, the operator presses the middle mouse button to close the contour and to finish the process.

During the contour-drawing process, the operator can change the contour detection parameters. In this way, for different parts of the contour, different detection parameters can be used.

Figure 2.2 shows a flow diagram showing the contour drawing process.

Contour Correcting. After the contour has been drawn, the operator can correct the contour. This can be necessary because the edge of the object is not entirely within the ROI, or because the contour detection method partly detected the wrong contour. Before correcting the contour, the contour detection parameters, like the width of the ROI, can be altered by the operator. The correction process consists of four steps:

1. Pick a point of the contour by pressing the left mouse button at the desired location.
2. Pick a second point of the contour by pressing the left mouse button at the desired location. Between these points, the contour will be altered.

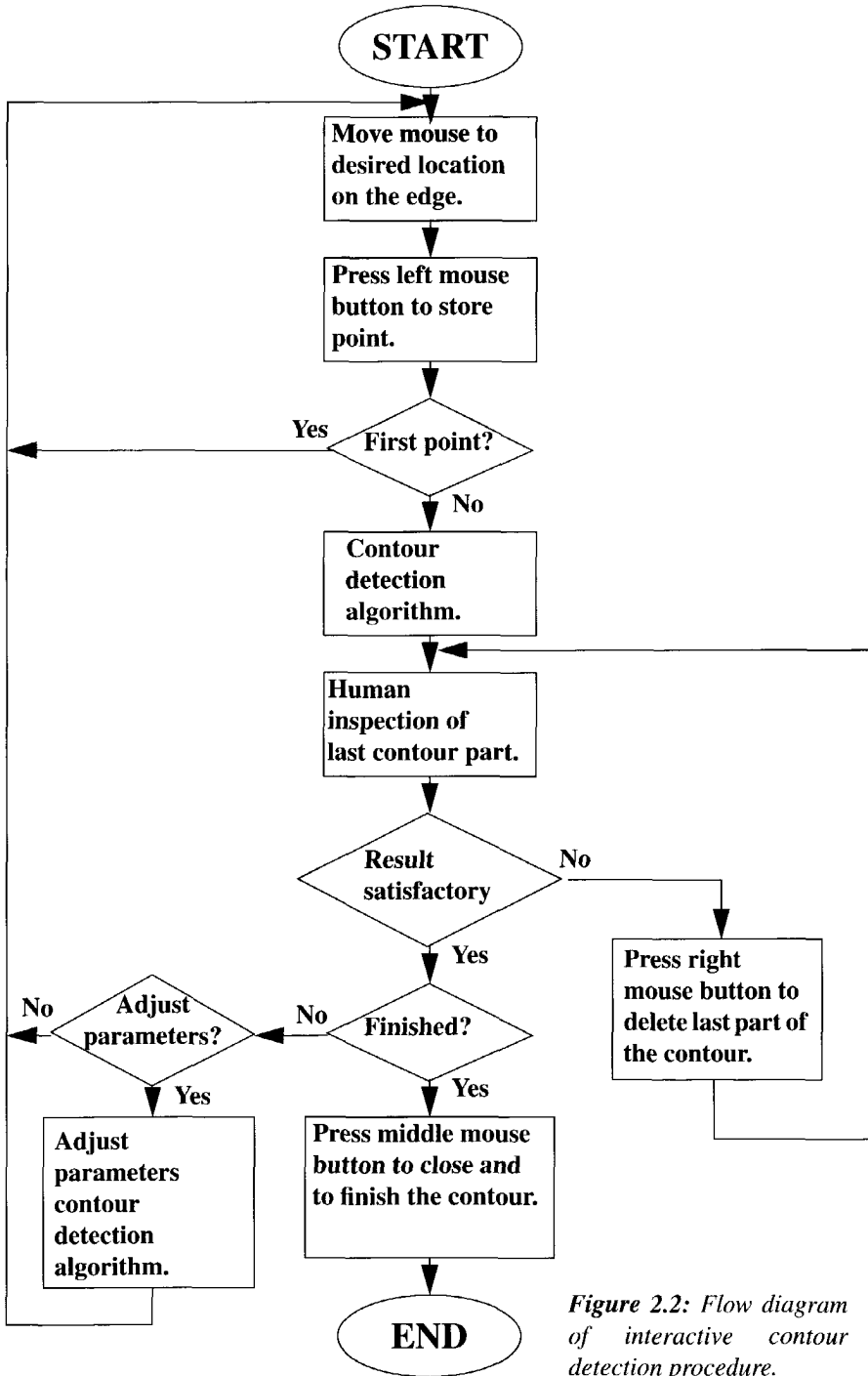


Figure 2.2: Flow diagram of interactive contour detection procedure.

3. Point at a location in the image and press the left mouse button, to provide a third point. An elastic line is shown in the image from the first point to the second point via the third point. When the mouse button is released, a ROI is defined using the three points.
4. The contour detection method calculates a contour with minimal costs in the ROI, from the first point to the second point via the third point.

In this way, the operator corrects the contour by cutting away part of the contour and replacing it with another part.

Contour Propagation. Tomographic images contain a stack of 2-D images, each containing a cross section of the scanned volume. Because these cross-sectional images are aligned, the 2-D cross sections of the 3-D object of interest are aligned as well. Because of this, it is possible to use the 2-D object contour detected in one section as an initial contour for the next section. The contour detection algorithm uses this initial contour to define the ROI, and detects the resulting contour within this ROI. This technique is called contour propagation and is often used in medical image analysis. In the interactive contour detection tool, contour propagation can be activated by pressing the button “Next Slice” or “Previous Slice” which results in the current contour being used as an initial contour in the next or previous slice.

Figure 2.3 shows a flow diagram of the complete Interactive Contour Detection System. This diagram shows the role of the human operator inside the process loop.

2.4 The Contour Detection Algorithm

The contour detection algorithm used in the described procedure consists of three steps: First, the generation of a cost matrix using, for example, gradient filters. Second, the optimization procedure that calculates an optimum path through the cost matrix using dynamic programming. Third, post processing of the contour in order to make it smooth. This three step approach makes the method very flexible. In this paragraph, the algorithm is explained very shortly. For a more extensive explanation we refer to Kaptein [Kaptein 1993].

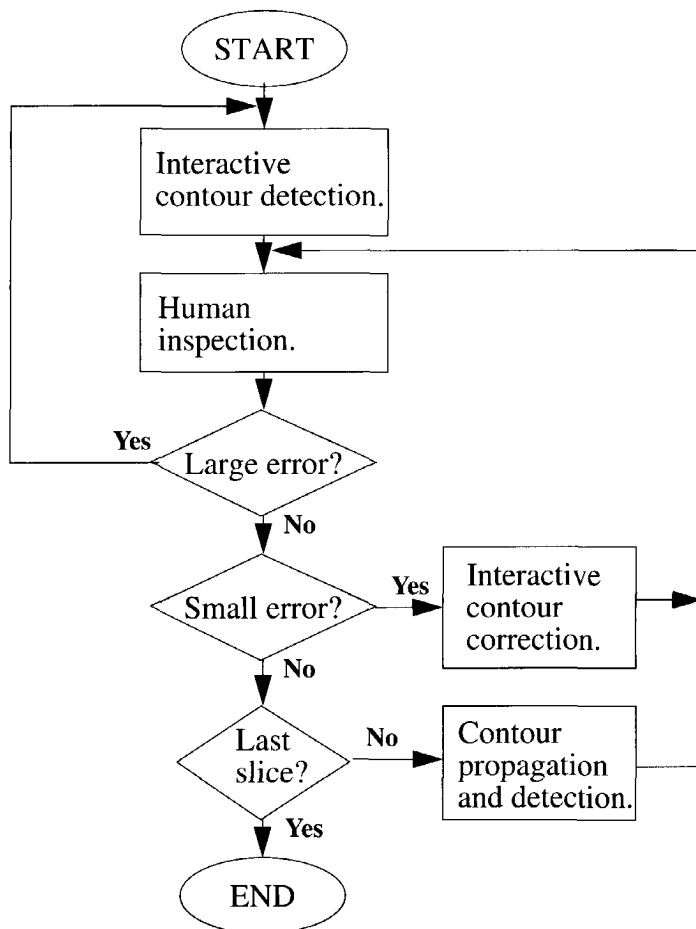


Figure 2.3: Flow diagram of complete Interactive Contour Detection System.

Generation of a cost matrix.

The cost matrix is generated by resampling the image data within the ROI to generate a rectangular matrix. In this matrix a filter is applied that generates the costs from the image data. Normally this filter is a gradient filter. This makes it possible to calculate the gradient in a direction perpendicular to the direction of the contour. Another advantage of filtering the resampled image data is that it is also possible to make the filter direction sensitive: This means that the algorithm can distinguish between a dark object on a light background and a light object on a dark background. It is also possible to filter the image data itself using one of the many existing gradient filters, or even other contour detection algorithms like the Canny edge detector [Canny 1986]. The generation of a good cost matrix for a specific application can be a difficult task.

The cost matrix used in this algorithm is generated using a very simple gradient filter. It is a matrix in which the values of the cells represent the costs that have to be paid to pass these cells.

Optimum path calculation. To calculate an optimum path through the cost matrix, we use a dynamic programming procedure. This procedure minimizes the cumulative total costs that have to be paid to follow a path from the first row to the last row in the matrix. The costs in each cell of the matrix that is passed by this path adds to these costs. Demands on this path are that it must be connected and closed. After an optimal path has been calculated, the path is transformed back from the resample matrix domain to the image domain.

Contour filtering. Because of the distortions in the image, and the transformations between the image domain and the resample matrix domain, the resulting contour is not smooth, and can even contain little loops. To smooth the contour, and to remove the little loops, three filters are applied on the contour:

1. A filter that removes the little loops by just cutting them off.
2. A third-order polynomial smoothing filter, which calculates a third-order polynomial through part of the contour and replaces contour points by their corresponding points on the polynomial.
3. A vectorization filter, which reduces the number of contour points using a vectorization algorithm [Douglas 1973].

Smoothing and vectorization of the contour is necessary when the contour is used as an initial contour for the next contour detection step because a non-smooth contour distorts the resampling algorithm.

2.5 Results

Finding the contour of the humerus bone. The first example shows coronal images of the humeral head from coronal MRI images of the Visible Human data set [NLM 1995]. In this example it is shown that with a minimum of mouse clicks, a 3-D object can be detected from an MRI image. For this experiment, the following settings were used:

- Width of the ROI: 11 pixels.
- Number of contour points for smoothing: 13. (The contour points have a distance of about 1 pixel from each other.)
- Vectorization error: 0.5 pixel.
- Gradient filter in the resample image domain, using direction sensitiveness.

In Figure 2.4 the contour propagation through the different image slices is shown. In slice a, the contour of the humeral head is detected. For the initial contour, only four mouse clicks were necessary. This contour is propagated through the slices b-j without intervention of the operator.

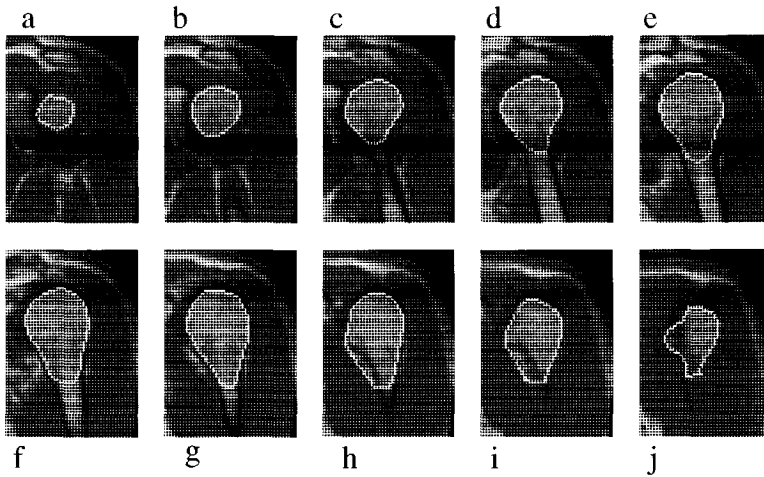


Figure 2.4: Contour detection of humeral head in coronal images of the human shoulder joint. The initial contour of image a is propagated through the image slices without correction.

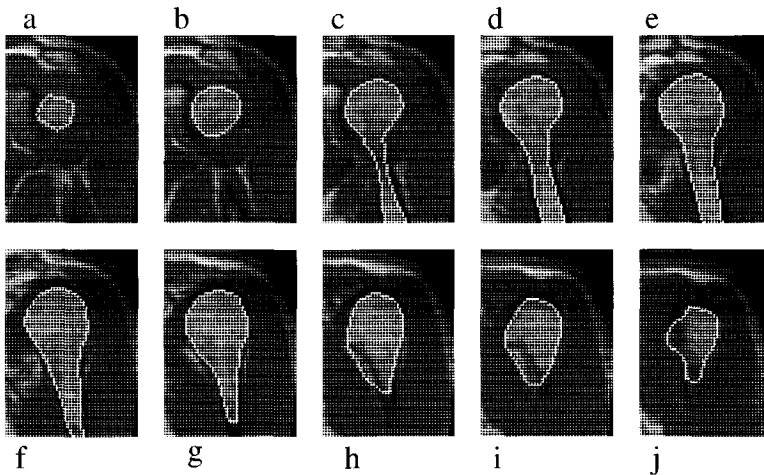


Figure 2.5: Contour detection of humeral head in coronal images of the shoulder joint. Intervention in slice c makes the detection of the stem of the humerus also possible.

In slice c, the stem of the humerus appears in the image. Because the contour detection algorithm seeks a contour in a ROI, the difference between slice b and slice c is too great for the algorithm to detect also the stem.

In slice h, part of the scapula bone is visible in the image as a false contour. This contour is probably stronger than the humerus contour within the ROI, so the contour detection method follows the wrong contour here.

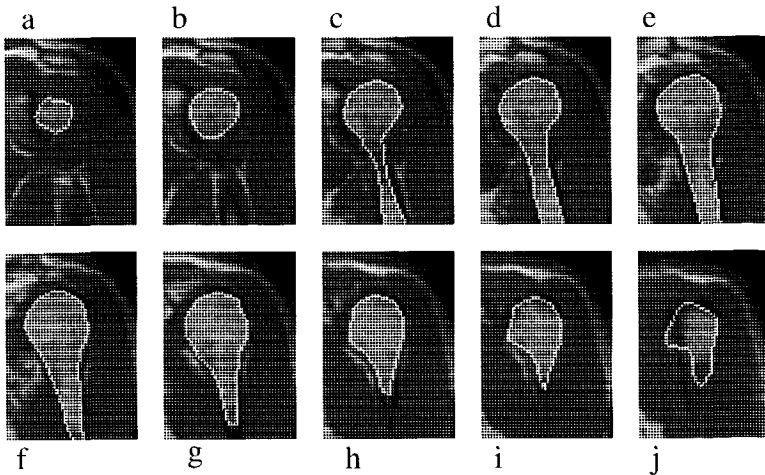


Figure 2.6: Contour detection of humeral head in coronal images of the shoulder joint. Intervention in slice h.

Slice j shows that once the contour detection method gets a wrong initial contour as input, the detected contour is wrong as well. This makes unsupervised contour propagation an unreliable tool.

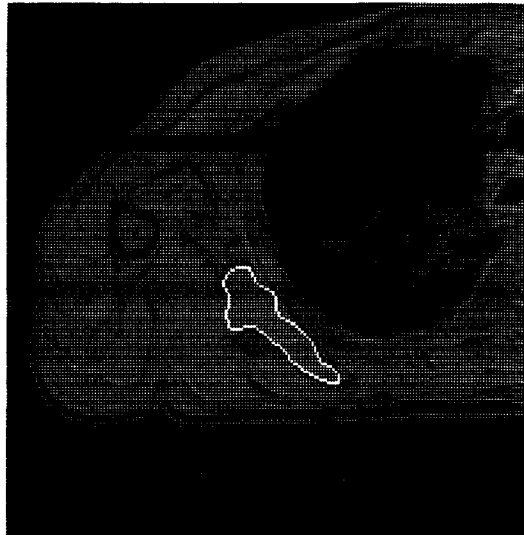
Figure 2.5 shows the same procedure as Figure 2.4, but now the operator corrected the contour in image slice c. We see that this correction is enough to detect the stem of the humerus in all following image slices.

Figure 2.6 shows the result after user intervention in image slice h. Now the detection is almost complete, except that in image slice j, the contour is not detected correctly. This is caused by a large difference between image slice i and image slice j. To correct the contour in slice j, it is faster to redraw this contour completely than using the correction method. This is because the correction method can only correct one local error at a time. Here we see two local errors.

With this example, we showed that with a few mouse clicks a complete 3-D object can be segmented from an MRI image. Using the extracted contours, we can generate and view a triangular surface model.

Detecting the muscles of the shoulder in an MRI data set. This example shows the application for which the interactive contour detection tool was originally designed: Detecting muscle contours from MRI images. Because the muscle contours do not have high contrast, detecting these contours is very difficult. Figure 2.7 shows an example of the subscapularis muscle detected in an MRI image slice. Using the propagation tools in combination with contour correction and in some cases redrawing of the complete contour we extracted a complete 3-D model of all the muscles of the shoulder from this data set. For some parts of the contours a lot of human interaction is necessary because these contour parts are not visible in

Figure 2.7: Contour of the subscapularis muscle, detected using the interactive contour detection tool.



the images. For the parts of the contours that are visible in the images, the interactive contour detection tool provides a great help for the human operator.

2.6 Discussion and Conclusions

2.6.1 Discussion

This paper shows a contour-based approach on interactive image analysis. At the moment, a lot of research focuses on using a watershed algorithm to segment an image into a large number of objects, followed by some kind of user interaction to join the objects of the oversegmented image. These region-based methods are very promising, but for detecting muscles in MRI images, a contour-based segmentation method is more suitable. Also for applications where a region-based approach can be used, the contour-based method as described in this paper provides good results, as shown in the first example.

To improve the presented method we can extend it by showing information to the human operator about the quality of the detected contour. For example, the local relative costs of the contour provide information about the local quality of the contour. The problem is that erroneous parts of the contour exist in two different situations: When the gradient of the contour in the image is not strong enough, and when another contour in the region of interest has a high gradient. So parts of the contour with lower or higher costs than the mean costs over the complete contour can be labelled as possibly erroneous.

Information about the continuity of the object in the third dimension can also be of interest to the operator. At the moment, this information is given by projecting the contours from the preceding and following image slice onto the current image slice

using a different colour. This simple clue provides enough information to the human operator about the continuity in the third dimension.

2.6.2 Conclusions

In this paper, an interactive contour detection procedure is presented. This procedure is very suitable in cases where tomographic data needs to be segmented. Benefits of the method are the generic usability, and the ease with which it can be extended with different gradient filters. Because the method is interactive, it can be used for many purposes without adaptation.

Chapter 3:

Different parameter sets for the Delft Shoulder Model.

Abstract. To investigate the sensitivity of the Delft Shoulder Model to its parameters, we used results from dissection experiments with different cadavers to obtain three sets of parameters for the shoulder model. These parameter sets were used for simulations with the shoulder model. Simulation results were analysed to investigate the sensitivity of the shoulder model to these geometrical parameters. The results show that the model is very sensitive to these parameters. From this, we can conclude that it is necessary to adapt the Delft Shoulder Model to an individual subject. Because of the complexity of the model and the unpredictable effects of model adaptation, the adaptation of the Delft Shoulder Model to the individual subject must be done with great care.

3.1 Introduction

The shoulder girdle is one of the more complex joints of the human body [Engin 1980]. It consists of the clavicle and the scapula, and provides a stable but moving base for the humerus. Because of the construction and possible movements of this base, the humerus has a large range of motion with respect to the thorax.

To gain a better understanding of the working of this joint, biomechanical computer models have been developed [Högfors 1987]; [Högfors 1991]; [Karlsson 1992]; [Helm 1994a]. These models comprise a number of rigid bodies describing the bones, and muscle lines of action describing the muscles. Joints are mostly modelled as ball-and-socket joints. The scapulo-thoracic gliding plane is a special kind of joint, and is modelled differently in the models that exist nowadays.

In most of these models, there are more muscle lines of action than strictly necessary from a mechanical point of view. To distribute the necessary joint moment over the different muscle lines, an objective function is formulated. This objective function consists of the minimization of certain costs like the total sum of the quadratic muscle stresses. It also contains a number of constraints.

Högfors developed a static 3-D model of the shoulder which is based on a cadaver study [Högfors 1987]; [Högfors 1991]; [Karlsson 1992]. Input for this model is the orientation of the humerus bone, and external moments and forces acting on this bone. The position and orientation of the scapula and clavicle are assumed to be related to this humeral orientation. This relation between the orientations of the constituent bones of the human shoulder is known as the scapulo humeral rhythm. The relation is consistent within one individual, but inter-individual differences are large [Högfors 1991]. In the model of Högfors, the scapulo-thoracic gliding plane is modelled as an elliptic cylinder. It is only used to calculate the direction of the

scapulo-thoracic reaction forces and does not provide kinematic constraints.

Van der Helm developed a 3-D dynamic model [Helm 1994a] on the basis of a cadaver study involving 7 cadavers [Veeger 1991a]; [Helm 1992]. This model needs external forces and moments as input. Orientation of the humerus as well as the scapula and clavicle are also necessary as input for this model. Because orientation of scapula and clavicle cannot be recorded in dynamic situations, input for this model can only be recorded in static situations. De Groot investigated the scapulo-humeral rhythm by using 2-D roentgen video. He showed that the velocity of arm movement has no significant effect on the scapulo-humeral rhythm, so it is possible to extrapolate the static information to dynamic situations [Groot 1998a]. The model of Van der Helm uses an ellipsoid to model the scapulo-thoracic gliding plane. This ellipsoid constrains the possible movements of the scapula as well as the direction of the scapulo-thoracic reaction forces.

This study focuses on what influence the parameters used in the model have on its simulation results. This study is performed using the shoulder model of Van der Helm. Parameter sets of three different cadavers were used to generate three models, each based on its own parameter set. An evaluation of the results of the simulations using these models gives insight in the sensitivity of the Delft Shoulder Model to these geometrical parameters. The goal of this study is to find out whether it is necessary to individualize the model. When individualization of the model is necessary, we want to know which parameters need to be adapted.

3.2 Method

3.2.1 Modelling and model parameters

An inverse dynamic musculo-skeletal model of the shoulder mechanism was developed by Van der Helm [Helm 1994a]. The input variables for this model are position, velocity and acceleration of the bones and external loads, whereas output variables are muscle forces calculated by means of an optimization criterion.

In a cadaver study data were acquired for inertia, geometry and muscle contraction parameters for this model [Veeger 1991a]; [Helm 1992]. Data from the left and right shoulder of 7 cadavers were recorded, which resulted in 14 data sets. On the basis of these data sets, one more or less median cadaver was chosen to build the original shoulder model of van der Helm. In this study, two other data sets were used to build two extra shoulder models in the same manner as the original one. Following the original publications, we call these data sets R2, R4 and R6, where R2 was used for the original shoulder model.

3.2.2 Input

Well-defined bony landmarks on the bones are used to connect the external palpation measurements of movements with the movements of the model. The recorded bony landmarks are used to calculate the bone orientations. In the model, the clavicle and scapula together with the thorax and the conoid ligament form a closed chain mechanism with only three degrees of freedom [Helm 1994a]. Because for the shoulder girdle six degrees of freedom were measured, the rotations of the bones of the shoulder model cannot be similar to the rotations recorded at the subject. De Groot developed an optimization procedure that minimizes the difference between the orientations of the scapula and the clavicle bone in the model and the measured orientations. This is done by altering the input coordinates for the shoulder model [Groot 1998b].

Because only two landmarks can be distinguished on the clavicle, the axial rotation of the clavicle cannot be recorded [Pronk 1991a]; [Helm 1995]. Axial rotation has been estimated by minimizing the rotations in the AC joint. In the shoulder model, the axial rotation of the clavicle is fully determined by the conoid ligament, which is assumed to be rigid. Kinematic input for the model are the three angles determining the orientation of the humerus bone. For the shoulder girdle, the y- and z-coordinate of point AC, and the x-coordinate of the point TS determine the three degrees of freedom. (See Appendix A for a definition of coordinate systems and rotations).

3.2.3 The bones

The bones in this model are modelled as rigid objects, which are connected by ideal ball-and-socket joints. Together with the scapulo-thoracic gliding plane, modelled as an ellipsoid, and the conoid ligament, modelled as a rigid truss, these joints prescribe the possible motions of the shoulder girdle.

3.2.4 The muscles

A special method has been developed to model the mechanical effect of muscles with large attachment sites [Helm 1991a]. According to this method, each muscle is modelled by means of 1 to 6 muscle lines of action. Because some of the muscles of the shoulder girdle are wrapped around bony contours, special curved lines of action are used for these muscles. These muscles are wrapped around simple geometric objects, like a ball for the humeral head, a cylinder for the humeral shaft, and an ellipsoid for the thorax.

Table 3.1 Results for a selection of anthropometric data of the three cadavers used in this study.

	R2	R4	R6
Gender	M	F	M
Age	90 years	86 years	82 years
Weight	72.9 kg	71.3 kg	74.9 kg
Stature	172.7 cm	164.2 cm	167.6 cm
Chest depth	19.70 cm	25.30 cm	22.10 cm

Table 3.2 Length of Clavicula and Conoid ligament and dimensions of the Scapula of the three models of the shoulder.

	R2	R4	R6
Length Clavicle	15.8 cm	14.5 cm	15.9 cm
Length Conoid ligament	1.83 cm	1.32 cm	1.38 cm
Distance AI-TS (length internal border)	11.3 cm	11.0 cm	10.9 cm
Distance AC-TS	11.9 cm	10.0 cm	13.0 cm
Angle (AC-TS-AI)	105 degree	109 degree	98 degree

3.3 Results

Analyzing and comparing the simulation results of these three data sets gives insight in the sensitivity of the shoulder model to geometric parameters. Table 3.1 shows a selection of anthropometric data of the three cadavers used in this study. As can be seen from this table, the differences between the cadavers are small, so we do not expect large differences in kinematic results between the different models.

3.3.1 Kinematic analysis

Model parameters. Important parameters for the kinematics of the model, are the length of the clavicle (Table 3.2), the shape of the scapulo-thoracic gliding plane (Table 3.3), and the length of the conoid ligament. They prescribe the possible movements of the model. In the original data set, the length of the conoid ligament of cadaver R4 is 8.2 mm, but this model is not able to reach all the measured positions. The length of the ligaments has not been measured directly, but has been calculated from the insertion locations of the ligaments. This makes these measurements unreliable. Literature shows the average length of the conoid ligament to be about 13 mm [Salter 1987]. The length of the ligament of cadaver R4 was changed to 13.2 mm. Pronk analysed the functions of the ligaments of the shoulder girdle [Pronk 1993]. He concluded that the function of the conoid ligament is to counteract the axial rotating moments about the longitudinal axis of the clavicle by the m. Deltoideus and m. Trapezius. He also concluded that the function of the ligaments in preventing extreme joint translations could not be analysed. Table 3.3 shows the parameters for the ellipsoid model of the thorax. There is no relation between these parameters and the stature or chest depth data of Table 3.1. The ellipsoid parameters have been calculated by fitting an ellipsoid model through measured points on the thorax. The X-Centre was defined to be zero, and the main axes of the ellipsoid were aligned with the global coordinate system. The large differences in the Y-Centre location and Y-Axis length are caused by the high interaction between these parameters, which makes them very sensitive for variations in the input for the fitting procedure.

Table 3.3 Parameters of ellipsoid of the three shoulder models

	R2	R4	R6
X-Centre	0.0 cm	0.0 cm	0.0 cm
Y-Centre	-29.6 cm	-23.0 cm	-15.8 cm
Z-Centre	7.8 cm	5.4 cm	6.6 cm
X-Axis length	15.3 cm	13.7 cm	13.3 cm
Y-Axis length	40.4 cm	31.4 cm	25.6 cm
Z-Axis length	13.0 cm	13.0 cm	11.1 cm

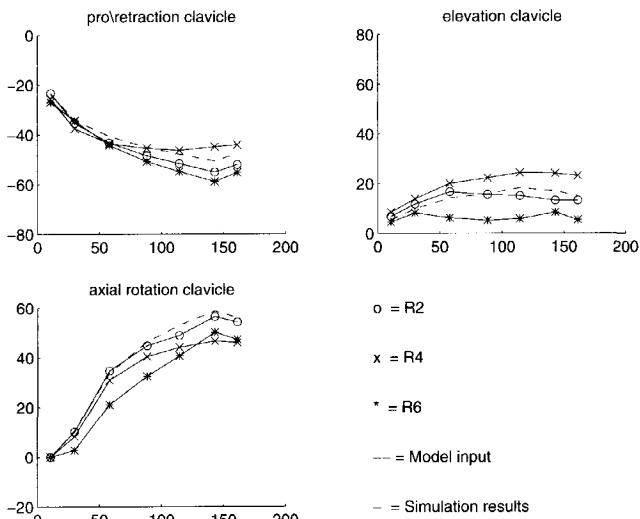


Figure 3.1: Rotations of clavicle (degrees) as a function of humeral elevation angle (degrees) for an Unloaded ABduction movement (ABU).

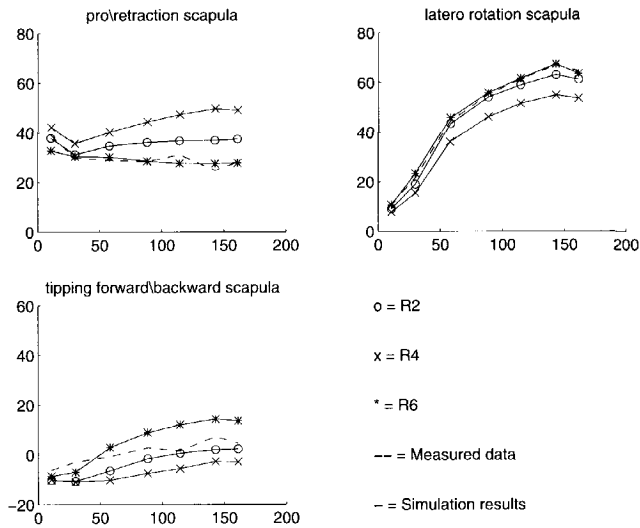


Figure 3.2: Rotations of scapula (degrees) as a function of humeral elevation angle (degrees) for an unloaded abduction movement (ABU).

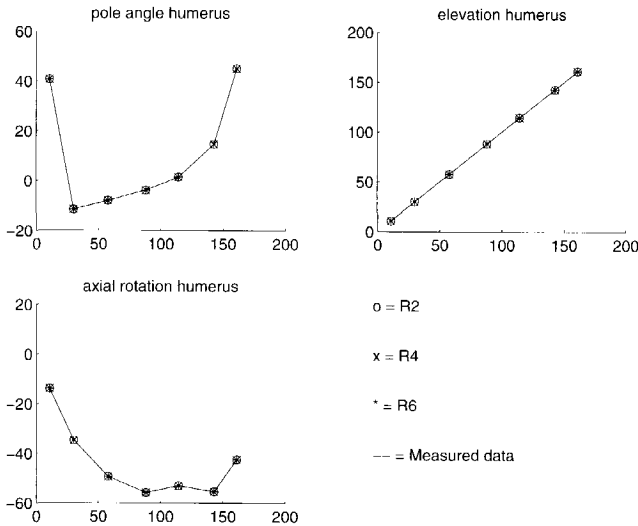


Figure 3.3: Rotations of humerus (degrees) as a function of humeral elevation angle (degrees) for an unloaded abduction movement (ABU).

Note: Because there is no difference between the data from R2, R4, and R6, the lines are plotted on top of each other.

Movements. For the kinematic analysis of the shoulder model, two types of movements are analysed: the Unloaded humeral ABduction movement (ABU) and the Unloaded humeral forward flexion (or ANtcflexion) movement (ANU). For both the movements, seven positions were measured. These input data is the mean of the recorded data from ten healthy subjects [Helm 1994b]. Because of the constraints imposed by the kinematic structure of the model, not all positions could be reached exactly.

In Figure 3.1, Figure 3.2, and Figure 3.3, we see the simulated and measured rotations of the clavicle, scapula and humerus during a humeral abduction movement. In Figure 3.1 we see that the simulated elevation angle of the clavicle of cadaver R6 is ten degrees below the measured angle of the clavicle. For the axial rotation of the clavicle, we also see a larger difference for the data of R6. R4 also has a larger difference at higher humeral elevation angles. These differences in axial rotation can be caused either by the fact that we estimate the axial rotation of the clavicle or because the assumption that the conoid ligament is rigid is not valid. Figure 3.2 shows the simulated and measured rotations of the scapula. Here the differences between measured and simulated rotations for cadaver R4 are larger than these differences between the data of the rotations for R2 and R6. Figure 3.3 shows

Table 3.4 Mean of the absolute differences and standard deviation in orientation (degrees) between measured and simulated rotations for unloaded humeral abduction movement (ABU).

	R2	R4	R6
pro\retraction clav.	2.9 (1.6)	2.8 (1.7)	5.1 (2.9)
elevation clav.	2.1 (1.1)	5.8 (1.7)	7.4 (4.4)
axial rot. clav	1.7 (1.3)	6.0 (4.5)	9.2 (4.6)
pro\retraction scap.	6.2 (4.0)	14.0 (7.8)	2.1 (2.3)
latero rotation scap.	2.3 (1.1)	8.5 (3.0)	0.9 (0.6)
tipping forw.\ backw. scap.	4.3 (2.2)	8.0 (2.2)	6.1 (2.9)

Table 3.5 Mean absolute difference and standard deviation in orientation (degrees) between measured and simulated rotations for unloaded humeral forward flexion movement (ANU).

	R2	R4	R6
pro\retraction clav.	1.9 (1.6)	3.2 (1.7)	4.0 (2.9)
elevation clav.	2.3 (1.7)	9.0 (0.6)	5.5 (4.2)
axial rot. clav	1.4 (1.2)	11.2 (10.7)	6.4 (3.2)
pro\retraction scap.	7.6 (5.8)	19.8 (9.8)	2.7 (1.7)
latero rotation scap.	2.6 (0.9)	11.8 (4.7)	1.5 (1.2)
tipping forw.\ backw. scap.	7.1 (2.3)	2.1 (1.5)	3.3 (2.2)

the simulated and measured rotations of the humerus. Because in the model there are no restrictions on the rotations of the humerus, there is no difference between the measured rotations and rotations resulting from the simulations. Table 3.4 shows the differences for the clavicle and scapula rotations for the humeral abduction movement. The model of cadaver R4 simulates the measured movement least good, whereas the model of R6 simulates it best. Table 3.5 shows the differences between clavicle and scapula rotations for the humeral forward flexion movement. Also for this movement, the model of cadaver R4 is less capable of simulating the measured movements.

In general, we see that large differences between measured and simulated movements of the shoulder girdle can exist. The large differences for the model of cadaver R4 are caused by some kinematic difference between the model and the mean geometry of the measured subjects. The data show that the main parameters influencing the kinematics are the shape of the ellipsoid and the sizes of the clavicle and scapula. The relatively short clavicle length of cadaver R4 may be the cause of the problems.

Moment arms. In biomechanical models, moment arms can be considered as the most important parameters influencing the calculated muscle forces of the model. External loads acting on the model are to be compensated by joint moments. Joint moments are exerted by muscle moments, and muscle moments are the product of muscle force and muscle moment arm.

In the shoulder model, a muscle line of action is defined by its origo and insertion point, and, for some muscle lines, by its bony contour. So for each position and for each muscle line of action, moment arms are calculated.

To get some insight in the differences between these moment arms, simplifications are necessary: First the mean moment arm for each muscle is calculated by taking the mean moment arm over all muscle lines of action for the muscle lines belonging to that muscle. Second, because the model has three dimensions, each muscle line of action has a moment vector consisting of a moment arm for the x, y, and z component. The length of this moment vector is calculated. Third, because the moment arms vary with the humerus orientation, the mean moment arm is calculated over a complete movement.

In Figure 3.4, Figure 3.5, and Figure 3.6, the results of these calculations are displayed for a humeral abduction movement. In general, the moment arms for the model of cadaver R2 and R6 are similar, whereas for most muscles of cadaver R4, the moment arms for the model differ from those of model R2 and model R6. For a humeral forward flexion movement, similar results can be obtained. Appendix B shows the mean muscle moment arms as a function of humeral abduction angle for all muscles. This appendix shows us that the change in moment arms over the abduction movement is consistent for the three models for most muscles.

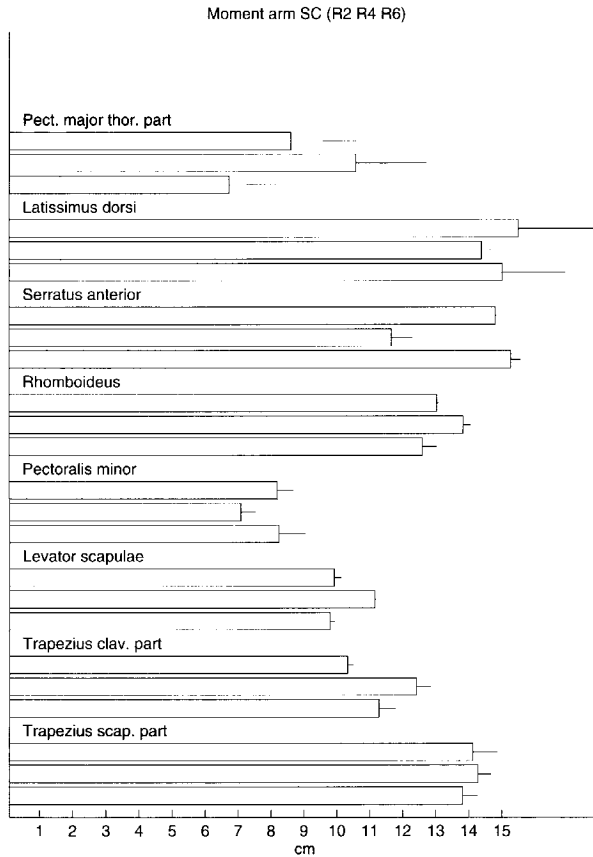


Figure 3.4: Mean of the moment arms around the SC-joint for a humeral abduction movement. The three bars are of the model of cadaver R2 (top bars), of cadaver R4 (middle bars), and of cadaver R6 (lower bars), respectively.

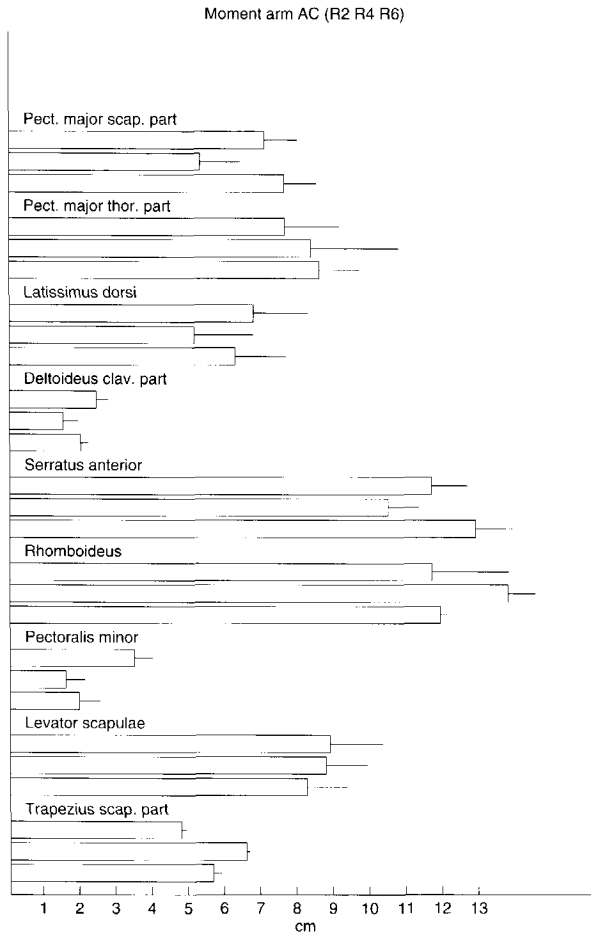


Figure 3.5: Mean of the moment arms around the AC-joint for a humeral abduction movement. The three bars are for the model of cadaver R2 (top bars), of cadaver R4 (middle bars), and of cadaver R6 (lower bars) respectively.

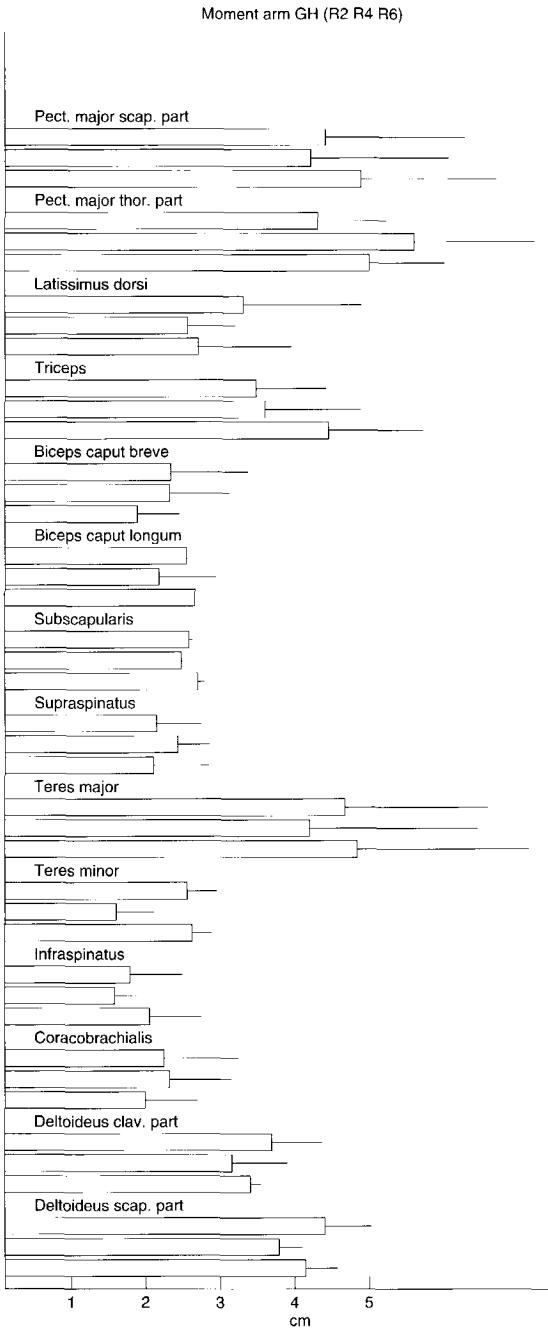


Figure 3.6: Mean of the moment arms around the GH-joint for a humeral abduction movement. The three bars are for the model of R2 (top bars), of R4 (middle bars), and of R6 (lower bars), respectively.

It also shows large differences between the moment arms between the models for the Serratus Anterior muscle. This is because moment arms of the Serratus Anterior muscle are very sensitive to the shape of the thorax and the direction of the muscle fibres.

3.3.2 Dynamic analysis

Because in the shoulder model, the number of muscle lines of action is far greater than the number of degrees of freedom, there is not a unique way to distribute the necessary joint moment over the different muscle moments. To solve this problem, an optimization algorithm is used. For the optimization algorithm different criteria can be used. For this experiment we used a minimalization of the quadratic muscle stresses. Besides this criterion, the optimization procedure also has to obey the earlier-mentioned constraints:

- The joint reaction force vector of the glenohumeral joint has to point inside the glenoid cavity.
- The points *trigonum spinae* (TS) and *angulus inferior* (AI) may only apply compressive forces acting on the thorax.
- The conoid ligament may only apply a pulling force between its insertion points.
- Moment balance needs to be established for each joint.

Muscle force. Figure 3.7 shows the mean muscle forces during an abduction movement. Here we see that the small differences in moment arms between the different models are amplified by the nonlinear behaviour of the optimization algorithm, resulting in larger differences in muscle forces. We also see that there is no direct relation between differences in moment arms and differences in muscle force. To see whether the different models use different strategies (or muscles) to compensate the necessary joint moments, we can have a look at the joint moments. Figure 3.8 shows these moments for the z-axis of the glenohumeral joint. This is the abduction moment. The contribution from each muscle to compensate the external moments is plotted as a function of the humeral elevation angle. We see that for model R2 and R6, these moments are quite similar. The Subscapularis of model R4 behaves very differently at low elevation angles. For the model of R6 at 60 degrees elevation angle, the thoracic part of the Pectoralis Major is active, as well as the Latissimus Dorsi. It is unlikely that the behaviour of model R6 at a humerus elevation angle of 60 degrees is normal. Unfortunately no explanation could be found for this behaviour after thorough analysis.

Joint reaction forces. Because the shoulder model is so complex, it is very difficult to compare the muscle forces and muscle moment arms directly. It is better to look at the results of the muscle forces, which are the joint reaction forces.

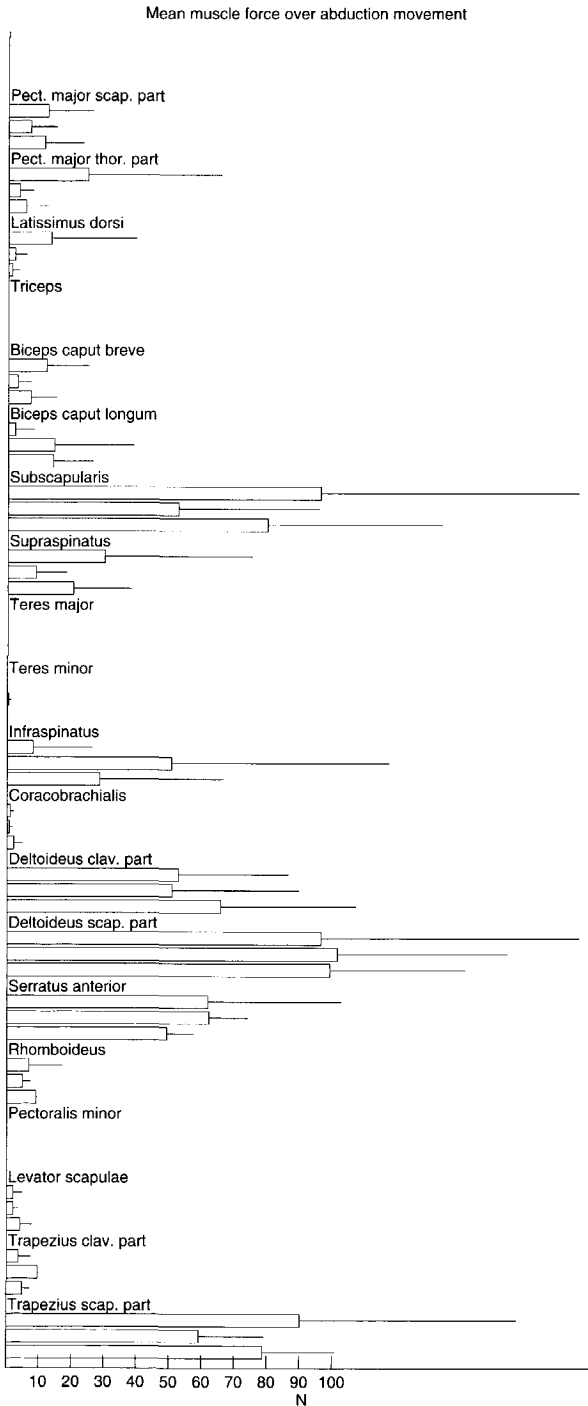


Figure 3.7: Mean of the muscle forces (N) for each muscle during an abduction movement. The three bars are for the model of cadaver R2 (top bars), of cadaver R4 (middle bars), and of cadaver R6 (lower bars), respectively.

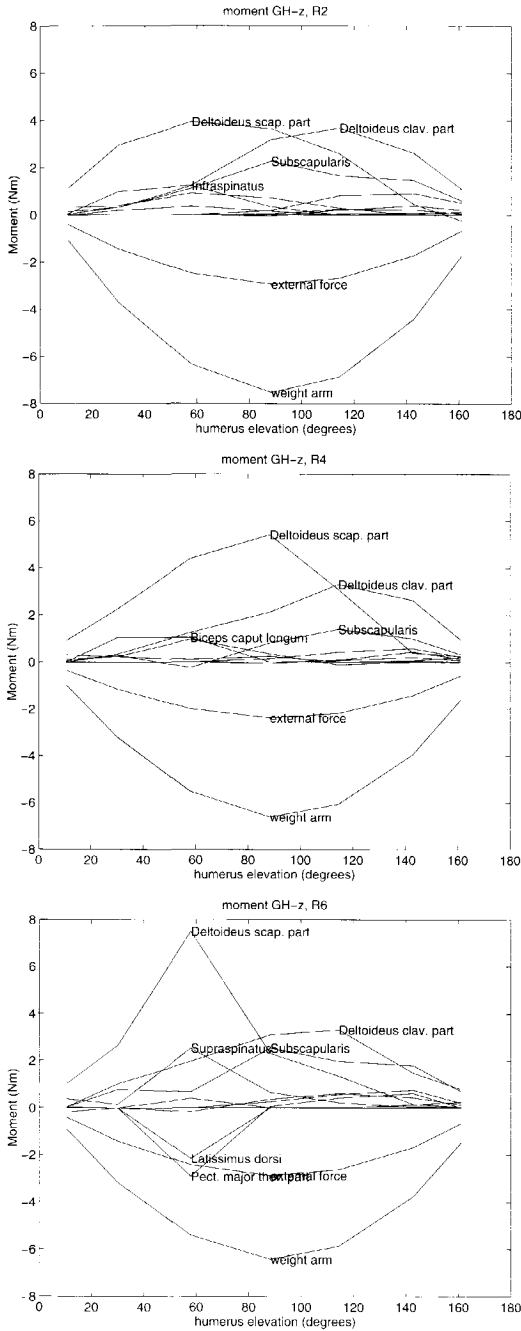


Figure 3.8: Moments (Nm) around the z-axis of the glenohumeral joint as a function of the humeral abduction angle for the models of cadaver R2, R4 and R6.

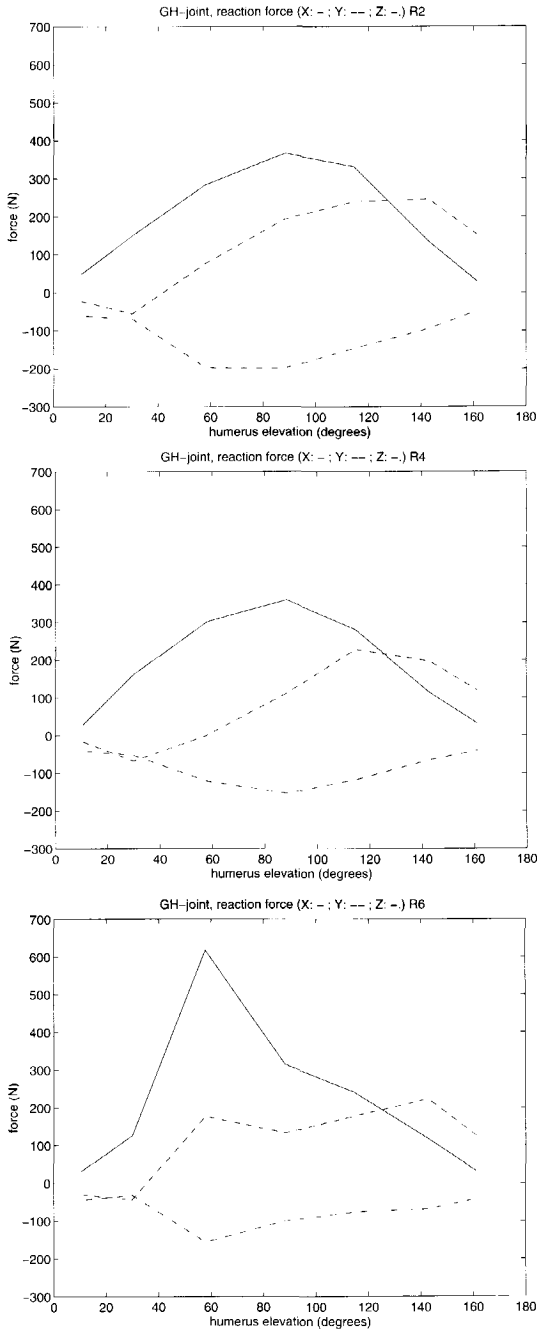


Figure 3.9: Reaction forces in the Gleno-humeral joint as a function of humeral abduction angle for the models of cadaver R2, R4, and R6.

In Figure 3.9 the reaction forces in the glenohumeral joint are plotted for an abduction movement. One can see that these forces are almost similar for the models of cadaver R2 and R4. The model of cadaver R6 is very different at a 60 degrees elevation angle. For the other elevation angles, the forces are in the same order of magnitude as those of the models of cadaver R2 and R4.

3.4 Discussion and Conclusions

The main conclusion of this paper is that the Delft Shoulder Model is sensitive to parameter variations. This does not imply that the parameters of the shoulder model should be adapted to the individual subject for which we simulate the measured movements. Changing the parameters of the model can result in an unpredictable instability, as we saw with the model of cadaver R6 at a humeral abduction of 60 degrees.

Adapting the model to the measured movements can be necessary for specific situations. The kinematics of the model depend to a great extent on the parameter set that is used. For the parameter set of cadaver R4, the mean difference between the measured and the simulated rotations can be as much as 20 degrees. Such differences are too great to call the simulation results reliable. It will be interesting to perform further research on simulations with the shoulder model with measured input from different subjects.

It might be possible that for a specific subject, the model of cadaver R4 or R6 gives better simulation results than the model of cadaver R2. The main reason for this would be that this subject would be kinematically more compatible with this specific parameter set.

Before deciding to fine-tune, or to adapt the parameters of the model, one should think of the use of the model. Simulations in this study show large differences in muscle force, but only small differences in joint reaction force. As long as muscle force cannot be measured directly, it is not possible to improve muscle force predictions. Muscle activation patterns can be validated by means of EMG, so muscle activation patterns are an interesting result of model simulations for validation purposes.

Further research is to be done on the influence of the thorax model on the moment arms of the Serratus muscle, and on the kinematics of the shoulder model.

Based on the research of this paper, we conclude that:

- Different parameter sets show different simulation results on a kinematic and a dynamic level.
- The model of cadaver R2 shows the most consistent results on a kinematic and dynamic level.
- In certain configurations the shoulder model can produce results that are not con-

sistent with what is expected (R6 at 60 degrees humeral abduction).

- There are only small differences between the moment arms of the models based on the shoulders of different cadavers.
- When the same kinematic input is used for the model, large differences in rotations exist for different parameter sets.

Chapter 4:

Parameters for a musculoskeletal model of the human shoulder.

A comparison between an MRI and a dissection experiment.

Abstract. The increase in the possibilities of modern computers have led to an increase in the use of biomechanical computer models. Parameters for these models are obtained from dissection experiments or MRI data. Validation of these models is difficult because measuring muscle forces is impossible. This paper describes which parameters can be found, and how these parameters can be obtained from MRI data in order to build a biomechanical model of the human shoulder. The goal of this study is to investigate whether it is possible to adapt a generic model of the human shoulder to an individual subject using MRI data of that subject, in order to use an individualized shoulder model in medical practice. To this end, MRI images of a cadaver have been made, and the same cadaver has been used in a dissection experiment. This makes it possible to compare the parameters obtained from the MRI data with the parameters obtained using the dissection data. It was concluded that muscle contours cannot be extracted from MRI images without much human interaction. This makes this method not suitable for medical practice. Although MRI data is very suitable to obtain a limited set of geometric parameters necessary to build biomechanical models, it is not possible to build a complete biomechanical model exclusively on the basis of MRI data.

4.1 Introduction

The increase in the possibilities of modern computers has led to an increase in the use of biomechanical computer models. For the shoulder, the early models were used for analysing the possible movements [Pronk 1991a]. Later, inverse dynamics were added to calculate the necessary joint moments as a function of external moments and movements. These models were used to calculate the load on the human body as a result of an external load during specific tasks. These models could also calculate muscle forces by using an optimization criterion to provide load sharing between the different muscles in static and dynamic situations [Högfors 1987]; [Högfors 1991]; [Helm 1991a]; [Helm 1994a]; [Nieminen 1995]; [Niemi 1996]. The muscle forces are important because they restrict the maximal possible external load on the human body. They are also important because phenomena like fatigue and energy consumption take place in the muscles and the muscle forces are the main influencing factor on the joint reaction force. So quantitative data on muscle forces is necessary to analyse muscle functions, muscle load and joint reaction forces.

In building these models, a lot of information about the shoulder is needed. For the kinematics, the location and possible movements of the joints must be known.

For a dynamic analysis, the mass and inertia of the different moving parts should also be known. When muscles are included in the model, muscle moment arms must be known for all possible positions of the model, as well as muscle fibre direction and fibre type. For some joints with one degree of freedom, like the knee joint, a relation can be described between the muscle moment arm and the joint angle [Spoor 1992]. To joints with more degrees of freedom, this method is not applicable. Then, moment arms are calculated in the model: A muscle is modelled as one or more muscle lines of action between origo and insertion. For curved muscle lines, different modelling approaches are used. Best known are the centroid line method [Jensen 1975] and the bony contour method. The bony contour method defines a bony contour around which the muscle lines are wrapped around [Helm 1991a]. To calculate the load sharing between muscles, one must know the maximum possible muscle force for each muscle. This is usually a function of the cross-sectional area of the muscle. More sophisticated dynamic models use a special muscle model to include muscle dynamics [Happee 1994]; [Happee 1995].

To obtain all these data for the human shoulder, several cadaver studies have been executed [Högfors 1987]; [Veeger 1991a]; [Helm 1992]; [Klein Breteler 1997]; [Klein Breteler 1999]. Because these studies ask a lot of effort and skill, only a few good and complete data sets are available.

Nowadays, with the help of computer tomography techniques it is also possible to use non-invasive techniques to obtain information from the inner body. The advantages are great: It is possible to obtain the data from a living human being in different postures. The problem of comparing cadavers from an elderly population with young healthy subjects is solved, and a complicated cadaver experiment is not necessary. The necessary images are freely available from the Visible Human project [NLM 1995], or they can be obtained using standard hospital equipment like MRI- and CT-scanners.

Different methods and techniques on obtaining the necessary information from these images have been described in the literature:

Spoor and van Leeuwen [Spoor 1992] compared moment arms of the knee muscles from MRI and from tendon travel. They concluded that the tendon travel method is more accurate than the technique using MRI, but MRI is the only admissible technique for *in vivo* measurements. Fukunaga et al. [Fukunaga 1992] calculated the cross-sectional area of human leg muscles using MRI. They concluded that MRI can be used to determine muscle volumes. These volumes are used to calculate the Physiological Cross-Sectional Area (PCSA), defined as the product of the muscle volume and the cosine of the angle of pennation divided by the mean fibre length. For this, the pennation angle and the fibre length on individual muscles were obtained from cadaver studies. In the same study it was concluded that the Anatomical Cross Sectional Area (ACSA), defined as the area of the cross section taken perpendicular to the length axis of the muscle, cannot be used to calculate the

maximum possible muscle force. Koolstra et al. [Koolstra 1989]; [Koolstra 1990]; [Koolstra 1992] have published a method to calculate muscle lines of action of human masticatory muscles reconstructed from MRI images. They concluded that the critical factor in the process they used was the reliability with which the outlines of the muscles could be traced from the images. They were able to estimate the orientation of masticatory muscle lines of action with an average reproducibility of about five degrees.

From literature we see that different methods have been used to obtain parameters from tomographic images. To build a complete biomechanical model of the human shoulder, we need the following geometrical parameters:

- Location of bony landmarks.
- Location and shape of bony contours.
- Location of joint rotation centres.
- Location and shape of muscle attachments.
- Muscle volume.
- Muscle architecture (muscle fibre direction).
- Muscle optimum length.
- Muscle dynamic parameters such as the force length relation and force velocity relation.

Until now, the muscle architecture, like pennation of muscle fibres and muscle fibre direction could not be obtained from MRI images. Optimum muscle length and dynamic parameters cannot be obtained from MRI images. Earlier research on this topic showed that the Delft Shoulder Model is not very sensitive to these variables [Westen 1993].

It was not possible to obtain the muscle moment arms of the shoulder directly from the MRI images. The 3-D structure and the complexity of the shoulder makes it necessary to build a 3-D reconstruction of the muscles and the bones so the necessary parameters can be extracted from this 3-D reconstruction. The purpose of this paper is to investigate the possibilities to extract model parameters *in vivo* from MRI images in order to build individualized models of the human shoulder.

Questions to be answered are:

- What parameters can be extracted?
- How accurately can these parameters be extracted?
- How much effort does it take to extract these parameters?
- Can data from an MRI experiment be validated by comparing them with data from a dissection experiment?
- Is it possible to build individualized models of the human shoulder by obtaining model parameters from MRI data for each subject for whom the model is used?

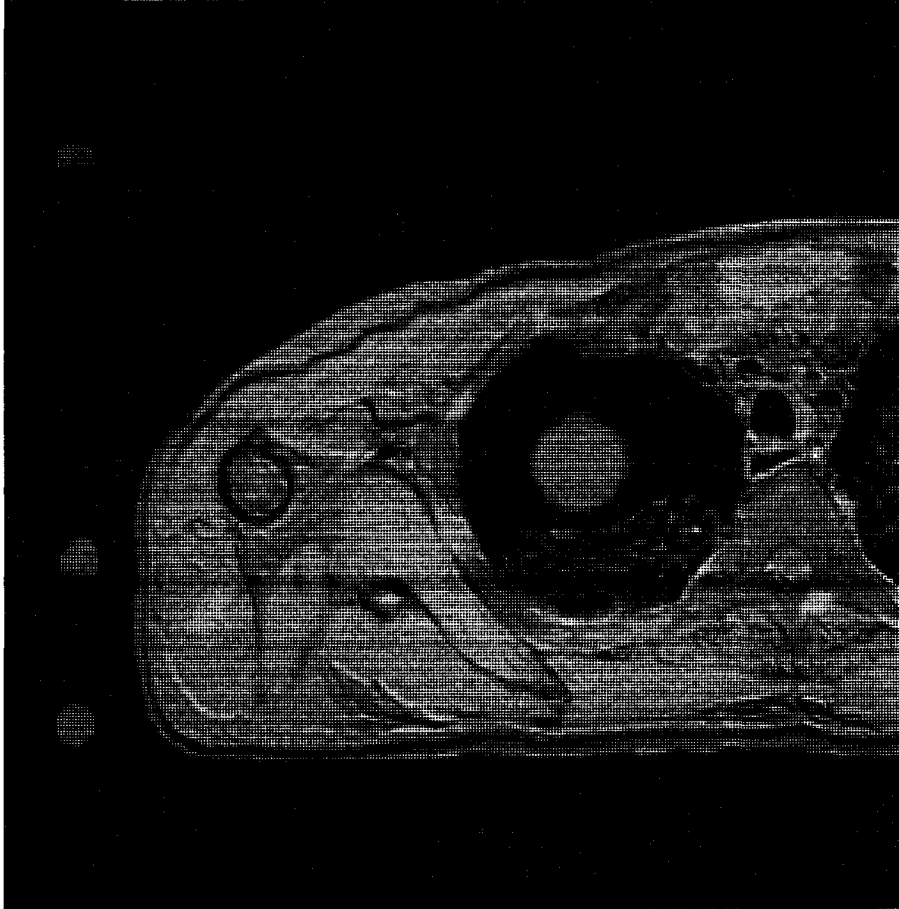


Figure 4.1: A typical example of the applied MRI images: A transverse cross section of the cadaver. The three dots on the left side are a cross-section of the frame used for calibration and test purposes. The large dot inside the lung is a cross section of a ping-pong ball, used for calibration and test purposes.

To answer these questions, MRI images of an embalmed cadaver were made. The same cadaver was subsequently used in a dissection experiment. This makes it possible to validate the results of the MRI experiment using the data from the dissection experiment.

4.2 Method

MRI images were made of the embalmed upper body of a 57 year old man for which Philips Gyroscan T5 with a magnetic field of 0.5 Tesla was used. The specimen was placed in the MRI scanner on a PVC plate. For reference, a water-filled frame and six water-filled spheres were scanned simultaneously. The field of view was 300 by 300 mm with 256 by 256 pixels in an image. The slice thickness was 5 mm with 0 mm space in between slices. In this study, images of the complete shoulder region were made in transverse, sagittal and frontal direction. This made it possible to compare results from images with different orientations.

After the MRI experiment the same specimen was used by another researcher in a dissection experiment [Klein Breteler 1997]; [Klein Breteler 1999]. In this experiment, the specimen was fixed in a stainless steel frame. In every segment of the skeleton, four or five screws were driven. These screws were used as reference points. Before the dissection started, the position of these screws, as well as the position of sixteen palpable bony structures were measured by means of the palpator [Pronk 1991b]. In the dissection experiment, location of joint rotation centres of the shoulder bones were measured together with the shape of the glenoid. The locations of origo and insertion of the muscles of the shoulder and upper arm were measured. The muscles were weighed and their length and fibre length were measured using a string and ruler.

The MRI images were processed on a computer. See Figure 4.1 for a typical example of the MRI images used. Using an interactive contour detection procedure [Kaptein 1996], the contours of the muscles, bones and reference objects were extracted from the images. In this procedure the contour drawn is instantaneously attached to the contours in the images instantaneously. This is done using a model-based contour detection algorithm based on dynamic programming techniques. This tool also facilitates the use of contour propagation through the different image slices. This procedure was used to speed up the contour extraction and to investigate the possibilities of using a complete model-based approach in which user interaction is reduced to a minimum. The problem with obtaining muscle contours from MRI images is that all the muscles have the same grey values. The only way in which two muscles can be distinguished is by detecting the very thin fascia and fat tissue that surrounds each muscle.

Because the purpose of this study is to investigate the possibilities of obtaining model parameters for a biomechanical model of the human shoulder from MRI images, not all muscles of the shoulder were processed. The processed data is presented in the following section.

4.3 Results

4.3.1 Reference measurements

To get an idea of the accuracy of the MRI scanner and the image-processing routines, six water-filled spheres and a water filled-frame were scanned simultaneously with the cadaver.

The frame was placed next to the cadaver. It exists of two parallel tubes in line with the axes of the main MRI tube. These tubes are 183.9 millimetres apart and connected by three tubes at a 29.6 degree angle with the main tubes. The inside diameter of all these tubes is 13.5 mm.

Estimating a cylinder through the contours of the frame tubes extracted from the MRI data makes it possible to compare the distance between these tubes from the MRI data with the measured distance. For all MRI data sets, this distance was 185.3 millimetres, so the relative error for this distance is less than one percent. The relative error in the estimated cylinder diameter is less than three percent.

The spheres placed at different locations around the cadaver had an inside radius of 18.5 millimetre. A ball was estimated through the contours extracted from the MRI images. For most spheres and MRI data sets, the radius could be estimated within 0.1 millimetre from the measured radius. Only for the sphere placed closely to the wall of the MRI tube the radius was estimated to be between 18.8 and 19.0 millimetre. For the spheres that showed in MRI data sets with different orientations, also the estimated location of the centre could be compared. This resulted in a difference between the different MRI data sets of one millimetre in horizontal and vertical direction. In the longitudinal direction of the MRI tube, the difference is two millimetres.

Different MRI data sets were made because the cadaver was too large for one scan. Because of this, the cadaver was shifted in between the different scans using the calibrated sliding table of the scanner. The MRI images of these different data sets should be exactly aligned with each other, but a 3-D reconstruction of the frame showed a shift between the images of the two MRI data sets. Template matching between two images of the sets that should be aligned showed a shift over 2 pixels horizontally and 1 pixel vertically. This is a shift of 2.4 millimetres. For the other data sets, only one other horizontal shift was found, of one pixel. From these reference measurements we can conclude that the MRI imaging and contour extraction process is accurate enough for the purpose of estimating parameters for a biomechanical model of the shoulder. No corrections were done to account for these small shifts.

4.3.2 Coordinate systems

In relating external measurements to a biomechanical model it is important to use a well-defined coordinate system. For the shoulder, coordinate systems are defined for each bony structure. The global or main coordinate system is defined with respect to the thorax.

This thorax coordinate system is defined by four bony landmarks: Incisura Jugularis (IJ); Processus Xyphoideus (PX); the 7th Cervical vertebra (C7); and the 8th Thoracic vertebra (T8). These are almost the same as v/d Helm used in his work [Helm 1994b]; [Helm 1995]; [Helm 1997]. The origin of the system is located in the point IJ. The y-axis is defined parallel to the line from halfway between PX and T8 to halfway between IJ and C7 directed from caudal to cranial. The x-axis is perpendicular to the mid-sagittal plane through the points IJ, C7 and halfway between PX and T8 directed from the left to the right shoulder. The z-axis is perpendicular to the y- and x-axis, directed from front to back. In Figure 4.2 a schematic picture is given of the coordinate system and the different points used in the shoulder model. See appendix A for a more detailed description of the coordinate system that was used.

In the dissection experiment, landmarks like C7 and T8 are sometimes difficult to distinguish. This is not a big problem because these points only determine the direction of the coordinate system. The direction of the coordinate system only changes a little when for example T9 is palpated instead of T8.

In the MRI images, the coordinates of all bony landmarks were pointed out directly. Coordinates in this paper are defined in millimetres with respect to the thorax coordinate system as defined in this paragraph, unless stated differently.

4.3.3 Skeletal points

Skeletal points like joint rotation centres and bony landmarks are very important because they determine the kinematics of the shoulder mechanism. In the dissection experiment, these parameters are derived from measuring the articular surface of the dissected bones directly. We used the contours of the bones to estimate these parameters from MRI images. Using cutting planes, we separated relevant areas of these contours from the rest of the points. These cutting planes are defined by hand for which the MRI image and a 3-D reconstruction of the model is used. The separated points were used for estimation of the model parameters. [Lelieveldt 1994]

The sterno-clavicular joint (SC-J) was estimated by calculating the mean of the points at the clavicular joint surface. The clavicular joint surface was separated from the clavicle contours by means of a cutting plane. The acromio-clavicular joint (AC-J) was estimated fully automatically. This was done by taking the points of the clavicle that were less than 10 millimetre from the scapula and vice versa. The mean of these points on the clavicle and the scapula was used to define the AC-joint. The glenohumeral joint (GH-J) parameters were obtained by separating the glenoid

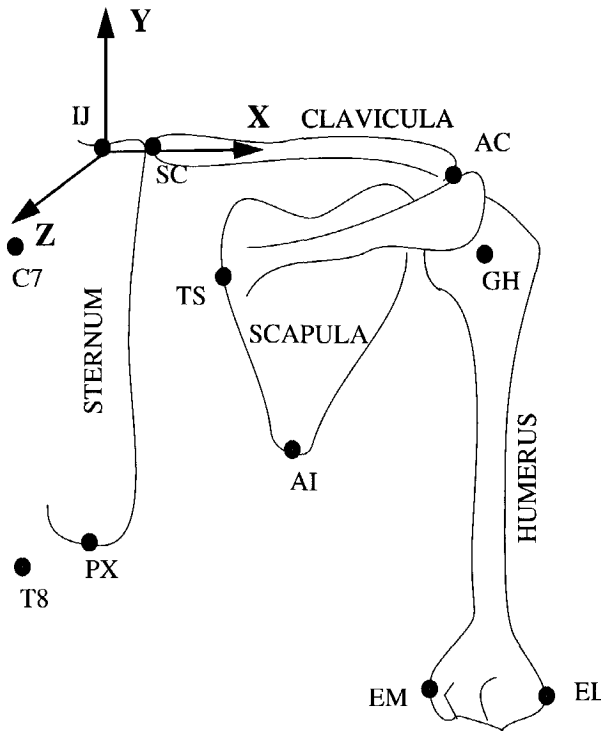


Figure 4.2: Dorsal view of the shoulder girdle.

Thorax coordinate system with location of joint rotation centres and bony landmarks.

Origin: Incisura Jugularis;
X-axis: left to right;
Y-axis: caudal to cranial;
Z-axis: ventral to dorsal.

IJ Incisura Jugularis
PX Processus Xiphoideus
C7 7th cervical vertebra
T8 8th thoracic vertebra
SC sterno-clavicular joint
AC acromio-clavicular joint
GH gleno-humeral joint
EM epicondile medialis
EL epicondile lateralis
TS trigonum spinae
AI angulus inferior

points from the contours of the humerus using two cutting planes. One of these cutting planes was in the transverse direction to separate the head of the humerus from the rest of the humerus. The second cutting plane was in the sagittal direction to separate the glenoid from the rest of the humeral head. Through these humeral head points, a ball was fitted. The centre of this ball is defined to as the GH-Joint.

A number of bony landmarks necessary for defining local coordinate systems was pointed out directly in the MRI images.

4.3.4 Comparing points from the MRI experiment with points from the dissection experiment.

If we compare the point locations obtained from the MRI experiment with point locations from the dissections, we encounter some difficulties caused by the fact that in between the MRI experiment and the dissection experiment the cadaver had to be moved. As a result of this handling, joints have rotated a bit, which makes a direct comparison of the coordinates impossible. For this reason, we compared the distances between the points on the same bone. This was done by calculating the error between DM_{mri} ; the distance matrix of the points from the MRI data and DM_{diss} ; the distance matrix of the points from the dissection experiment. A distance matrix contains the distances from all points to all other points in the system.

Table 4.1 E_{diff} Difference between the distance matrix from MRI locations and the distance matrix from dissection locations in millimeters. The locations within the bold lines are on the same bone, so there the difference between MRI and dissection data should be small.

	Thorax			Clavicle			Scapula			Humerus		
	IJ	PX	C7	T8	SC-J	AC	AC-J	AI	TS	GH-J	EL	EM
IJ	0.0	74.3	13.5	-49.6	0.4	-10.9	-4.3	-25.2	-4.4	-3.3	-23.2	-32.3
PX	74.3	0.0	65.1	23.4	71.8	66.0	69.6	17.0	66.8	62.3	-36.3	-51.6
C7	13.5	65.1	0.0	-82.9	12.0	-8.4	-3.4	-39.3	-32.5	1.6	-42.5	-48.2
T8	-49.6	23.4	-82.9	0.0	-48.7	-29.8	-26.7	-5.3	-33.3	-10.5	15.9	20.3
SC-J	0.4	71.8	12.0	-48.7	0.0	-8.0	-1.8	-25.7	-2.1	-1.9	-24.9	-33.4
AC	-10.9	66.0	-8.4	-29.8	-8.0	0.0	-1.9	-0.8	-3.1	9.1	1.7	-3.1
AC-J	-4.3	69.6	-3.4	-26.7	-1.8	-1.9	0.0	-1.0	0.3	6.9	-1.6	-5.1
AI	-25.2	17.0	-39.3	-5.3	-25.7	-0.8	-1.0	0.0	3.4	6.4	-16.3	-14.7
TS	-4.4	66.8	-32.5	-33.3	-2.1	-3.1	0.3	3.4	0.0	13.3	-9.0	-9.2
GH-J	-3.3	62.3	1.6	-10.5	-1.9	9.1	6.9	6.4	13.3	0.0	-1.9	-2.7
EL	-23.2	-36.3	-42.5	15.9	-24.9	1.7	-1.6	-16.3	-9.0	-1.9	0.0	-2.4
EM	-32.3	-51.6	-48.2	20.3	-33.4	-3.1	-5.1	-14.7	-9.2	-2.7	-2.4	0.0

Table 4.1 gives the difference between the two distance matrices E_{diff} in millimetres.

$$E_{diff} = DM_{mri} - DM_{diss} \quad (4.1)$$

Positive values in this matrix mean that the distance between the two points in the MRI data set is larger than the difference in the dissection data set. The points in the boxes in bold type do not suffer from changes in position of the cadaver between the MRI and dissectioning experiment because they are on the same bone. From this table we can conclude that the correspondence between the MRI and dissection data of the points on the clavicle, scapula and humerus is good. However, the differences

between the thorax points are large. The cause for this is that in the dissection experiment, PX could not be reached by the palpator. Instead of this point, another point on the sternum was measured. Also C7 and T8 could not be measured well because fat tissue underneath the skin made good palpation impossible. In the MRI images, it was very difficult to identify the vertebrae C7 and T8.

The coordinates of the points in the thorax coordinate system are shown in Table 4.2. A comparison between these data and the data from Table 4.1 shows that the bones must have moved with respect to each other between the MRI and the dissection experiment. This was to be expected because in the MRI experiment the cadaver was lying on its back, whereas in the dissection experiment, the cadaver was fixed in an upright position. Part of the differences between the points in this table are caused by the fact that the thorax coordinate system is defined by means of the measured points. Differences in these points between the MRI and the dissection experiment cause differences in coordinate systems. From the nature of the differences, we see that the arm moved about 40 millimetres in y-direction downwards, which is in agreement with what is to be expected when rotating the cadaver from a lying to a upright position.

4.3.5 Bony contours

The procedure to estimate the GH-Joint was also used to fit a sphere through the Tuberculum Majus and Tuberculum Minus points. This sphere and the sphere fitted through points of the GH-joint are used as bony contours for muscles that pass the gleno-humeral joint.

Part of the humerus shaft is modelled as a cylinder. This cylinder is used as a bony contour for the Teres Major. The cylinder was fitted through points separated from the humerus contours for which three cutting planes were used.

Part of the thorax is modelled as an ellipsoid. This ellipsoid model has two functions in the shoulder model: It is used as a bony contour for the Serratus Anterior, and it is used for the Scapulothoracic Gliding Plane. For fitting the ellipsoid, we localized by hand points on the outside of the ribs of the thorax; semi-automatic contour detection of the outside of the thoracic cage was impossible. Points on the front, side and back of the thorax were used to fit the ellipsoid. The x-coordinate of the centre of this ellipsoid is zero by definition, so the ellipsoid is symmetric with respect to the midsagittal plane of the human body. The axes of the ellipsoid are aligned with the thorax coordinate system.

4.3.6 Bony contours: MRI vs dissection.

A comparison of the bony contours of the MRI experiment with the bony contours obtained from the dissection experiments involves the same problems as stated in Paragraph 4.3.4.

In Table 4.3, the parameters of the balls fitted through the head of the humerus

Table 4.2 Coordinates of skeletal points in the thorax coordinate system. Comparison between points obtained from MRI-data and points obtained from dissection data. The distance between the points is shown in the dist column in millimeters.

	x-mri	y-mri	z-mri	dist	x-diss	y-diss	z-diss
IJ	0.0	0.0	0.0	0.0	0.0	0.0	0.0
PX	-1.7	-210.2	-20.4	78.7	-9.8	-132.7	-31.9
C7	0.0	54.4	138.7	14.5	0.0	54.1	124.2
T8	1.7	-89.3	159.0	82.6	9.8	-171.5	156.1
SC-J	21.1	-6.9	12.8	1.6	20.3	-8.2	12.4
AC	145.7	67.5	58.2	47.1	165.0	26.6	71.4
AC-J	146.2	59.6	60.6	42.0	157.0	20.3	70.8
AI	98.7	-85.1	152.5	42.5	102.5	-127.3	155.7
TS	67.5	33.6	151.0	45.6	74.9	-11.2	155.8
GH-J	171.9	20.5	50.4	41.1	170.8	-17.9	65.0
EL	217.8	-253.1	119.7	69.2	215.5	-302.2	71.0
EM	154.4	-255.6	136.9	60.6	156.9	-307.3	105.4

are compared with the corresponding parameters from the dissection experiment. This table also shows the 40 millimetre difference in the y-direction that we saw in the previous paragraphs. It shows that for the ball fitted through the GH-joint the difference in radius is very small. For the ball fitted through the Tuberculi, the difference is larger. The most probable cause for this is the fact that a sphere is not an exact approximation of the Tuberculi. This makes the results very sensitive to the part of the humeral head used for fitting this ball.

In Table 4.4 the parameters of the cylinder fitted through the humeral shaft are compared with the parameters obtained from the dissection experiment. The differences in the z-position for the parameters from the dissection experiment are not in agreement with the parameters of the GH-joint from the dissection experiment.

Table 4.3 Parameters of the spheres used as bony contours for the humeral head. Comparison between MRI data and dissection data in millimeters.

	center-x	center-y	center-z	radius
GH-J (MRI)	171.9	20.5	50.4	23.3
GH-J (diss)	170.8	-17.9	65.0	24.4
GH-Tub (MRI)	170.0	22.2	54.1	24.9
GH-Tub (diss)	171.8	-19.9	62.3	27.2

Table 4.4 Parameters of the cylinder used as bony contour for the humerus shaft. Comparison between MRI data and dissection data. x , y , z are the coordinates of the position vector of the central axis, (dx, dy, dz) is the normalized direction vector of the central axis of the cylinder in millimeters.

	x	y	z	dx	dy	dz	radius
Humerus (MRI)	162.0	0.0	55.4	-0.09	0.94	0.32	7.9
Humerus (diss)	156.3	0.0	-0.12	-0.00	0.92	-0.40	9.0

Table 4.5 Parameters of the ellipsoid used as bony contour for the thorax. Comparison between MRI data and dissection data. $A-x$, $A-y$, $A-z$ are the lengths of the axes of the ellipsoid in millimeters.

	center-x	center-y	center-z	A-x	A-y	A-z
Thorax (MRI)	0.0	-107.6	62.9	137.5	157.8	94.6
Thorax (diss)	0.0	-139.3	68.0	139.1	198.2	85.4

This is caused by an error in processing the data of the dissection experiment.

In Table 4.5 the parameters of the ellipsoid fitted through the thorax are compared with the parameters obtained from the dissection experiment. It shows that the largest difference is in the y -direction. This is the long axis of the ellipsoid, for which the fitting procedure is most sensitive. This sensitiveness is caused by the interaction between the y -coordinate of the center location of the ellipsoid ($center-y$) and the length of the ellipsoid axis in y -direction ($A-y$). Because the points through which the ellipsoid is estimated cover only a small part of the ellipsoid, $A-x$ and $A-y$ have

interaction with the center location. For the other directions, the differences are small, relative to the accuracy of the measurement methods.

4.3.7 Muscle attachments

The muscles are connected to the bones at the muscle attachment locations. These locations determine the muscle line of action and thus influence the muscle moment arm. In the dissection experiment, the optical centroids of the muscle attachments are measured on the bones by means of the palpator. In the MRI experiment, two methods were used to determine muscle attachment locations.

The first method uses the muscle and bone contours extracted from the MRI images. The points of the muscle contours with a small distance to the points of the bone contours were defined as muscle attachment points. For some muscles, like the Infraspinatus and the Subscapularis, as part of the muscle is adjacent to the bone without being attached to it, but this cannot be detected on the MRI images. To solve this problem, parts of the bones were marked to be areas where no muscles are attached. Using this method, we detected the muscle attachment areas on the scapula of the Teres Major, the Teres Minor, the Infraspinatus, and the Subscapularis.

The second method was used for muscles with a line-shaped muscle attachment site. For these muscles, the attachment locations could not be found by means of the first method, because the detected muscle contours were not well defined at these locations. The attachment locations of these muscles were marked on the MRI images by a human operator. Using this method, we modelled the muscle attachment lines on the humerus of the Teres Major, the Subscapularis, and the Teres Minor. For the clavicle and scapula, we used the same procedure to detect the attachments of the Deltoid muscle.

The muscle attachment points were used to define a point, line, or plane shaped muscle attachment model. This was done using the method described by Van der Helm [Helm 1991a]; [Helm 1992]. Because the muscle fibres cannot be detected in the MRI images, the muscle architecture cannot be individualized; in MRI images it is necessary to use a generic muscle architecture model for each muscle as obtained from the dissection experiment.

4.3.8 Muscle attachments: MRI vs dissection

We compared muscle attachments from the MRI experiment with muscle attachments from the dissection experiment by using local coordinate systems for each bone. In this way, the displacements of the bones as described in Paragraph 4.3.4 are accounted for. One must keep in mind that because these local coordinate systems are defined with respect to bony landmarks, the difference in the location of these landmarks between the MRI and the dissection data (Table 4.1) also applies to the difference for the muscle attachments.

In the dissection experiment we did not measure muscle attachment contours. For

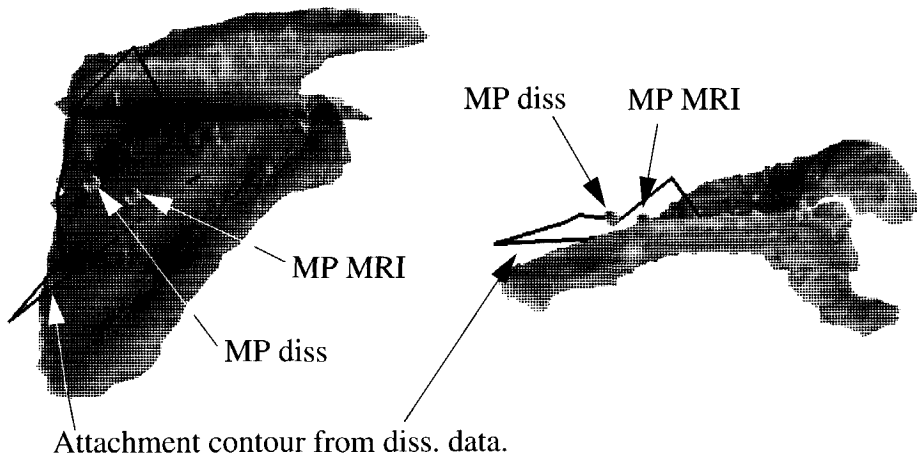


Figure 4.3: Muscle attachment contour of Infraspinatus Muscle. (Dorsal view and Caudal view). This visualisation shows that there is a great distance between the muscle attachment in the dissection data and the Scapula bone.

each muscle, we decided in how many parts it was to be divided; for each part, we measured the geometrical centre as the attachment of the muscle line of action [Klein Breteler 1997]. For this reason, it is not possible to compare the muscle contours directly.

For plane shaped muscle attachments, the middle (or Mean Point) of the muscle attachment contour from the MRI scans can be compared to that from the dissection experiment. We call this the Distance between Mean Points (DMP). A second value that can be compared is the mean distance from the points of the dissection experiment to the muscle attachment plane as defined by the MRI experiment. We call this MDP (Mean Distance to Plane). Results for the measured muscles can be found in Table 4.6. In this table, we see that for the Teres Major, Teres minor and Subscapularis the results are satisfactory. For the Infraspinatus muscle, both the DMP and the MDP are large. This may be caused by a measurement error or a data-processing error in the dissection experiment. Figure 4.3 shows the large distance between the muscle attachment contour of the Infraspinatus muscle and the Scapula.

For line-shaped muscle attachments we use three values to evaluate the difference between the data from the dissectioning experiment and those from the MRI experiment: 1) the mean distance from the dissectioning points to the muscle attachment line as defined by the MRI experiment; 2) the minimum distance from the dissectioning points to the muscle attachment line as defined by the MRI experiment; 3) the maximum distance from the dissection points to the line as defined by the MRI experiment. Results for the measured muscles are given in

Table 4.6 Results for plane-shaped muscle attachments on scapula bone calculated in local scapula coordinate system. *MDP* = Mean Distance from dissection points to Plane through MRI points. *DMP* = Distance from Mean of dissection Points to mean of MRI points. (mm)

	MDP (STD)	DMP
Origo Teres Major	5.0 (0.9)	5.8
Origo Teres Minor	1.9 (1.5)	4.0
Origo Infraspinatus	10.4 (8.1)	18.3
Origo Subscapularis	3.9 (3.1)	7.6

Table 4.7 Results for line-shaped muscle attachments calculated in local coordinate systems. *MD* = Mean Distance from dissection points to line through MRI points. *MinD* = Minimum Distance from dissection points to line through MRI points. *MaxD* = Maximum Distance from dissection points to line through MRI points. (mm)

	MD (STD)	MinD	MaxD
Insertion Teres Major	8.7 (1.8)	7.2	10.8
Insertion Teres Minor	9.3 (3.5)	7.3	13.2
Insertion Infraspinatus	23.4 (2.2)	21.2	26.1
Insertion Subscapularis	14.9 (3.8)	8.9	19.6
Origo Deltoid (Scapular part)	21.2 (15.4)	3.8	47.3
Origo Deltoid (Clavicular part)	7.6 (6.2)	3.0	16.8

Table 4.7. In this table, we see that for most muscles, the difference between the dissection data and the MRI data is great. We consider the data for Teres Minor and Teres Major to be satisfactory, but those for the Infraspinatus and Subscapularis are not within the expected accuracy. For the scapular- and clavicular- part of the Deltoid, We expect that the data for the scapular and clavicular part of the Deltoid from the MRI experiment are not correct because these muscle attachments are known to attach to the complete spine as the data from the dissectioning experiment shows.

4.3.9 Visual inspection of line shaped muscle attachments

By means of a 3-D reconstruction of the muscle contours and bone contours as defined in the MRI experiment, the MRI data can be visualized. On top of these 3-D models, the data from the dissection experiment can be projected. By means of these 3-D models, the difference between the MRI and the dissection experiment can be analysed in more detail.

Insertion Infraspinatus muscle.

The insertion of the infraspinatus muscle is on the great tuberosity of the humerus. A comparison of Figure 4.4 with anatomical information suggests that we measured the insertion too close to the glenoid in the dissection experiment. In the MRI experiment, the insertions seems to be located a little too low.

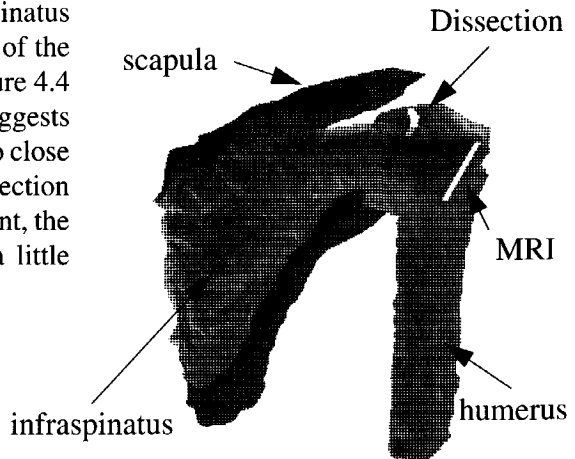


Figure 4.4: Insertion Infraspinatus muscle.

Insertion Subscapularis muscle.

The insertion of the Subscapularis muscle is on the lesser tuberosity and the front of the capsular ligament of the shoulder joint. A comparison of Figure 4.5 with anatomical information suggests that we measured the insertion too large and too close to the glenoid in the dissectioning experiment. In the MRI experiment, the insertion seems to be extended a bit too far to the lower side.



Figure 4.5: Insertion Subscapularis muscle.

Insertion Teres Major muscle.

The insertion of the Teres Major muscle is on the inner bicipital ridge of the humerus. A comparison of Figure 4.6 with anatomical information suggests that we measured in both the MRI and the dissection experiment the insertion at the right location. The insertion of the MRI experiment fits the 3-D reconstruction of the muscle better, but this is because both the insertion and the 3-D reconstruction come from the same data set.

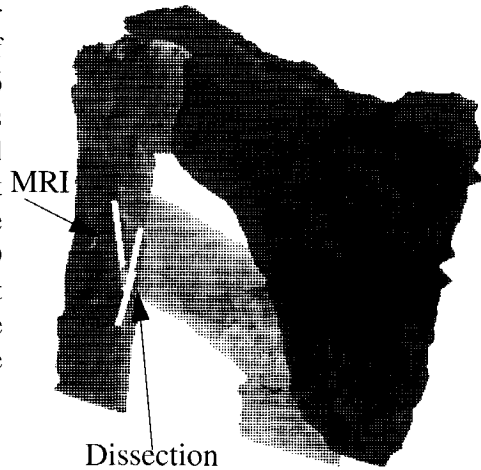


Figure 4.6: Insertion Teres Major muscle.

Insertion Teres Minor muscle.

The insertion of the Teres Minor muscle is on the lowest of the three impressions of the great tuberosity. A comparison of Figure 4.7 with anatomical information suggests that we measured the insertion of the Teres Minor Muscle in the MRI experiment a little too low, located more on the humeral shaft than on the humeral head. The 3D reconstruction of the muscle itself suggests that this is the right location.

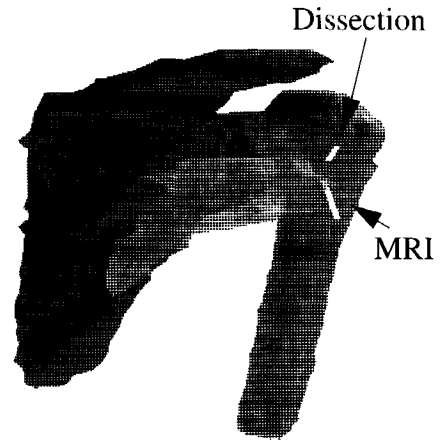


Figure 4.7: Insertion Teres Minor muscle.

Origo Deltoid muscle (anterior part).

The origo of the anterior part of the Deltoid muscle is on the upper side of the outer part of the clavicle. A comparison of Figure 4.9 with anatomical information suggests that in both the MRI experiment and the dissection experiment the origo of the Deltoid muscle is a little small. It should be extended further towards the distal end of the clavicle.

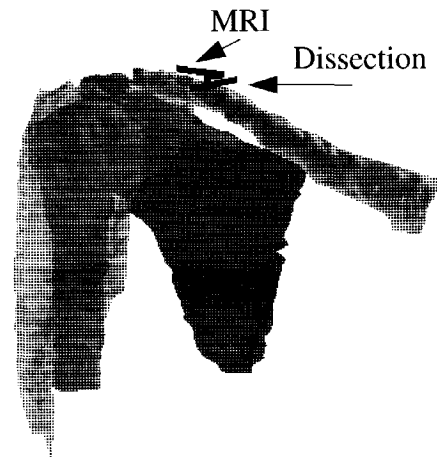


Figure 4.8: Origo Deltoid muscle (anterior part).

Origo Deltoid muscle (posterior part).

The origo of the posterior part of the Deltoid muscle is on the upper part of the acromion and the upper part of the spine. In the 3-D reconstruction a large part of the muscle itself lacks, so that the origo reconstructed from the MRI data is too short. The origo resulting from the dissection data conforms better to the anatomical information.

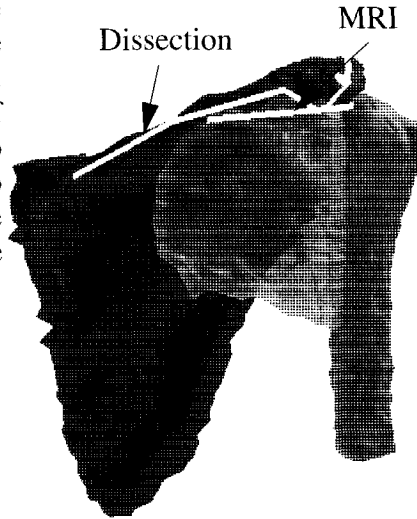


Figure 4.9: Origo Deltoid muscle (posterior part).

Inspection Infraspinatus muscle.

The insertion of the infraspinatus muscle is modelled as a line. In the MRI images on the right (Figure 4.10), the lowest and highest point of this line are marked. The top two images show these marks for the dissection data. The bottom two images show these marks for the MRI data.

In the images showing the points from the dissection data we can clearly see that the location of the infraspinatus muscle insertion is wrong. The insertion seems to be on top of the humerus head, on the position were the Supraspinatus muscle inserts.

The slice numbers also show the large difference between the dissection data and the MRI data. The slice numbers go from caudal to cranial with 5 mm space in between.

The images with the points from the MRI data show the right locations. Of course it is easier to validate this statement when looking at the 3-D MRI data set on a computer screen.

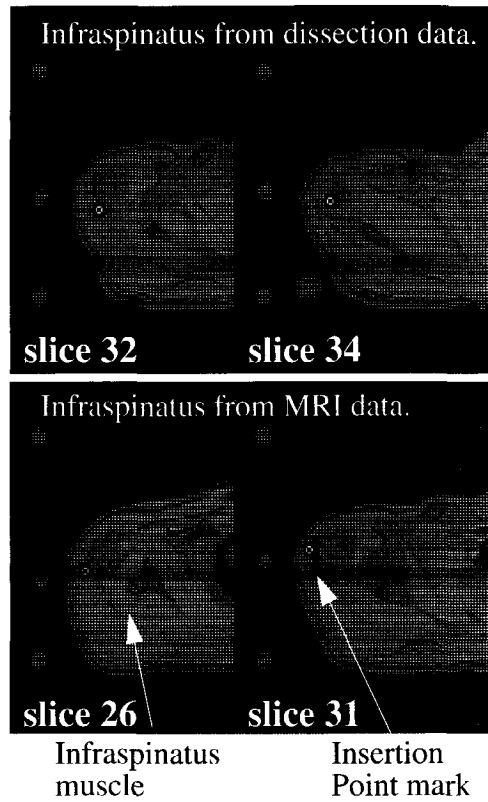


Figure 4.10: MRI images of Infraspinatus muscle. The slice thickness of this scan is 5 mm.

4.3.10 Muscle volume

Literature showed that obtaining the muscle cross-sectional area directly from MRI images does not give a good approximation of the Physiological Cross Sectional Area (PCSA) [Fukunaga 1992]. The best method to calculate the PCSA is to divide the muscle volume by the optimal muscle fibre length. [Fukunaga 1992]

To calculate the muscle volume, we multiplied the area of the muscle contours extracted from the MRI images by the slice thickness. For the dissection experiment, we separated and weighed the muscles. Assuming that the muscles have the same specific mass as water, we calculated the muscle volume. For the Teres Major, the Teres Minor, and the Infraspinatus, the results are presented in Table 4.8.

Table 4.8 Comparing muscle volumes calculated using MRI data with muscle volumes calculated using weighing of the dissected muscles.

Muscle	Volume MRI (cm ³)	Volume weighing (cm ³)
Teres Major	101.1	96.4
Teres Minor	34.4	29.8
Infraspinatus	112.1	113.0
Sphere	27.5	26.3 ^a

a. Calculated using the radius of the sphere (18.45 mm).

Seeing that the volume of the sphere is calculated very accurately, we can conclude that the applied method of calculating the volume of an object defined by extracted contours of an MRI image is very good. We also see that the difference between the muscle volume calculated using the two different methods is small. One must keep in mind that if MRI is used, the optimum fibre length cannot be measured. Thus for calculating the PCSA using MRI, one must use values from the literature for the optimum fibre length of each muscle.

4.3.11 Discussion

This paper showed a comparison between an MRI experiment and a dissection experiment for obtaining model parameters for a biomechanical model of the human shoulder. Unique is that for both these experiments the same cadaver was used, which makes validation of the method possible. Because in the MRI experiment not all muscles were processed, a complete comparison was not possible, but the results clearly show the possibilities and problems of these techniques.

The most important problem is the quality of the MRI images. Therefore to obtain images for the shoulder one must make images of a large part of the human body, the scan time is in the order of minutes. This results in many image distortions, as the subject has to be moved. A second problem is that it is not possible to make a complete data set in one scan. Moving the subject in between scans changes its posture a little bit. Also the natural movement of the subject as a result of the heart beat and the blood flow results in image distortions. Together with the problem of distinguishing the different muscles by detecting the very thin muscle fascia these problems make it very difficult to distinguish the muscles of the shoulder. In the experiment described in this paper, these problems were partly avoided by using a cadaver and by applying user interaction to segment the images. In future situations where MRI images of patients are used these problems cannot be avoided however.

It is difficult to compare the parameters obtained from MRI images with the parameters obtained from the dissection experiment because the cadaver was moved in between these experiments. Markers visible in both data sets were not available. For future experiments like this, we strongly advise the use of nonmetal markers in all the bones of the cadaver. However, the use of bony landmarks made it possible to compare the data sets. Most of the bony landmarks could be compared and the difference between both data sets was less than 5 millimetres. Only the bony landmarks on the thorax could not be reproduced. The reason for this is that these landmarks could not be detected well in the MRI nor in the dissection experiment. Because often these landmarks cannot be detected, the thorax coordinate system is defined in such a way that errors in the location of these landmarks result in small differences in the thorax coordinate system.

The location of bony landmarks, bony contours and joint rotation centres can be detected very well by means of MRI image data. The locations of the SC joint and AC joint were detected within a 2 millimetre difference. For the GH joint, this difference is a bit larger. The location of bony landmarks can be measured with the same accuracy as the locations of joint rotation centres. Also bony contours like the ball fitted through the head of the humerus and the ellipsoid fitted through the thorax points can be measured accurately when MRI data are used.

Muscle attachment locations are more difficult to obtain from MRI data because one cannot handle the muscles directly. A comparison between the MRI data and the dissection data reveals errors of 8 to 21 millimetres. The most important cause for these errors is the interpretation of the human operator who identifies the muscle attachment. The largest differences are caused by errors in the dissection experiment. For example the images showing the insertion of the infraspinatus muscle show that this insertion has been pinpointed at the wrong location.

Estimating muscle volume by means of MRI images is very well possible. Comparing the results with data obtained from weighing the dissected muscles shows a relatively small difference of 1 to 14 percent. Such differences are presumably caused by errors in the contour detection.

In general we can conclude that MRI images are very suitable for obtaining model parameters for a model of the shoulder. The advantages are that one does not have to destruct the subject during the experiment, so that it is always possible to reproduce the measurements and the data afterwards. Also the experiment is cheaper and faster than a dissection experiment and does not need a cadaver. Human interaction is needed for performing an MRI experiment. The human operator acquires anatomical knowledge of the human body to add the structures that are not visible in the MRI images.

The main disadvantage of using MRI images is that interaction with the data, like pulling muscles to find attachment sites, is not possible. The current quality of the MRI images requires a lot of user interaction to segment the MRI images. The

direction of muscle fibre cannot be detected in MRI images. In the dissection experiment described in this paper, muscle fibre length was measured for each muscle part. Because the muscle attachments and muscle architecture cannot easily be extracted from MRI images, transformation of a generic shoulder model as described by Kaptein (chapter 6 of this thesis) is more suitable for the daily practice in a medical environment.

4.3.12 Conclusions

- Using MRI, one can usually extract the same parameters as from a dissection experiment. Only muscle architecture (fibre direction) cannot be detected with MRI.
- The accuracy of MRI depends on the quality of the images. It is difficult to find the exact muscle attachment locations of some muscles, but most geometric parameters can be detected within an accuracy of five millimetres.
- Because automatic segmentation is not possible in MRI, parameter extraction from MRI images must be done by a human operator who has knowledge about the human body. In comparison with a dissection experiment, using MRI images is much less time consuming. With the right tools and enough practice, extracting a limited set of parameters from MRI images takes only a number of days. A dissection experiment takes a number of months.
- The chance that MRI data contain errors is smaller than that data from a dissection experiment are erroneous, because the circumstances for MRI data processing are better. Also it is possible to check parameters from MRI data afterwards because the source of the data is still available. The accuracy of dissection data, especially for muscle attachments and muscle architecture is much better.
- It is not possible to build individualized models of the human shoulder on a routine basis by obtaining parameters from MRI images because obtaining the parameters takes too much time.

Chapter 5:

Estimating muscle attachment contours by transforming geometrical bone models.

Abstract. For individualization of a biomechanical model, it is necessary to estimate the muscle attachments of the person to whom it is to be adapted. One of the methods to estimate muscle attachments is to use model transformations to transform a model with known muscle attachments to the bones of a person. We hypothesize that the location and shape of muscle attachment sites correlate with the shape of the bones they are attached to. If this hypothesis holds, it is possible to predict the location of muscle attachments when the shape of the bones is known. To validate this hypothesis, geometric models of three sets of shoulder bones were built. These models consist of 3-D surface models of the scapula, clavicle, and humerus, with the muscle attachment contours connected to them. By means of geometric transformations, the models were transformed, so the muscle attachments of the different data sets could be compared. Using these techniques, fifty percent of the muscle attachment contours could be predicted with high accuracy. The muscle attachment contours that could not be predicted were all influenced by measurement errors. For thirty percent of the muscle attachment contours it was not possible to distinguish the interindividual differences from the inaccuracies of the method used. From this study, we concluded that most muscle attachment contours can be predicted by means of geometric models of the bones.

5.1 Introduction

In biomechanical research, models are used, among others, to simulate the movements of parts of the human body. For the shoulder, this started with complete shoulder specimens, where part of the muscles replaced were by threads [Fick 1877]; [Mollier 1899]. These techniques are still used [Wuelker 1995], but more and more computer models become available [Högfors 1987]; [Högfors 1991]; [Karlsson 1992]; [Helm 1994a]; [Niemi 1996]; [Maurel 1998]. These computer models are often based on cadaver measurements [Högfors 1987]; [Veeger 1991a]; [Helm 1991a]; [Karlsson 1992]; [Klein Breteler 1997]. Medical imaging techniques, such as CT and MR imaging, supply data that can be used for biomechanical models [Koolstra 1992]; [Kalra 1995]. In 1995 data from The Visible Human Project became available, providing a large and detailed data set used by a large group of researchers [NLM 1995]. A biomechanical shoulder model was made based on these data [Maurel 1998]. Questions that can be asked for all these methods of obtaining data are: What is the quality and the reproducibility of these measurements? Is it justifiable to use specific models, based on data of only one subject, in a general manner?

In our laboratory, a biomechanical model of the human shoulder has been developed [Helm 1994a]. This model, also known as the Dutch Shoulder Model, is based on the measurements of one out of a group of seven cadavers [Helm 1992]. In the dissection experiment fourteen shoulders were dissected, and only one set was used to build the biomechanical shoulder model. The data from the other shoulders were stored for later use.

This shoulder model is used to analyse the kinematic [Pronk 1991a] and dynamic behaviour of the shoulder in order to improve the diagnosis, treatment, and prevention of shoulder disorders [Helm 1994b]. The model needs the positions and orientations of the shoulder bones as input, as well as the external forces. Using an optimization scheme, the model predicts the muscle forces for the different muscles.

Quantitative validation of the Dutch Shoulder Model is very difficult: Measuring muscle forces *in vivo* is not possible. Moreover the relation between EMG and muscle force is only partly known [Niemi 1996]; [Groot 1998b]. From qualitative validation of the model by means of EMG, it was concluded that the model can predict muscle activities for a number of situations; kinematic and dynamic situations [Helm 1994b]; timing of muscle activities during fast goal-directed arm movements [Happee 1995]; wheelchair propulsion [Helm 1996]; principal actions [Groot 1998b].

In chapter 3, we showed that the Dutch Shoulder Model should be adapted to the individual subject. Especially adaptation of the kinematic parameters is very important. To get a better agreement between the simulation results of the model and the measured data of a specific person, we must base the model on the geometry of that specific person. As shown in chapter 2 of this thesis, obtaining geometric model parameters for a specific person can be done using medical images. The problem is that it is not possible to determine the muscle architecture by means of MRI, and that the whole process from MRI to model parameters is very complicated and time consuming. In this paper, we propose a method of obtaining muscle attachment contours by transforming geometric surface models of the bones and muscle attachments of a generic shoulder model to geometric surface models of the bones of a specific person.

The specific bone models are obtained from MR images or CT images. They are transformed by means of rotation, scaling, and translation as well as by deformation. Because the muscle attachment contours of the specific shoulder model are transformed together with the surface model of the bone, adapted muscle attachment contours result from transformation. If this method works for muscle attachment contours, it can also be used for other geometrical model parameters, like joint rotation centres. The adapted shoulder model built by means of these transformed muscle attachment contours has the muscle architecture of the generic model and the geometry of the measured subject.

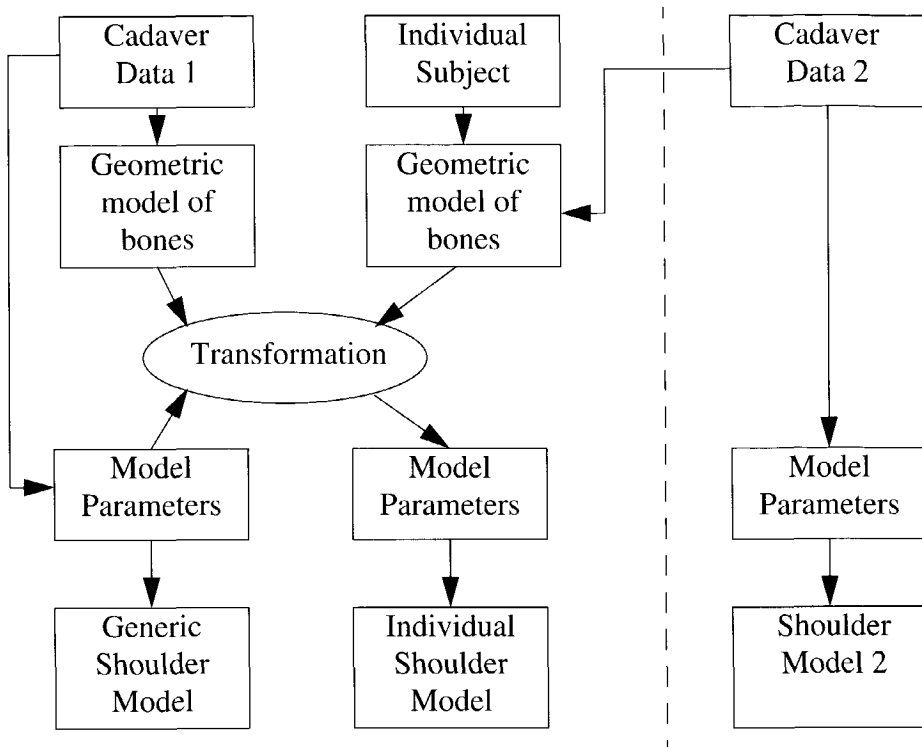


Figure 5.1: Schematic view of the method to individualize the Dutch Shoulder Model using geometric models of the bones.

- The generic shoulder model is built from cadaver data 1.
- The individual shoulder model is built by transforming the model parameters of the generic shoulder model, by means of geometric data from the individual subject.
- To validate this method, a second cadaver is used to build a second shoulder model. This model can be compared with the individual shoulder model, built using the transformation method.

In this paper, the following questions are answered:

- Is it possible to predict the muscle attachment sites of a specific shoulder model using only the geometry of the bones of a specific subject?
- What is the quality of these predicted muscle attachments?

5.2 Methods

In Figure 5.1 the transformation process is explained; the generic shoulder model is based on model parameters from cadaver data 1. By means of a geometric model of the bones of cadaver data 1 and a geometric model of the bones of an individual subject, the model parameters are transformed into the subject. From these model parameters, an individualized shoulder model is built.

To validate this method, we used data of three cadavers. From these data, geometrical models of the bones are built, and their muscle attachments and other model parameters are measured. One of these data sets is used for the generic shoulder model. The other two are used to build an individual shoulder model for validation of the proposed method. After transformation of the bone models, the transformed muscle attachments and other model parameters can be compared with the original model, to validate whether it is defensible to obtain parameters through transformation.

5.2.1 Model parameters from a cadaver experiment.

In the past, a cadaver study involving seven cadavers was performed to acquire data for inertia, geometry and muscle contraction parameters [Helm 1992]. This study resulted among others in muscle attachment contours measured on the shoulder bones of the cadavers with respect to a local coordinate system defined by five metal markers. The markers used for this experiment were Pozidriv screws (2.5 x 12 mm). They were necessary to define local coordinate systems for each bone with respect to a global coordinate system for the whole body. All data were described with respect to coordinate systems defined by bony landmarks. During the cadaver experiment the locations of these screws were measured using a 3-D spatializer called the Palpator [Pronk 1991b]. The palpator was estimated to have a standard deviation of 0.96 mm per coordinate or 1.43 mm in absolute distance [Pronk 1991b]. For the study of Veeger and Van Der Helm, seven cadavers were used [Veeger 1991a]. From this large data set, the data on one cadaver was used to build the generic shoulder model [Helm 1994a]. For the experiment described in this paper, we also used the data from two other cadavers. From now on, we call these cadavers R2 (the generic shoulder model), R4 and R6, which refers to the original publication [Veeger 1991a].

5.2.2 Geometric bone models

After the cadaver dissection experiment of Veeger and Van der Helm, the bones of these cadavers were dried, fixated and stored for later use. For this research, CT images of these bones (humerus, clavicle and shoulder blade) were made at Leiden University Medical Centre by means of a Philips CT scanner. The resulting CT images consist of about 120 image slices of 512 x 512 voxels. The dimension of one

Figure 5.2: CT-image of a left and right shoulder blade and a left and right clavicle. In both the shoulder blades and in the top clavicle, a metal screw can be seen.

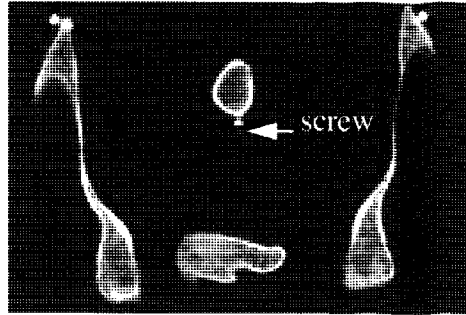
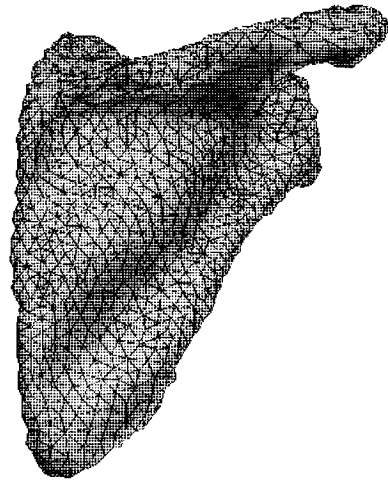


Figure 5.3: 3-D reconstruction of the right shoulder blade of cadaver R2. This model consists of 1717 nodes connected by 3430 triangular patches.



voxel is $0.54 \times 0.54 \times 3.0$ mm. See Figure 5.2 for a typical example of a CT image. With the help of a semi-automatic contour detection method, contours of these bones were extracted [Kaptein 1996]. Between these contours, triangular elements were defined to form a surface model using the techniques described by Boissonnat [Boissonnat 1988]. A typical surface model of a humerus or scapula consists of about 1700 points, connected by 3300 triangular surface patches (Figure 5.3). A typical surface model of a clavicle consists of about 500 points, connected by 1000 triangular surface patches.

5.2.3 Mapping of palpated data to the bone models

To find a mapping between the surface models obtained from the CT images and the muscle attachment contours and other model parameters obtained from the dissection experiment, we used the screws as reference markers. With the help of a mouse, the locations of these screws were pointed out in the CT images and displayed on a computer screen. The difficulty in this procedure is estimating the location of the head of the screws while the slice distance of the CT-images is 3 mm

Table 5.1 Error matrix M_{ERROR} for the humerus of cadaver R2. (mm)

	S 1	S 2	S 3	S 4	S 5	S 6
S 1	0.0	-12.1	-12.3	-4.7	4.7	-6.0
S 2	-12.1	0.0	2.2	2.3	8.4	-1.3
S 3	-12.3	2.2	0.0	0.3	6.6	-3.3
S 4	-4.7	2.3	0.3	0.0	6.4	-3.6
S 5	4.7	8.4	6.6	6.4	0.0	-1.2
S 6	-6.0	-1.3	-3.3	-3.6	-1.2	0.0

(Figure 5.2). We calculated a distance matrix DM_{CT} , containing the distances between the screw locations from the CT images with respect to each other. For the screw locations obtained by means of a 3-D spatializer a distance matrix DM_{SP} was defined. With both distance matrices, the screw locations from the CT images were mapped to their corresponding screws from the spatial data. The subtraction of the CT distance matrix from the spatial distance matrix results in the error matrix:

$$M_{ERROR} = DM_{CT} - DM_{SP} \quad (5.1)$$

A typical example of such an error matrix is given in Table 5.1. Because the values in the first and fifth row (or column) of the error matrix are larger than the mean of the values, we can conclude that screw S1 and screw S5 are wrongly detected. Possible causes of these erroneously detected screws can be that the screws have changed position during the years (they have been removed once for another experiment) or that there has been a mistake in the spatializing or CT image pointing process. The error for the other screws is relatively small compared to the 3 millimetres slice thickness of the CT images. By means of the screw locations of screws S2, S3, S4 and S6, a transformation (rotation and translation) is defined by means of techniques described by Spoor and Veldpaus [Spoor 1980]. The residual error between the screw locations from spatial data and CT images is shown in Table 5.2. From this table, we can conclude that the screws are very suitable for finding a transformation between spatial data and CT images.

Table 5.2 Residual error (and standard deviation) between screw locations in spatial data and screw locations in CT data. (mm)

	Scapula	Clavicle	Humerus
R 2	1.1 (0.4)	2.5 (1.5)	2.8 (1.9)
R 4	1.1 (0.7)	0.5 (0.2)	2.6 (0.3)
R 6	2.4 (0.8)	2.7 (1.1)	3.6 (0.7)

5.2.4 Transformation of the bone models

We now have three different data sets consisting of geometric bone models with their corresponding digitized muscle attachment contours. Transformation of these models is done in two steps: First, a transformation is defined based on the inertia properties of the models. For this transformation only translation, rotation and scaling are used. Second, the surfaces of the models are transformed to each other, allowing local deformations of the models. This is done by defining a force field between the two surfaces and slowly deforming the model in an iterative manner [Kaptein 1996a]; [Kaptein 1996b]; [Redert 1998]. After transformation, the surfaces of the two bones are exactly mapped on each other in the sense that the points of one surface lie on the other surface and vice versa.

5.3 Results

After the transformation of the 3-D model of the bones, the measured muscle attachment contours should be located on the surface of these bones. By checking the distance between the mapped muscle attachment contours and their corresponding projection contours on the surface of the bone models, the accuracy of the measurements can be checked. We calculate for each muscle attachment contour the mean distance from the muscle attachment contour points to the surface of the corresponding bone surface. Results are displayed in Figure 5.4, from which we see that for most muscles, the distance between muscle attachment contours and the surface of the bone model is relatively small. The three measurements having a distance larger than twenty centimetres are the distances from the humerus bone to the insertion of the biceps muscle. This muscle is not inserted on the humerus bone, so this distance is supposed to be great. The two muscles with a distance between ten and fifteen millimetres are the origo of the Biceps Caput Breve of R2 and the origo of the Coracobrachialis of R2. These attachments have probably not been measured well. In appendix C, these distances are displayed separately for each muscle. If we

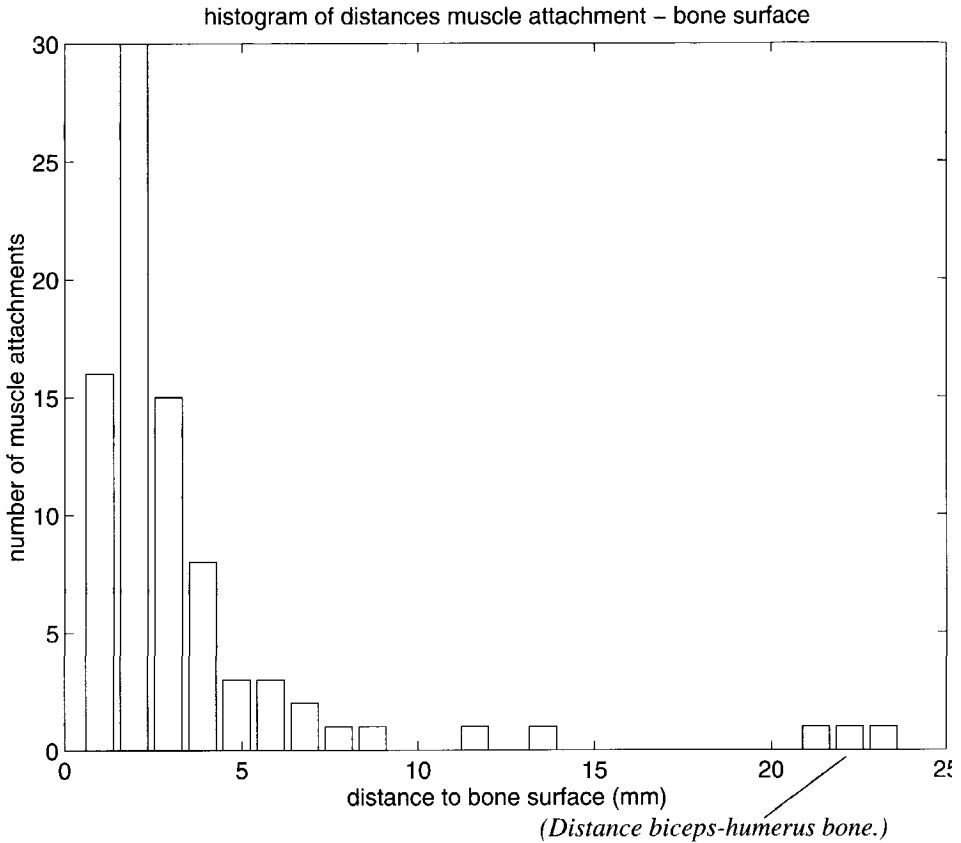


Figure 5.4: Histogram of mean distances from spatial muscle attachment contours to their corresponding bone surfaces for all 84 muscle attachment contours of the shoulder muscles of R2, R4 and R6.

For the biceps, we show the distance from the insertion to the humerus bone, because the shoulder model used in this paper does not contain a lower arm.

measured correctly, we can conclude from these data that 85 percent of our data set is measured and processed correctly.

To check whether the muscle attachments correspond with the bone shape, we transformed the data from R4 and R6 to R2. This resulted in three sets of muscle attachment contours (R2, R42, R62), connected to the geometry of R2. If the assumption that the muscle geometry corresponds with the bone geometry holds, there should be no difference between these three muscle attachment data sets. We checked this in two different ways:

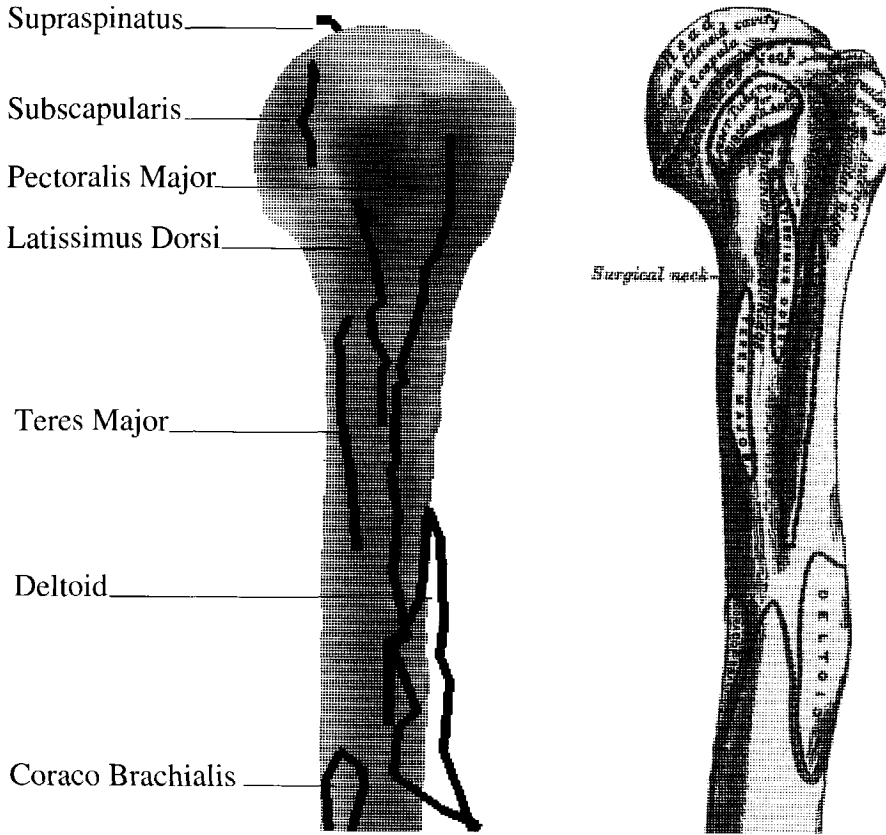


Figure 5.5: Visual check of attachment contours of humerus bone.

Right: Anterior view of left humerus. (from Gray's Anatomy [Gray 1994])

Left: Anterior view of right humerus of R2 (mirrored).

From this figure, we concluded that the attachments of the Supraspinatus and Subscapularis are wrong.

Firstly, we checked the attachment contours visually with the help of a 3-D visualisation tool called Geomview [Geomview]. The data were compared with data from different Anatomy Atlases [Gray 1994]; [Guyton 1985]. With this check, interpretation errors made during the cadaver experiment can be found. In Figure 5.5 a typical example of such a visual check is given for the upper part of the humerus bone. In this image, it is clear that the Supraspinatus muscle of R2 is not attached to the Greater Tuberosity of the humeral head, and that the Subscapularis is not attached to the Lesser Tuberosity of the humeral head. No misplacement of other muscles was detected in this image.

Table 5.3 Categorization of muscle attachment contours into 5 different types.

large: min.dist > 5 mm

mean.dist > 7 mm

max.dist > 12 mm

small: min.dist < 5 mm

mean.dist < 7 mm

max.dist < 12 mm

Type 1 Slide or length difference in direction

min.dist < 5 mm

mean.dist < 7 mm

max.dist > 12 mm

Type 2 Shift perpendicular to direction

min.dist > 0 mm

mean.dist > 0 mm

max.dist < 12 mm

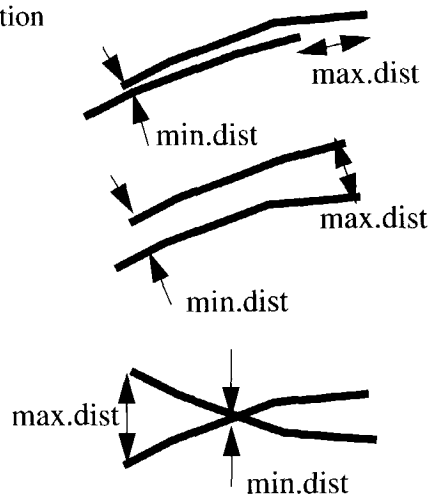
(not small)

Type 3 Cross, or different directions

min.dist < 5 mm

mean.dist > 7 mm

max.dist > 12 mm



Secondly, we checked the correspondence of the data sets by analysing the difference between the attachment contours. To this end the minimum distance, the mean distance, and the maximum distance between the attachment contours were calculated. Using the results of these calculations, we categorized the attachment contours in five types (Table 5.3). As an example, we will analyse the results for the insertion of the Subscapularis muscle. In Table 5.4 all the results for this muscle are shown, together with the labelling of the different parts of the table. The visual check suggests that the muscle attachment of R2 is wrong. The attachments of R2, transformed from R4 (R24), and R2, transformed from R6 (R26) are right. This also shows in the distances of the attachment contours from R2 to R24, and from R2 to R26, which are large and the distance of the attachment contour from R24, to R26, which is small. The distance from the attachment contours to the bone surfaces is small for all data sets. From this, we conclude that the data are correct.

In appendix D the results for all muscles are shown and analysed. It shows that for 45 percent of the muscles, the differences are small in relation to the quality of the data. 15 percent of the muscles is classified as having a large difference, but all of these muscle attachments are qualified wrong by the visual inspection, which

Table 5.4 Typical example of analyzing the results of the Insertion of the Subscapularis muscle. (R24 = Data of R2, transformed from R4)

data set	muscle name	attachment type	conclusion from visual check			distances to bone surface (mm, (standard deviation))
Insertion Subscapularis (line)						
R2		Wrong position				2.0 (1.6)
R24		Right position				1.8 (1.9)
R26		Same as R24				2.7 (1.4)
R2-R24	8.3	11.2	14.6	LARGE		
R2-R26	10.3	12.3	14.3	LARGE		
R24-R26	0.5	4.2	10.7	SMALL		
	distance from - to	min dist.	mean dist.	max dist.	type	visual check



means that the most likely cause of these differences are measurement errors. 15 percent of the muscle attachments has a difference of type 1, 10 percent of the muscle attachments has a difference of type 2, and 15 percent of the muscle attachments has a difference of type 3. It must be noted that all the muscle attachments having a type 2 difference were also qualified as wrong by the visual inspection. From this we can conclude that prediction of muscle attachments based on the bone geometry is very well possible. In the data set of Van der Helm, the muscles on the head of the humerus, like the Infraspinatus, Subscapularis, Supraspinatus, and Teres Minor, contain measurement errors.

To investigate the interindividual differences in muscle geometry, one must use a greater number of cadavers, in combination with a very well standardized dissection protocol.

5.4 Discussion

In this paper, we looked at the differences between muscle attachment data from three different cadavers, obtained during one dissection experiment. In most cases, researchers have difficulties enough to obtain one data set, so they have no other measurements they did themselves with which they can compare their data. When they compare their data with measurements from other research groups, they only do so in a qualitative way, because the differences between the different groups in obtaining and presenting the data is so large that a quantitative comparison is not fruitful.

When using only one data set to build a biomechanical model, one can question whether this model is generally applicable. Because there are interindividual differences, using such a “generic” model may be problematic. Moreover, the quality of its data is not controlled. In most cases, a biomechanical model is not tested for its general applicability.

Not only is validation of the model difficult, the differences between model simulation results and measured data can also be explained in different ways. This makes the use of mechanical models in medical practice very difficult. For gaining insight in the mechanisms that play a role in the human body, these mechanical models are of course very important. The techniques that are described in this chapter can help to validate the data obtained from a cadaver study and can be used to correct for errors in the cadaver experiment.

5.5 Conclusions

By checking the distance between the muscle attachment contours and their corresponding bone surfaces, we have shown that 85 percent of the muscle attachments were measured correctly.

We have also shown that it is possible to predict muscle attachment locations on the basis of the geometry of the bones of a specific subject. To establish this, we had to transform 3-D surface models of these bones into each other. For 45 percent of the muscle attachments, the prediction of the muscle attachment is of good quality in relation to the accuracy of the measurements. Measurement errors were the reason why there was a great divergence between 15 percent of the measured and observed muscle attachments. For about 40 percent of the muscle attachments, the prediction error could have been caused by inter individual differences. It is necessary to repeat this experiment with a larger data set and a better dissection protocol to gain an insight into the inter individual differences.

Chapter 6:

Adapting the Delft Shoulder Model on the basis of measured movements.

Abstract. Because of its special structure, the shoulder joint is a unique joint in the human body. To investigate the influence of the motion constraints incorporated in the Delft Shoulder Model have on its simulation results, we measured the abduction and anteflexion movements of ten different subjects. These measurements were used as input for simulations of the Shoulder Model, using parameter sets from three different cadavers in sequence. Simulation results show that the orientations of the shoulder bones in the simulations are different from the measured orientations. This difference is caused by the motion constraints of the Delft Shoulder Model. As a result of these differences between simulated and measured orientations, other simulation results like muscle force are also different. To reduce these differences we introduced and tested an adaptation scheme, which adapts the parameters of the thorax model based on an optimization of the difference between measured and simulated bone orientations. It is concluded that after adaptation, the differences between measured and simulated bone orientations are smaller, reducing the simulation errors caused by these differences.

6.1 Introduction

The shoulder girdle is a chain of bones connecting the upper extremity to the thorax. It consists of the clavicle, connected to the thorax, and the scapula, connected to the clavicle. The scapula by itself slides over the thorax so that the shoulder girdle acts like a closed chain mechanism. The humerus is connected to the scapula. Because of the special structure of the shoulder girdle, the humerus has a large range of motion.

To gain a better understanding of how this joint functions, biomechanical computer models have been developed [Högfors 1987]; [Högfors 1991]; [Karlsson 1992]; [Helm 1994a]; [Maurel 1998]. These models consist of a number of rigid bodies describing the bones, and muscle lines of action describing the muscles.

In shoulder models it is especially important to be able to characterize the relative position of the scapula [Nieminen 1995]. The orientation and position of the scapula influence the moment arms and muscle length of most shoulder muscles. The orientation of the scapula is also important because it influences the direction of the gleno-humeral joint reaction force vector, which should point inside the glenoid cavity to provide joint stability. [Karlsson 1992]; [Helm 1994a]

Joints are mostly modelled as ball-and-socket joints. The scapulo-thoracic joint, modelling the connection between the scapula and thorax, is a special kind of joint, and is differently modelled in the models that exist nowadays.

The way the scapulo-thoracic joint is modelled in the existing shoulder models

influences the orientation of the scapula to a great extent. First a short survey of the different models will be given in order to present the problems and difficulties caused by the way the scapulo-thoracic joint is modelled.

In the model of Högfors the scapulo-thoracic joint is not modelled as a kinematic joint. In his model, a scapulo-thoracic gliding plane is modelled as an elliptical cylinder, scaled to contact the scapula, determining the direction of scapulo-thoracic reaction forces at two locations on the scapula [Högfors 1987]. Unfortunately, the exact locations of these points are not mentioned in the publication. In this model the number of degrees of freedom (DOFs) of the shoulder girdle is six, but the orientation of the scapula and clavicle are related to the orientation of the humerus. This relation is also known as the scapulo-humeral rhythm [Codman 1934]. The advantage of using the scapulo-humeral rhythm is that humeral angles are the only kinematic input for the model. This makes it very easy to use the model in a practical environment because no orientations of the bones of the shoulder girdle have to be measured. The problem is that the variation on the shoulder rhythm is large [Högfors 1991]; [Karlsson 1992]; [Groot 1998b]; [Groot 1997a]. De Groot made a regression model for the scapulo-humeral rhythm, which can predict scapular angles within a 95% confidence interval of 11 to 18 degrees for all scapular rotation angles [Groot 1998b]; [Groot 1997a]. The scapulo-humeral rhythm used in the model of Högfors is a 'handmade' extrapolation of the results given by Högfors, providing quantitative data for the rhythm over a limited range of movements for the arm [Högfors 1991]; [Karlsson 1992].

The Delft Shoulder Model of Van Der Helm et al. (Figure 6.1) uses an ellipsoid fitted to measured points of the thorax to model the scapulo-thoracic joint [Helm 1994a]. This ellipsoid surface determines the kinematics of the scapula by forcing the points Trigonum Spinae (TS) and Angelus Inferior (AI) of the scapula to be at a constant distance from this surface. This reduces the number of DOFs of the shoulder girdle by two. At the same points, TS and AI, the scapulo-thoracic reaction forces apply. These forces are directed perpendicularly to the ellipsoid surface. In the Delft Shoulder Model, measured scapular positions are used as input, so it is not necessary to use a scapulo-humeral rhythm. If the scapula and clavicle orientations are not measured, it is possible to calculate these orientations from a scapulo-humeral rhythm by using de Groot's regression formula, be it with less accuracy. The number of DOFs are reduced more by modelling the conoid ligament as a rigid beam between the scapula and clavicle. This ligament only influences the axial rotations of the clavicle, which cannot be measured well [Helm 1995]. So the number of DOFs of the Delft Shoulder Model is three for the shoulder girdle and three for the GH-joint.

An advantage of using the same surface for both the kinematics and for applying forces on the scapula is that the model is mechanically consistent. Another advantage is that it makes it possible that the Delft Shoulder Model can be used in forward dynamic simulations. A disadvantage of the Delft Shoulder Model is that it is

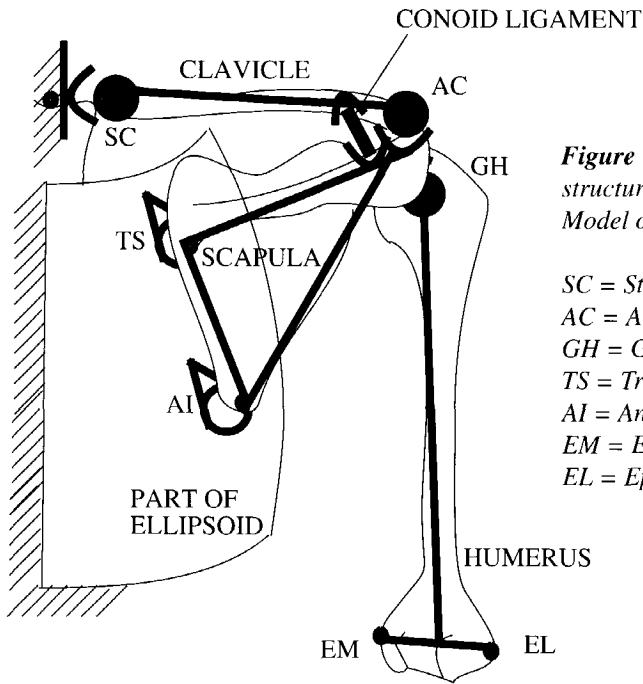


Figure 6.1: Kinematic structure of the Delft Shoulder Model of Van Der Helm et al.

SC = Sterno-Clavicular joint
 AC = Acromio-Clavicular joint
 GH = Gleno-Humeral joint
 TS = Trigonum Spinae
 AI = Angulus Inferior
 EM = Epicondyle Medialis
 EL = Epicondyle Lateralis

difficult to measure the scapula and clavicle orientations. An even more important disadvantage is that due to kinematic incompatibility between the model and the subject, the orientations of the bones of the model and the measured orientations of the bones of the subject differ. For the scapula, deviations up to ten degrees occur [Helm 1994b]. This is partly because the model structure does not match the real life situation exactly: In the model joints are modelled as ideal rotational joints, while in real life translations in the joints occur. A more important cause for the incompatibility between model and subject is that the numerical values of the parameters of the model differ from those of a given subject. However, one must keep in mind that when a scapulo-humeral rhythm is used, differences of the same order of magnitude or larger exist. When the scapular and clavicular orientations are not measured, these differences are unknown.

The model of Niemi is based on the model of Högfors [Niemi 1996]. In this model, the scapulo-humeral rhythm is not used. The movement of the scapula is constrained to a vertical plane that slides on the surface of a cylinder. The orientation of the scapula is calculated by measuring the horizontal distance from the inferior and superior angle of the scapula to the spine [Nieminen 1995]; [Niemi 1996]. The advantage of this model over the model of Högfors is that it does not depend on the scapulo-humeral rhythm.

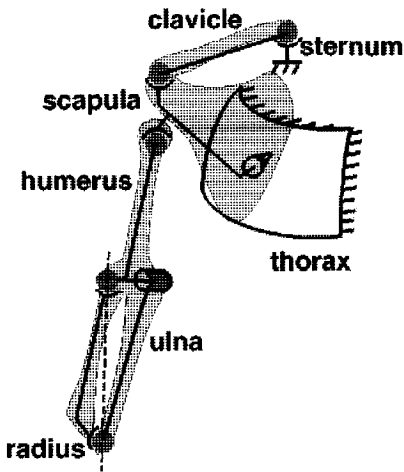


Figure 6.2: Kinematic structure of the model of the CHARM project. [Maurel 1998]

Its disadvantage is that the orientation of the scapula is not measured, so the extent of disagreement between the orientation of the scapula in the model and of the measured subject remains unknown.

In the model built in the CHARM project (Figure 6.2) the scapulo-thoracic joint is also modelled by means of an ellipsoid surface [Maurel 1998]. In this model, only one point of the scapula is constrained and must have a constant distance to the ellipsoid surface. Therefore in this model, the number of DOFs for the shoulder girdle is five. Unfortunately, it is not clear from the paper whether this point is also the point where the scapulo-thoracic reaction force applies. From a mechanical point of view there should be more than one point on the scapula where the scapulo-thoracic reaction force applies to preserve the stability of the scapula.

So in comparison with other models of the shoulder, in the Delft Shoulder Model differences between a measured subject and the model make that the orientations of the scapula of the model are different from the measured orientations. These problems are caused by the differences in morphological parameters between the model and the subject, in combination with the difference in kinematic structure between the model and subject. The kinematic structure of the model has been selected for its mechanical consistency.

To overcome problems caused by differences between model and measured subject, biomechanical models are often scaled [Högfors 1987]; [Högfors 1991]; [Niemi 1996]; [Nussbaum 1996]. Because such scaling has never been validated, the question arises whether scaling actually improves or deteriorates the simulation results.

Blankevoort showed that model simulations can be improved by adapting some model parameters that are unknown or of an uncertain nature [Blankevoort 1996]. He adapted the parameters of a three-dimensional model of the human knee by

optimization of the motion characteristics of the model relative to the corresponding experimental data.

This paper focuses on the problem of kinematic incompatibility between the parameters of the Delft Shoulder Model and those of measured subjects. As a result of this incompatibility the orientations of the bones in the model are different from the orientations of the bones measured in the subject. The cause of these differences is the fact that due to motion constraints in the model, the shoulder girdle has three degrees of freedom, whereas five angles are measured. To get some insight in the possible consequences of this incompatibility, simulation results of movements of different subjects will be evaluated for models based on different cadavers. This results in a large number of different subject-model combinations. For some subject-model combinations the kinematic differences are very large, resulting in different model simulation results. In the second part of this paper, a new method for parameter adaptation is presented and results are evaluated. The goal of this parameter adaptation method is to reduce the kinematic differences between model input and model simulation results, while preserving the original model parameters as much as possible. This is important because model simulation results are sensitive to kinematic values, like the orientation of the scapula. The parameter adaptation method is based on changing weak parameters such as the parameters of the ellipsoid model and the length of the conoid ligament that influence the motion constraints of the shoulder model.

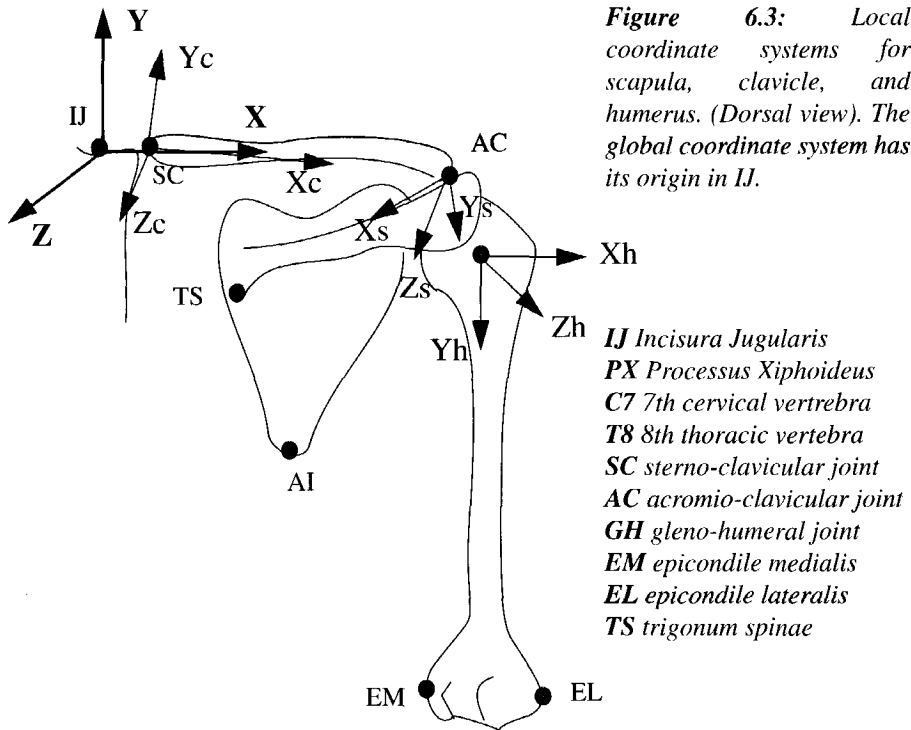
6.2 Method

6.2.1 Kinematic differences

A cadaver study has been performed in order to acquire data for inertia, geometry and muscle contraction parameters for a dynamic finite element model of the human shoulder [Helm 1992]; [Veeger 1991a]. In this study, data on the left and right shoulder of seven cadavers has been recorded, resulting in fourteen data sets. From these data sets, one more or less median cadaver was selected to build the Delft Shoulder Model. In the study presented in this paper, two other data sets were used to obtain two extra parameter sets for the same shoulder model, using the same procedure as for the original set. Following the original publication, we call these data sets R2 (right shoulder of cadaver number 2), R4 and R6, where R2 was used for the Delft Shoulder Model of Van Der Helm et al. [Helm 1994a].

6.2.2 Input

To analyse the Delft Shoulder Model, researchers doing earlier studies used a mean movement measured from ten different healthy subjects [Helm 1994b]; [Groot 1998b], or used measurements from only a few subjects [Helm 1996]. In this study,



we use data on ten different subjects, of whom we measured a humeral abduction movement and a humeral forward-flexion movement. The measured bony landmark locations are used to calculate rotation matrices describing the bone orientations. Bone orientations are defined as the orientations of their local coordinate system with respect to the thorax coordinate system. Figure 6.3 shows the local coordinate systems for the different bones. These definitions are according to the definitions of Van der Helm [Helm 1995]. (See also Appendix A). Figure 6.4 shows the measured bone orientations as a function of humeral abduction for the ten different subjects. It shows that the scapula and humeral movements differ considerably between individuals.

6.2.3 The Shoulder Model

The Delft Shoulder Model used in this study consists of a thorax connected to a clavicle by a ball-and-socket joint, modelling the Sterno-Clavicular (SC) joint. The clavicle is connected to the scapula by a ball-and-socket joint, modelling the Acromio-Clavicular (AC) joint. Two points of the scapula, the Angelus Inferior (AI) and Trigonum Spinae (TS), are bounded to have a constant distance to the thorax, which is modelled by an ellipsoid surface. This surface is called the scapulo-thoracal gliding plane. Between the scapula and the clavicle lies the conoid ligament which is

modelled as a rigid beam, connected by ball-and-socket joints at both ends. The humerus is connected to the scapula by a ball-and-socket joint, modelling the glenohumeral (GH) joint. The bones are modelled as rigid objects. See Figure 6.1 for a graphical presentation of the kinematic structure of the model.

As a result of this structure, the shoulder girdle has three degrees of freedom: Three at the SC-joint, three at the AC-joint, reduced by two by the scapulo-thoracal gliding plane and reduced by one by the conoid ligament. These three degrees of freedom are determined by the input, chosen to be the y-coordinate of point AC, the z-coordinate of point AC, and the x-coordinate of point TS. Rotations of the humerus are entered with respect to the thorax.

Because in this study we are only looking at the bone orientations, the modelling of the muscles is not described.

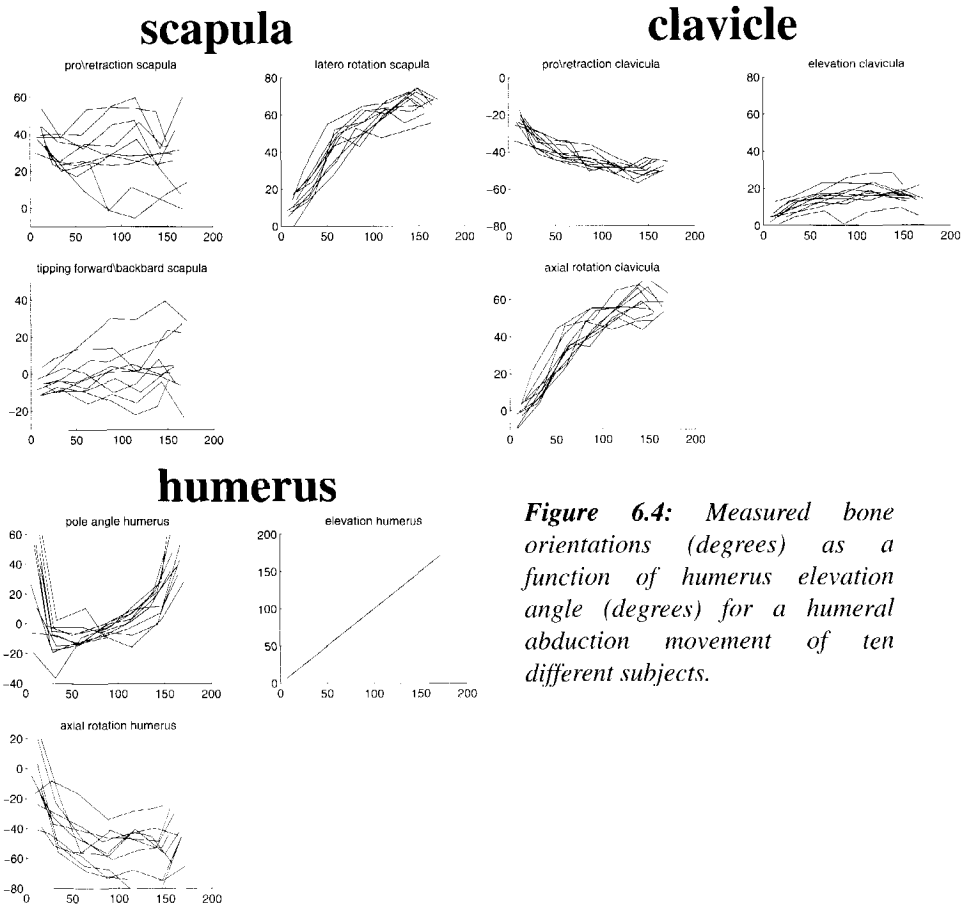


Figure 6.4: Measured bone orientations (degrees) as a function of humerus elevation angle (degrees) for a humeral abduction movement of ten different subjects.

6.2.4 Model simulations

If the difference between the bone orientations of a measured subject and those of the Delft Shoulder Model is large, we say that the subject and the model are kinematically incompatible. An optimization procedure has been developed to calculate bone orientations for the shoulder model that resemble the measured orientations as closely as possible [Groot 1998b]. This optimization procedure minimizes for each simulation step p the criterion function J_p , Eq. (6.1), under the constrained conditions A_1 , A_2 and A_3 , Eq. (6.2). The output of this optimization procedure is C_x^m , C_y^m , C_z^m , S_x^m , S_y^m , and S_z^m .

$$J_p = \left\{ \left\{ \begin{array}{l} (C_y^m - C_y^s)^2 + (C_z^m - C_z^s)^2 + (C_x^m - C_x^s)^2 + \\ (S_y^m - S_y^s)^2 + (S_z^m - S_z^s)^2 + (S_x^m - S_x^s)^2 \end{array} \right\} / 6 \right\} \quad (6.1)$$

$$\begin{aligned} |\text{ellipsoid} - \text{TS}| &= \text{const}_1 && \langle A_1 \rangle \\ |\text{ellipsoid} - \text{AI}| &= \text{const}_2 && \langle A_2 \rangle \\ |L_{\text{conoid}}| &= \text{const}_3 && \langle A_3 \rangle \end{aligned} \quad (6.2)$$

In these formulas, C denotes the clavicle, S the scapula, the subscripts y , z and x the Cardan rotations around the global axes. The superscripts m and s are the model angles and subject angles. L_{conoid} is the length of the conoid ligament. The three constants are derived from the cadaver experiment.

Figure 6.5 is a block diagram of the procedure.

6.2.5 Adapting the shoulder model

The difference between the bone orientations during simulations and the measured bone orientations of the subjects exists because the model and the measured subject are kinematically incompatible. There is a number of parameters in the shoulder model influencing these kinematics: The joint locations of the clavicle, the length of the conoid ligament, the ellipsoid parameters, and the locations of TS and AI on the scapula. The parameters of the clavicle and scapula are relative with respect to the ellipsoid. So, adaptation of all clavicle, scapula and ellipsoid parameters is not necessary.

Taking a closer look at how these parameters are obtained in the original cadaver experiment, we see that the joint rotation centres are measured directly as the centre points of the joint contact surface. The ellipsoid parameters are estimated by fitting an ellipsoid through points on the thorax. Pronk showed that an ellipsoid is a good description of the thorax from a geometrical point of view [Pronk 1991a], though in the shoulder model the ellipsoid is used to restrict the motions of the scapula. The

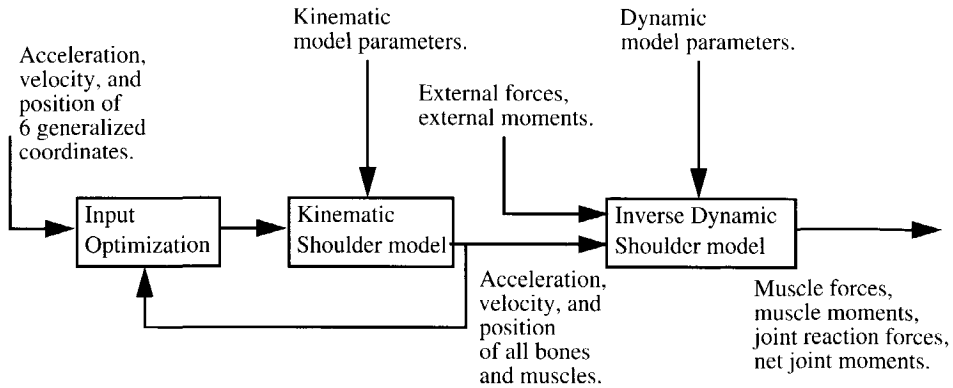


Figure 6.5: Block diagram of the shoulder model. Input variables are the 6 generalized coordinates, and for the inverse dynamic simulations the external forces and moments. Output variables are the acceleration, velocity and position of all bones and muscles, and for the dynamic simulations the muscle forces, muscle moments, net joint moments, and joint reaction forces. Because the kinematic shoulder model has only three free variables to steer six degrees of freedom, the input for this model has been optimised.

constant distances $const_1$ and $const_2$ in Eq. (6.2) between the TS and AI point and the ellipsoid were not measured directly, but derived from palpation measurements of the initial geometry of the cadaver. In vivo, these distances might be different and change due to activities of the adjacent muscles. The length of the conoid ligament was not measured directly either. For these reasons, the ellipsoid parameters and the length of the conoid ligament were chosen as the parameters that should be adapted.

6.2.6 Object function

To adapt these ellipsoid parameters we need an object function. The original ellipsoid was estimated by minimizing the distance D from a number of points measured on the thorax of the cadaver to the ellipsoid, Eq. (6.3), under the constraint that the ellipsoid is symmetrical in the mid sagittal plane, Eq. (6.4). See Van der Helm [Helm 1992] for a method to calculate the distance from a point to an ellipsoid. Following the numbering of Eq. (6.2) we call the constraint A_4 :

$$D = \text{dist}(\text{ellipsoid} - \text{thoraxpoints}) \quad (6.3)$$

$$M_x = 0 \quad \langle A_4 \rangle \quad (6.4)$$

The ellipsoid parameters are defined as the centre of the ellipsoid,

$M = [M_x, M_y, M_z]$, and the axes of the ellipsoid $A = [A_x, A_y, A_z]$, which are aligned with the thorax coordinate system. The following thorax points are used for fitting the ellipsoid: the origo of the serratus anterior muscle, palpated points on part of the thorax where the scapula is located, and palpated points on part of the thorax where the serratus anterior muscle is wrapped around the thorax. It is necessary to use the points of the serratus anterior muscle because the ellipsoid model is also used as a bony contour for this muscle. This means that the muscle lines of action of the serratus muscle are wrapped around the same ellipsoid model to provide the mechanical consistency of the model.

Because the goal of the model adaptation is to minimize the difference between measured and simulated bone orientations, this difference is added to the object

Table 6.1 Mean differences in orientation (degrees) between measured and simulated clavicle orientations for an unloaded humeral abduction movement. (ROWS = Subjects, COLUMNS = Models and angle*)

Subj	2 pr	2 el	2 ax	4 pr	4 el	4 ax	6 pr	6 el	6 ax
1	6.6	5.7	5.2	10.1	4.9	4.1	7.1	1.9	10.0
2	3.9	3.2	2.3	5.0	1.3	2.5	5.7	6.1	9.5
3	1.5	0.9	4.2	3.0	0.9	2.4	2.7	7.3	16.1
4	7.4	3.5	2.0	6.0	2.0	6.1	5.3	11.8	28.5
5	5.0	5.9	3.3	6.6	2.5	1.6	6.4	6.8	27.5
6	3.1	3.7	9.8	3.8	2.2	11.2	4.1	9.8	21.0
7	1.9	1.7	8.9	2.8	0.8	11.1	5.9	6.6	5.6
8	4.9	2.8	7.9	9.5	1.6	3.7	5.6	5.4	14.9
9	3.6	5.0	5.2	6.8	2.5	2.0	4.9	4.1	26.0
10	2.5	2.1	2.8	4.0	1.1	4.8	3.9	6.0	3.1
mean	4.0	3.5	5.2	5.8	2.0	5.0	5.2	6.6	16.2
std	1.9	1.7	2.8	2.3	1.2	3.5	1.3	2.8	9.2
max	7.4	5.9	9.8	10.1	4.9	11.2	7.1	11.8	28.5
min	1.5	0.9	2.0	2.8	0.8	1.6	2.7	1.9	3.1

(*pr = Pro\Re traction, el = Elevation, ax = Axial rotation)

function used to calculate the ellipsoid model. As a result we get the calculated optimal ellipsoid parameters from cadaver data in combination with measured movements of a subject. So the error criterion that is to be optimised can be written as:

$$E = D + w \left\langle \sum_{p=1}^{np} \frac{J_p}{np} \right\rangle \quad (6.5)$$

In this function, D is the distance from the thoraxpoints to the ellipsoid model, Eq. (6.3), J_p is the criterion for posture P , np is the number of postures, w is the weighing

Table 6.2 Mean differences in orientation (degrees) between measured and simulated scapula orientations for an unloaded humeral abduction movement. (ROWS = Subjects, COLUMNS = Models and angle*)

Subj	2 pr	2 ro	2 ti	4 pr	4 ro	4 ti	6 pr	6 ro	6 ti
1	19.7	6.7	11.1	26.0	7.4	11.5	14.1	2.1	5.5
2	6.8	3.5	3.9	13.8	5.7	4.8	2.5	1.0	5.8
3	3.0	1.1	4.6	7.3	3.1	5.4	4.0	2.2	5.7
4	7.1	5.1	7.1	4.8	3.2	6.4	8.3	2.9	10.0
5	6.0	3.7	8.0	4.2	2.6	6.2	6.4	2.8	8.6
6	6.2	3.0	7.6	7.6	4.6	6.2	7.1	3.4	9.2
7	3.0	2.3	3.3	7.6	4.6	2.6	5.4	3.4	9.2
8	23.5	6.5	15.4	28.5	7.9	16.5	19.7	3.3	10.0
9	13.7	2.7	12.2	21.4	3.7	9.4	9.6	2.7	5.7
10	5.9	2.5	4.9	12.4	5.0	6.8	1.5	1.1	4.0
mean	9.5	3.7	7.8	13.4	4.8	7.6	7.9	2.5	7.4
std	7.1	1.8	4.0	8.9	1.8	4.0	5.5	0.9	2.2
max	23.5	6.7	15.4	28.5	7.9	16.5	19.7	3.4	10.0
min	3.0	1.1	3.3	4.2	2.6	2.6	1.5	1.0	4.0

(*pr = Pro\Re traction, ro = Latero rotation, ti = Tipping forward\backward)

factor ($w=10$) necessary to balance the two different criteria. For this optimization, also the three constraints A_1 , A_2 , and A_3 from Eq. (6.2) must hold for each posture. Because we want to have an ellipsoid model suitable for the whole range of motion for a particular subject, the postures used in this optimization must contain the whole range of motion. For the experiments in this paper, we used a humeral abduction and a forward-flexion motion for the optimization, totalling fourteen positions. The criterion function has many local minima, so it is important to choose the right starting value for the minimization function. Several tests showed that using the parameters of the ellipsoid obtained by minimizing criterion function D , Eq. (6.3), as starting value, gives the best results.

Table 6.3 Mean differences in orientation (degrees) between measured and simulated clavicle orientations for an unloaded humeral abduction movement. The models used for these simulations have been adapted to the measured movements. (ROWS = Subjects, COLUMNS = Models and angle*)

Subj	2 pr	2 el	2 ax	4 pr	4 el	4 ax	6 pr	6 el	6 ax
1	3.2	2.8	5.7	4.0	2.6	5.2	6.9	6.6	28.6
2	1.5	3.6	2.9	2.0	2.1	2.4	5.9	5.5	18.2
3	1.4	0.7	3.8	1.9	0.7	3.1	2.1	6.4	17.3
4	6.2	1.6	1.8	3.3	5.1	6.3	5.9	9.1	31.3
5	5.3	3.4	3.1	4.0	1.8	1.6	5.1	5.3	15.9
6	3.0	2.3	10.5	2.7	1.5	10.6	5.7	9.2	14.3
7	1.8	2.4	8.6	3.0	0.9	9.1	4.8	3.5	18.4
8	3.9	3.8	7.5	4.8	3.5	7.2	3.2	6.8	24.2
9	2.9	4.3	4.5	3.0	1.5	4.8	5.5	6.5	44.0
10	1.7	2.4	2.5	2.0	1.3	2.9	3.4	2.5	10.9
mean	3.1	2.7	5.1	3.1	2.1	5.3	4.8	6.1	22.3
std	1.6	1.1	2.9	1.0	1.3	3.0	1.5	2.1	10.0
max	6.2	4.3	10.5	4.8	5.1	10.6	6.9	9.2	44
min	1.4	0.7	1.8	1.9	0.7	1.6	2.1	2.5	10.9

(*pr = Pro\Re traction, el = Elevation, ax = Axial rotation)

6.3 Results

Using the optimization procedure as explained in Subsection 6.2.4, we calculate the input for the models of cadaver R2, R4, and R6 for the ten different subjects. In Table 6.1 the differences between measured and simulated clavicle orientations are shown for each parameter set and for each subject. Table 6.2 shows the differences between the measured and the simulated scapula orientations for each parameter set and for each subject.

As can be seen, the shoulder model cannot simulate all measured movements well. The reason for this is that the difference between the kinematic structure of the

Table 6.4 Mean differences in orientation (degrees) between measured and simulated scapula orientations for an unloaded humeral abduction movement. The models used for these simulations have been adapted to the measured movements. (ROWS = Subjects, COLUMNS = Models and angle*)

Subj	2 pr	2 ro	2 ti	4 pr	4 ro	4 ti	6 pr	6 ro	6 ti
1	2.6	2.1	2.3	3.1	2.1	3.1	4.6	3.4	2.9
2	1.6	2.6	3.0	1.8	2.4	3.3	2.7	2.4	3.5
3	1.9	0.9	2.7	2.7	1.4	2.8	3.1	2.9	3.8
4	5.7	3.7	6.5	4.5	3.0	5.9	8.5	3.6	6.6
5	4.7	1.8	7.1	3.2	2.5	5.8	4.5	3.1	7.4
6	5.3	3.4	6.9	5.0	4.2	6.4	7.3	3.5	9.0
7	2.7	2.3	4.0	3.2	2.5	3.7	3.2	2.0	4.7
8	3.1	4.6	3.3	3.9	2.8	3.3	5.3	10.2	7.7
9	4.2	4.8	5.1	3.1	1.9	5.5	4.9	2.8	4.9
10	2.0	2.3	3.1	1.8	1.1	2.8	3.1	1.8	2.5
mean	3.4	2.9	4.4	3.2	2.4	4.3	4.7	3.6	5.3
std	1.5	1.2	1.8	1.0	0.9	1.5	1.9	2.4	2.2
max	5.7	4.8	7.1	5.0	4.2	6.4	8.5	10.2	9.0
min	1.6	0.9	2.3	1.8	2.1	2.8	2.7	1.8	2.5

(*pr Pro\Re traction, ro = Latero rotation, ti = Tipping forward\backward)

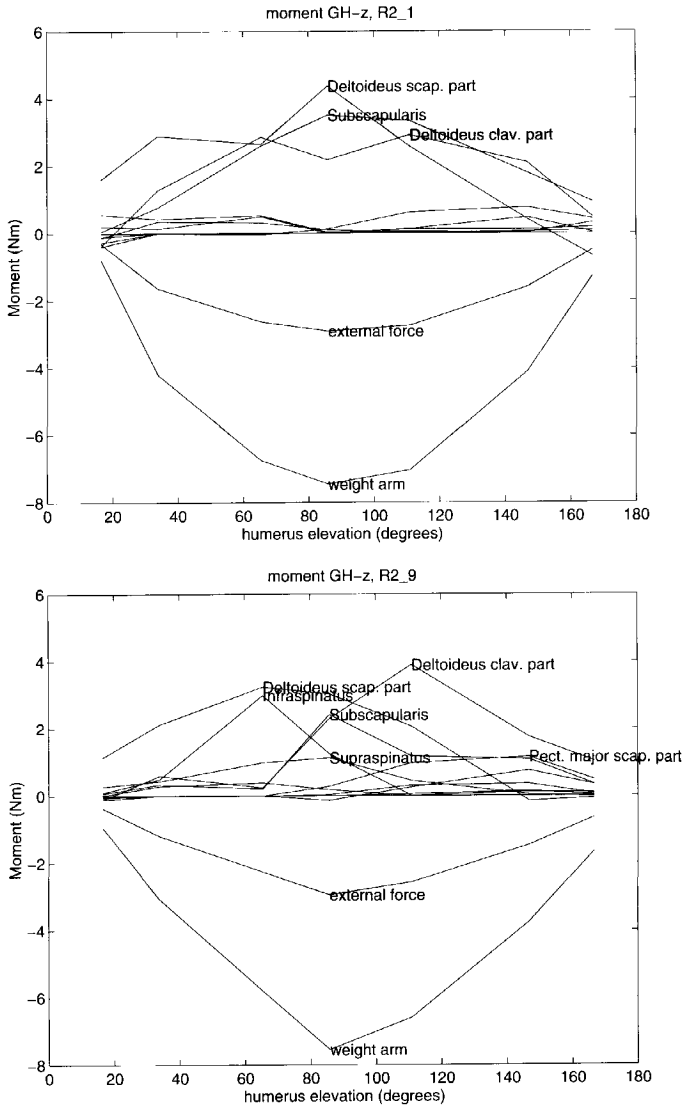


Figure 6.6: Moment balance around the z-axis of the gleno-humeral joint for the same shoulder model, R2, with input from subject no. 1 and subject no. 9. The difference between these graphs is caused by the difference in bone orientations of the two subjects.

model and the measured subject is too large. These tables also show that the model of cadaver R2 has smaller differences than the model of cadaver R4 and R6. For cadaver R4, the differences are the largest. In Table 6.1 we see that the difference between the axial rotation of the clavicle in the model results and in the measured data is largest. The reason for this is that the axial rotation of the clavicle was not measured directly on the subject because only two landmark points on the clavicle were available. We estimated the axial rotation of the clavicle by minimizing the joint rotations in both the SC and AC joint. In the shoulder model the axial rotation of the clavicle is caused by the conoid ligament, which provides a constant distance between its attachment site on the scapula and its attachment site on the clavicle. This is a model assumption, necessary to counteract the muscle forces acting on the clavicle. The differences between measured and simulated orientations of the scapula are in general larger than those of the clavicle.

Because of the difference in measured and simulated bone orientations, the moment arms of the forces acting on these bones will be different. This will result in different muscle forces and moments. For example in Figure 6.6, we see the moment balance around the z-axis of the gleno-humeral joint for an unloaded humeral abduction movement for two different subjects. The only cause for the differences in the two graphs is the difference between their input angles. The influence of this difference on the moment balance is very clear: The first graph shows more or less one group of muscles counteracting the weight of the arm. In the second graph the infraspinatus and supraspinatus contribute to the necessary moment at lower elevation angles, whereas the clavicular part of the deltoid muscle contributes at higher elevation angles. The contribution of the scapular part of the deltoid muscle is the same in both the graphs. We see from this example that the moment balance depends to a great extent on the input angles of the shoulder model, so it is important that the bone orientations of the shoulder model agree with the measured bone orientations.

Table 6.6 shows the parameters of the ellipsoid model calculated solely on the basis of geometrical information, Eq. (6.3). We see large differences between the different parameters sets for M_y and A_y . This is because these parameters have a high interaction with each other. Table 6.5 shows the parameters of the ellipsoid model calculated using a combination of geometrical information and measured bone orientations (Eq. (6.5)). Note that the difference in parameters between the two optimization methods is very small.

Using a shoulder model with parameters adapted to the measured bone orientations, the model simulations described in the previous paragraph were repeated. The resulting differences between the measured and the modelled orientations of the bones of the shoulder are shown in Table 6.4 and Table 6.3. As can be expected, for the majority of the simulations, the differences have become smaller.

Table 6.5 Adapted parameters of ellipsoid of the three shoulder models. Mean values and standard deviations for 10 subjects.

	R2 (cm)	R4 (cm)	R6 (cm)
M_x	0	0	0
M_y	-27.3 (3.1)	-21.9 (2.1)	-15.6 (0.8)
M_z	7.5 (0.6)	4.4 (0.6)	6.7 (0.7)
A_x	14.9 (0.3)	13.6 (0.2)	13.2 (0.2)
A_y	40.3 (2.4)	31.6 (1.3)	26.4 (1.3)
A_z	11.5 (1.7)	11.2 (1.5)	10.9 (1.7)
Length Conoid Ligament	1.8 (0.2)	1.0 (0.1)	1.3 (0.2)

Table 6.6 Parameters of ellipsoid of the three shoulder models, calculated using only geometrical information.

	R2 (cm)	R4 (cm)	R6 (cm)
M_x	0.0	0.0	0.0
M_y	-29.6	-23.0	-15.8
M_z	7.8	5.4	6.6
A_x	15.3	13.7	13.3
A_y	40.4	31.4	25.6
A_z	13.0	13.0	11.1
Length Conoid Ligament	1.8	1.3	1.4

The axial rotation of the clavicle still has large differences, but these are caused by the badly modelled axial rotation of the clavicle in the measurements and in the shoulder model

Looking at the simulation results, we checked the moment-balance around the z-axis of the gleno-humeral joint of all simulations. It was to be expected that the improvement in orientation reproduction of the shoulder model also leads to a change in simulation results. So, for the models of the parameter sets of cadaver R4 and R6, the simulation results changed considerably. For the model of cadaver R2, the change in simulation results was small.

6.4 Discussion and Conclusions

In this study, we used input data measured on ten healthy subjects for simulations of a shoulder model using three different parameter sets. The outcome yields thirty different simulation results.

The ten subjects were asked to elevate their arm according to a certain protocol. Measuring the orientations of the bones of the shoulder showed that the subjects used different shoulder blade orientations to support their arm for the given task. This can be caused by the fact that they use different muscle activation strategies, or that their motion constraints forces them to do so. A combination of the two is most likely.

Model simulations using the shoulder model have shown that the different bone orientations result in different muscle activation patterns. Simulations using shoulder models based on different data sets show that the muscle activation patterns also depend on the muscular structure and attachment sites. From these simulations, we cannot conclude whether the cause of the different bone orientations is the muscle activation strategy or the mechanical structure.

Adapting parameters of a model by optimization of the output of the model will always result in improved simulation results. It is important to check whether the adapted parameters are still valid. In the shoulder model, the ellipsoid model has three functions: Restricting the possible motions of the scapula, applying forces on the scapula, and forming a bony contour for the serratus anterior muscle. For the first function, the parameters of the ellipsoid have been optimised. So for this function the ellipsoid model has the optimal parameters to match the recorded motion. The forces that are applied on the scapula by the ellipsoid are orthogonal with respect to the surface of the ellipsoid. Because the movements of the scapula are in the same plane as the surface of the ellipsoid, the change in force direction will be minimal. So this function is not in conflict with the optimised parameter set either. To provide a proper bony contour for the serratus muscle, we had to add the original criterion, Eq. (6.3), to the object function of Eq. (6.5). Otherwise the shape of the ellipsoid would have been very different, resulting in unrealistic moment arms. Checking the resulting moment arms of the serratus muscle derived from simulations using the

adapted ellipsoid parameters did not show any unrealistic moment arms.

We can conclude that simulation results of the shoulder model are sensitive to the input and the parameters of the model. By ensuring that the movements of the model correspond to the measured movements as closely as possible, the influence of the input is accounted for. So the proposed model adaptation technique is an improvement of the shoulder model. The maximum difference in scapula orientation has been reduced from 28.5 degree to 10.2 degree and the mean orientation difference of the scapula has been reduced from 7.2 degree to 3.8 degree. For the clavicle the improvement is smaller. The sensitivity of the model to the model parameters is an uncertain factor that cannot be minimized. As no proper model validation method is available, it is not possible to adapt the muscular structure of the shoulder model to individual subjects.

Chapter 7:

Concluding remarks.

Discussion

The main goal for this project was to individualize the Delft Shoulder Model using medical imaging techniques. Adaptation of the model to each individual subject (or patient) should improve the model predictions with respect to that individual. This could be very useful in, for example, Computer Aided Surgery (CAS). Because the system is to be used in a medical environment, an important boundary condition is that the developed system is to use minimal human interaction. The reasons for starting this project were the developments in modern medical imaging techniques like MRI and in 3-D medical image analysis techniques. The expectations of the possibilities of these techniques were great, but now we know that the techniques are not yet as far as we hoped.

MRI techniques have greatly improved in the past years. New scanning algorithms and improved local coils reduced the scanning time and improved the resolution and the signal-to-noise ratio. For normal diagnostic research only a small volume is imaged because only specific organs or specific parts of the human body are of interest. To obtain model parameters for the human shoulder, a large volume needs to be scanned. This volume contains most of the spine, necessary for defining the body coordinate system. It also contains the shoulder and the complete humerus, necessary for defining the humeral coordinate system. In total, it is a volume of about 30x30x40 cm, depending on the size of the person. This implies that local coils cannot be used and that the subject needs to be moved by means of the calibrated sliding table of the scanner. Scanning such a large volume has three disadvantages. First, by scanning a large volume, the scanning time increases and the resolution decreases. This causes more artefacts, resulting from movements of the human body.

Second, in the study described in Chapter 4, moving the calibrated sliding table with the cadaver caused a shift of 2.4 millimetres. When a living subject is in the MRI tube, it is very likely that the subject will change posture and position a little during the sliding of the table. Corrections for these movements are possible, but moving the sliding table will certainly add to the overall error.

Third, scanning different parts of the body using local coils and combining the data to form a complete data set is not really an option. Many difficulties are expected from combining the data, while the scanning time of a complete session will be long because of the repositioning of the subject or patient in between scans.

CT is not really an alternative for MRI. The most important reason is that CT is less suitable for visualizing soft tissues than MRI. Especially muscle contours are not

visible in CT images. Another reason is that CT is believed to be more harmful to the human body than MRI.

The developments in 3-D medical image analysis techniques have been great during the past years. It is expected that due to the developments in computer techniques, better networking possibilities like Internet, Intranet, and the use of PACS¹, 3-D medical image analysis will be used more and more in the coming years. Automatic and semi-automatic applications are being developed for special purposes like the human heart and brain. Model-based techniques are already in use for different applications in these fields.

To investigate which parameters need to be adapted to individualize the Delft Shoulder Model and to investigate the accuracy that is necessary for these parameters, in Chapter 3, three different parameter sets were used for simulations with the shoulder model. It was concluded that the shoulder model is sensitive to its parameters and that changing the parameters can lead to unrealistic simulation results. It was shown that for one parameter set at a sixty-degree humeral abduction angle, muscle forces of the shoulder muscles became unrealistically high. These results are probably caused by some kind of instability or other unknown phenomenon in the shoulder model. A possible cause for this instability is a mismatch of the scapula orientation with respect to the humerus orientation. This calls for individualization of the model. The problem is that a change in model parameters also caused unpredictable simulation results, which makes parameter adaptation a difficult and hazardous operation.

Before fine tuning the parameters of the model, one should keep in mind the use of the model. When, for example, the model is used to predict the gleno-humeral contact force, model adaptation is not very useful because the gleno-humeral contact force is not sensitive to different parameter sets. When individual muscle forces are of interest, model adaptation can be useful because the force distribution over the different muscles depends on the individual muscle moment arms and on the muscle cross-sectional area.

Simulations using the three different parameter sets also showed that the kinematic compatibility between the model and test subject depends a lot on the kinematic parameters in the model such as the shape of the ellipsoid model and the length of the clavicle. It was interesting to see that the parameters of the cadaver originally used for the shoulder model show the best kinematic results, that is: The difference between the measured orientations of scapula and clavicle and the simulated orientations is the smallest.

In Chapter 4, the model parameters were obtained by means of MRI images of a cadaver in order to investigate how accurate model parameters obtained from MRI images are. Because the same cadaver was used in a dissection experiment, it was

1. Picture Archive and Communications Systems

possible to check the difference between the data resulting from the two techniques. This check showed that the data coming from both experiments are comparable. The problem with the data from MRI is that it is sometimes difficult to distinguish the exact muscle attachment locations. Extrapolation on the basis of anatomical knowledge about the structures is sometimes necessary. Another problem is that the muscle fibre direction is not visible in MRI images. This hampers modelling of muscles with multiple muscle lines of action based on fibre direction.

A big advantage of MRI is that the original data are not lost during the process. A dissection experiment is destructive by definition, so checking the data afterwards is not possible because the source of the data is lost. For this reason it is important that no errors are made during the dissection experiment. We found that having made an MRI data set of the cadaver before the dissection helps a lot when interpreting and checking the dissection data. Compared to the costs and amount of work of a dissection experiment, making an MRI image is not expensive.

The problem with the MRI images of the human shoulder is that the muscle contours are very difficult to distinguish. The interactive contour detection tool described in Chapter 2 makes the segmentation of tomographic images easier and a lot faster, but the signal-to-noise ratio of the images is such that even an experienced human being has difficulties in distinguishing between the different muscles, so automation is not possible at present.

In Chapter 5 a model transformation technique is shown and validated which is based on the shape of the bones. The assumption that the locations of the muscle attachments are related to the shape of the bones is checked and proven to be correct for the small data set of three cadavers that was available for this experiment. It is difficult to prove that an adapted model, based on a transformation of a generic model, provides better simulation results than the generic model itself. The simulation results of our experiments showed a higher correlation between the generic model and the transformed model than between the transformed model and the model of the cadaver that was used as a target model. As was to be expected, especially the muscle fibre direction of the transformed model was very much correlated with the muscle fibre direction of the source model, but different from the muscle fibre direction of the target model, so in this respect the model transformation technique is not useful.

In Chapter 6, another model transformation technique was presented. This technique is based on the optimization of the parameters determining the kinematic constraints of the shoulder model, for which end palpation data obtained from the subject are used. The ellipsoid is part of the kinematic structure of the model. We think that adaptation is defensible because the kinematic constraints are based on model assumptions, so calculating the parameters determining these constraints in a different way is comparable with using other model assumptions. Optimization is based on measured movements. The positions of the scapula during a complete

abduction and anteflexion movement are used to calculate an optimal thorax model. This thorax model ensures that the kinematic structure of the model is optimally adapted to the measured movements. So within the limitations of the model, kinematic differences between model and measured subject are minimal. Because this method uses measurement data that can be measured using standardized protocols that are already commonly used, this method is suitable for improving the simulation results of the shoulder model.

General Conclusions

It is possible to obtain some of the parameters for a biomechanical model from MRI images with reasonable accuracy. For this purpose, human interaction is necessary for image segmentation and parameter extraction. Problem is that the amount of human interaction necessary is far too great for successful usability in a clinical setting.

It is not possible to obtain all the parameters required for a biomechanical model of the human shoulder from MRI images. Parameters that cannot be obtained are: the direction and length of the muscle fibres. Muscle attachment locations can be obtained for most muscles. Automatic segmentation and analysis of MRI images of the human shoulder is not possible with the current quality of the MRI images.

It is possible to make model and subject kinematically more compatible. Advantages of this are that the difference in the orientations of the bones of the subject and the model becomes smaller, preserving the mechanical consistency of the model. This results in more accurate simulation results.

So we can conclude that individualization will not be possible in medical practice, but it is possible to reduce the kinematic incompatibility between the shoulder model and subject.

Future work

This research can form the basis of different possibilities for future research in the shoulder project. This section presents several possibilities for new projects:

Model parameters from MRI images. There is still a long way to go before MRI images of the human shoulder can be segmented semi-automatically for obtaining the model parameters the Delft Shoulder Model requires. In the MRI images, the muscle contours are difficult to distinguish and the complexity of the muscular structure of the human shoulder is too high. Using a model-based approach it is possible, but then the method depends greatly on model knowledge. This results in a method that is still based on parameters from an external source.

Building biomechanical models from MRI images will be done more and more in the future. We believe that it is very well possible, but one must keep in mind that for larger muscles the muscle fibre direction is an important factor that needs more investigation because the direction cannot directly be obtained from MRI images.

Kinematic adaptation. Chapter 6 describes the adaptation of part of the kinematic structure of the shoulder model based on measured movements. The purpose of this adaptation is to reduce the kinematic incompatibility between measured subject and model. It would be interesting to do more research on this topic. Some questions to be answered are:

- What are the effects of the model adaptation on the results of the dynamic shoulder model.
- What is better: Differences in orientation of the scapula and clavicle between simulation and measurements, or no differences in orientation, but using an ellipsoid model that is adapted during the simulation?
- What is better for the simulation results: Using a scapulo-humeral rhythm, or measuring the scapula and clavicle orientation?
- One of the assumptions in the Delft Shoulder Model is that the points TS and AI have a constant distance to the thorax during normal arm movements. It would be interesting to validate this assumption. The shape of the thorax and other necessary parameters for a kinematic shoulder model can be measured for an individual subject using MRI. Position and orientation of the scapula can be measured using a 3-D tracking device. The difference in orientation of clavicle and scapula between model simulations and measurements should be minimal. The distance between the measured points TS and AI and the reconstructed thorax surface should be constant. A problem in this experiment is that in the MRI tube, the subject is in a horizontal position and inactive. During a palpation experiment the subject is standing and active.

References.

- [Bassett 1990]. Bassett, R.W., Browne, A.O., Morrey, B.F., An, K.N., "*Glenohumeral muscle force and moment mechanics in a position of shoulder instability*", J. Biomechanics Vol. 23, No. 5, pp. 405-415, 1990.
- [Berquist 1987]. Berquist, T.H., Ehman, R.L., Richardson, M.L., "*Magnetic resonance of the musculoskeletal system*", Raven Press Inc. New York 1987.
- [Beylot 1996]. Beylot, P., et all., "*3D Interactive Topological Modeling Using Visible Human Dataset*", Computer Graphics Forum, 15, 3, C-33:C-44, Proc. Eurographics 1996.
- [Blankevoort 1996]. Blankevoort, L., and Huiskes, R., "*Validation of a three-dimensional model of the knee*", J. Biomechanics Vol. 29, pp. 955-961, 1996.
- [Brouwn 2000]. Brouwn, G.G. "Postural control of the human arm", PhD. Thesis University of Technology Delft, 2000.
- [Boissonnat 1988]. Boissonnat, J., "*Shape reconstruction from planar cross sections*", Computer vision, Graphics, and image processing, 44, pp. 1-29, 1988.
- [Canny 1986]. Canny, J., "*A computational approach to edge detection*", IEEE Transactions on Pattern Analysis and Machine Intelligence, vol. 8, no. 6, pp. 679-698, 1986.
- [Codman 1934]. Codman, E. A., "*The Shoulder*", Thomas Todd Comp. Boston, 1934.
- [Cohen 1991]. Cohen, L.D., "*On Active Contour Models and Balloons*", CVGIP: Image Understanding Vol. 53(2), pp. 211-218, 1991.
- [Cohen 1992]. Cohen, I., Cohen, L.D., Ayache, N. "*Using Deformable Surfaces to Segment 3-D Images and Infer Differential Structures*", CVGIP: Image Understanding Vol. 56(2), pp. 246-263, 1992.
- [Cool 1989]. Cool, J.C., "*Biomechanics of orthoses for sub-luxated shoulders*", Prosthetics Orthotics Int., 13 pp. 90-96, 1989.
- [Douglas 1973]. D.H. Douglas, T.K. Peucker, "*Algorithms for the reduction of the number of points required to represent a digitized line or its caricature*", The Canadian cartographer, 10(2), pp. 112-122, 1973.
- [Engin 1980]. Engin, A. E., "*On the biomechanics of the human shoulder complex*", J. Biomechanics, 13, 575-590, 1980.
- .
- .

- [Fick 1877]. Fick, A. E. and Weber, E., "*Anatomisch-mechanische Studie über die Schultermuskeln*", Verh. d. phys.-med. Ges. zu Würzburg 11, pp. 123-152, 1877.
- [Fukunaga 1992]. Fukunaga, T. et al., "*Physiological Cross-Sectional Area of Human Leg Muscles Based on Magnetic Resonance Imaging*", J. of Orthopaedic Research 10, pp. 926-934, 1992.
- [Geest 1994]. Geest, R.J. van der., e.a., "*Automated Detection of Left Ventricular Epi- and Endocardial Contours in Short-axis MR. Images*", Proc. computers in cardiology, pp. 33-36, 1994.
- [Gerbrands 1988]. Gerbrands, J.J., "*Segmentation of noisy images*", PhD Thesis University of Technology Delft, 1988.
- [Geomview]. Geomview, an interactive 3D geometry viewing program written at the Geometry Center. <http://www.geom.umn.edu>
- [Gingins 1996a]. Gingins, P., et al. "*Using V.H.D. to Build a Comprehensive Human Model*", The Visible Human Project Conference, Oct.7-8, 1996, Bethesda, Maryland, USA, 1996.
- [Gingins 1996b]. Gingins, P., et al. "*Modeling Using the Visible Human Dataset*", Proc. Medical Informatics Europe, IOS Press, 1996, pp. 739-743.
- [Gray 1994]. Gray, H., "*GRAY'S Anatomy*", Sixteenth edition, (first edition, 1905), ISBN 1-85958-018-1, 1994.
- [Groot 1992]. Groot, J. H. de, Van der Helm, F. C. T. and Arwert, H. J. "*The effect on the direction of arm force on muscle forces and the configuration of the shoulder mechanism*", Proc. 8th Meeting Eur. Soc. Biomechanics, Rome, Italy, pp. 78, 21-24 June, 1992.
- [Groot 1997a]. Groot, J.H. de, "*A three dimensional regression model of the scapulo-humeral thytm*", Proc. of the First Conference of the International Shoulder Group, ISBN 90-423-0008-6, Delft, the Netherlands, 26-27 Augustus, 1997.
- [Groot 1997b]. Groot, J. H. de, "*The variability of the shoulder motions recorded by means of palpation*", Clinical Biomechanics 12 (7/8), pp. 461-472, 1997.
- [Groot 1998a]. Groot, J. H. de, Valstar, E. R. and Arwert, H.J. "*Velocity effects on the scapulo-humeral rhythm*", Clinical Biomechanics 13, pp. 593-602, 1998.
- [Groot 1998b]. Groot, J.H. de, "*The Shoulder: A Kinematic and Dynamic Analysis of Motion and Loading*", doctoral thesis Delft University of Technology, ISBN 90-9011298-7, 1998.
- [Guyton 1985]. Guyton, A. C., "*Anatomy and physiology*", CBS College publishing, ISBN 0-03-063157-2, 1985.

- [Happee 1994]. Happee, R., "*Inverse dynamic optimization including muscular dynamics, a new simulation method applied to goal directed movements*", J. Biomechanics, 27(7), pp. 953-60, 1994.
- [Happee 1995]. Happee, R., Helm, F. C. T. van der, "*The control of shoulder muscles during goal directed movements, an inverse dynamic analysis*", J. Biomechanics, 28(10), pp. 1179-1191, 1995.
- [Helm 1991a]. Helm, F. C. T. van der, and Veenbaas, R., "*Modelling the mechanical effect of muscles with large attachment sites: application to the shoulder mechanism*", J. Biomechanics 24, pp. 1151-1163, 1991.
- [Helm 1991b]. Helm, F. C. T. van der, "*The Shoulder Mechanism: a dynamic approach*", doctoral thesis Delft University of Technology, ISBN 90-370-0055-X, 1991
- [Helm 1992]. Helm, F. C. T. van der, Veeger, H. E. J., Pronk, G. M., Van der Woude, L. V. H., Rozendal, R. H., "*Geometry parameters for musculoskeletal modelling of the shoulder system*", J. Biomechanics, 25, pp. 129-144, 1992.
- [Helm 1994a]. Helm, F. C. T. van der, "*A finite element musculoskeletal model of the shoulder mechanism*", J. Biomechanics 27, pp. 551-569, 1994.
- [Helm 1994b]. Helm, F. C. T. van der, "*Analysis of the kinematic and dynamic behavior of the shoulder mechanism*", J. Biomechanics 27, pp. 527-550, 1994.
- [Helm 1994d]. Helm, F.C.T. van der, Pronk G.M., "*The loading of shoulder girdle muscles in consequence of a glenohumeral arthrodesis*" Clinical Biomechanics 9, pp. 139-148, 1994.
- [Helm 1995]. Helm F.C.T. van der, Pronk G.M., "*Three-dimensional recording and description of motions of the shoulder mechanism*", J. Biomechanical Engineering 117(1), 2, 1995.
- [Helm 1996]. Helm, F. C. T. van der, and Veeger, H. E. J., "*Quasi-static analysis of muscle forces in the shulder mechanism during wheelchair propulsion*", J. Biomechanics 29, pp. 39-52, 1996.
- [Helm 1997]. Helm, F.C.T. van der, "*A standardized protocol for motion recordings of the shoulder*", Proc. of the First Conference of the International Shoulder Group, ISBN 90-423-0008-6, Delft, the Netherlands, pp. 26-27 Augustus, 1997.
- [Higgins 1993]. Higgins, W.E., Ojard, E.J., "*Interactive Morphological Watershed Analysis For 3D Medical Images*", Computerized Medical Imaging and Graphics, Vol. 17, Nos. 4/5, pp. 387-395, 1993.

- [Höhne 1992]. Höhne, K.H. and Hanson, W., "*Interactive 3D Segmentation of MRI and CT Volumes using Morphological Operations*", Journal of Computer Assisted Tomography 16(2) pp. 285-294, March/April, 1992.
- [Högfors 1987]. Högfors, C., Sigholm, G. and Herberts, P., "*Biomechanical model of the human shoulder-I elements*", J. Biomechanics 20, pp. 157-166, 1987.
- [Högfors 1991]. Högfors, C., Peterson, B., Sigholm, G. and Herberts, P. "*Biomechanical model of the human shoulder-II. The shoulder rhythm.*", J. Biomechanics 20, pp. 699-709, 1991.
- [Högfors 1995]. Högfors, C., Karlsson, D. and Peterson, B., "*Structure and internal consistency of a shoulder model*", J. Biomechanics 28, pp. 767-777, 1995.
- [Inman 1944]. Inman, V.T., Saunders, J.B., Abbott, L.C. "*Observations on the function of the shoulder joint*" Journal of Bone and Joint Surgery, 26A, pp. 1-30, 1944.
- [Jensen 1975]. Jensen, R. H., Davy, D. T., "*An investigation of muscle lines of action about the hip: A centroid approach vs. the straight line approach*" J. Biomechanics 8, pp. 103-110, 1975.
- [Jonker 1988]. Jonker, B. "*A finite element dynamic analysis of flexible spatial mechanisms and manipulators*", Doctoral thesis, Delft University of Technology, The Netherlands, 1988.
- [Kalra 1995]. Kalra, P. et all., "*Topological Modelling of Human Anatomy Using Medical Data*", Proc. Computer Animation '95, IEEE Computer Society, pp. 172-180, 1995.
- [Kaptein 1993]. Kaptein, B.L., "*Model based image analysis of NMR-images of the shoulder*", Msc. thesis Delft University of Technology, Man Machine Systems Group, Lab. for Measurement and Control, Dept. of Mechanical Engineering, 1993.
- [Kaptein 1996]. Kaptein, B.L., and Gerbrands, J.J., "*Interactive contour detection in tomographic data*", Proceedings of the 18th Annual International Conference of the IEEE Engineering in Medicine and Biology Society, Amsterdam 31 October - 3 November 1996.
- [Kaptein 1996a]. Kaptein, B. L., Reinders, "*Exact geometric matching of 3D triangular surface models*", internal report Delft University of Technology, 1996.
- [Kaptein 1996b]. Kaptein, B. L., "*Transformation of 3D models of human shoulder*", IBME conference Papendal, the Netherlands, ISBN 90-365-0845-2, 1996.

- [Karlsson 1992]. Karlsson D., and Peterson B., "Towards a model for force predictions in the human shoulder", J. Biomechanics 25, pp. 189-199, 1992.
- [Kass 1987]. Kass, M., Witkin, A., Terzopoulos, D., "Snakes: Active contour models", int. J. Comput Vision vol. 1, pp. 321-331, 1987.
- [Klein Breteler 1997]. Klein Breteler, M. D., "Measuring muscle and joint geometry for a shoulder model", Proc. of the First Conference of the International Shoulder Group, ISBN 90-423-0008-6, Delft, the Netherlands, 26-27 Augustus, 1997.
- [Klein Breteler 1999]. Klein Breteler, M. D., Spoor, C.W., Helm, F.C.T. van der, "Measuring muscle and joint geometry parameters of a shoulder for modeling purposes", J. Biomechanics 32, pp. 1191-1197, 1999.
- [Koolstra 1989]. Koolstra, J.H., et all, "An iterative procedure to estimate muscle lines of action in vivo", J. Biomechanics, Vol. 22, No. 8,9, pp. 911-920, 1989.
- [Koolstra 1990]. Koolstra, J.H., et all, "Computer-assisted estimation of lines of action of human masticatory muscles reconstructed in vivo by means of magnetic resonance imaging of parallel sections", Archs oral Biol. Vol. 35, No. 7, pp. 549-556, 1990.
- [Koolstra 1992]. Koolstra, J. H., Eijden, T. M. G. J. van, "Application and validation of a three-dimensional mathematical model of the human masticatory system in vivo", J. Biomechanics, 25(2), pp. 175-187, 1992.
- [Laursen 1997]. Laursen, B., Jensen, B. J., Sjogaard, G., "Shoulder muscle force predictions - Comparison of two models" Proc. of the First Conference of the International Shoulder Group, ISBN 90-423-0008-6, Delft, the Netherlands, 26-27 Augustus, 1997.
- [Leest 1996]. Leest O. de, et all. "Influence of glenohumeral prosthesis geometry and placement on shoulder muscle forces" Clinical Orthopaedics and Related Research. 320, pp. 222-233, 1996.
- [Lelieveldt 1994]. Lelieveldt, B.P.F., "Determination of morphological parameters from MRI-images for a biomechanical model of the shoulder", Thesis rapport A-676 (in dutch), Delft University of Technology, Faculty of Mechanical Engineering and Marine Technology, Man-Machine-Systems group, 1994.
- [Martin 1989]. Martin, P.E., et. all., "The use of magnetic resonance imaging for measuring segment inertial properties", Journal of biomechanics vol 22: pp. 367-376, 1989.
- [Maurel 1998]. Maurel, W., Thalman, D., "A Case Study on Human Upper Limb Modelling for Dynamic Simulation", CMBBE, 1998.

- [Meskers 1996]. Meskers, C.G.M., et al., "*In vivo estimation of the glenohumeral joint rotation center from scapula bony landmarks by linear regression*", J. Biomechanics 31 pp. 93-96, 1996.
- [Meskers 1998a]. Meskers, C. G. M., et. all., "*3D shoulder position measurements using a six degree of freedom electromagnetic tracking device*", Clin. Biomech. 13 pp. 280-292, 1998.
- [Meskers 1998b]. Meskers, C. G. M., "Quantitative assessment of shoulder function in a clinical setting: Methodological aspects and applications.", doctoral thesis Leiden University, 1998.
- [Meskers 1999]. Meskers, C. G. M., et. all., "*Calibration of the "Flock of Birds" electromagnetic tracking device and its application in shoulder research*", J. Biomechanics 32, pp. 629-633, 1999.
- [Mollier 1899]. Mollier, S. "*Über die Statik und Mechanik des menschlichen Schultergürtels unter normalen und pathologischen Verhältnissen*", Festschr. f. C. v. Kupffer, Jena, 1899.
- [Montgomery 1993]. Montgomery, K., Ross, M.D., "*A method for semiautomated serial section reconstruction and visualization of neural tissue from TEM images*". Biomedical Image Processing and Biomedical Visualization, Ascharya R.J. Goldgof D.B. (eds.) Prox SPIE, Salem, MA., pp 114-120, 1993.
- [Mungiole 1990]. Mungiole, M. and Martin, P., "*Estimating segment inertial properties: comparison of magnetic resonance imaging with existing methods*", J. Biomechanics 23, pp. 1039-1046, 1990.
- [NLM 1995]. National Library of Medicine, "*The Visible Human Project*", http://www.nlm.nih.gov/research/visible/visible_human.html
- [NLM 1996]. National Library of Medicine, "*The Visible Human Project Conference*", , National Institutes of Health William H. Natcher Conference Center Bethesda, Maryland USA., October 7 & 8, 1996,
http://www.nlm.nih.gov/research/visible/vhp_conf/vhpconf.htm
- [Niemi 1996]. Niemi, J., et all., "*A static shoulder model based on a time-dependent criterion for load sharing between synergistic muscles*", J. Biomechanics 29, pp. 451-460, 1996.
- [Nieminen 1995]. Nieminen, H. et all., "*Load-sharing patterns in the shoulder during isometric flexion tasks*", J. Biomechanics 28, pp. 555-566, 1995.
- [Nieuwenhuis 1989]. Nieuwenhuis, F.J.M, Pronk, G.M. "*An adjustable external fixator to perform a glenohumeral arthrodesis*", Progress in bioengineering. Eds. Paul J.P., Barbenel, J.C., Courtney, J.M., Kenedi R.M., pp 170-173, Adam Hilger, Bristol-New York 1989.

- [Nussbaum 1996]. Nussbaum, M. A., Chaffin, D. B., "Development and evaluation of a scalable and deformable geometric model of the human torso", *Clinical Biomechanics* Vol. 11, No. 1, pp. 25-34, 1996.
- [Olabarriaga 1997]. Olabarriaga S.D., Smeulders, A.W.M., "Setting the Mind for Intelligent Interactive Segmentation: Overview, Requirements, and Framework", IPMI 1997.
- [Orange 1994]. C.M. Orange, F.C.A. Groen, "Magnetic contour tracing" IEEE Workshop Visualisation and Machine Vision, Seattle, June 24, 1994
- [Philip 1994]. Philip, D.P., e.a., "Automatic detection of Myocardial Contours in Cine-Computed Tomographic Images", *IEEE Trans. Medical Imaging*, vol. 13(2), pp. 241-253, 1994.
- [Porrill 1994]. Porrill, J. and Ivins, J. "A semiautomatic tool for 3D medical image analysis using active contour models", *Med. Inform.* VOL. 19, No. 1, pp. 81-90, 1994.
- [Pronk 1991a]. Pronk, G.M., "The shoulder girdle, analyzed and modelled kinematically", doctoral thesis Delft University of Technology, ISBN 90-370-0053-3, 1991.
- [Pronk 1991b]. Pronk, G.M., Van der Helm, F.C.T., "The palpator: an instrument for measuring the positions of bones in three dimensions", *J. of Medical Engineering & Technology*, 15(1):15-20, 1991.
- [Pronk 1993]. Pronk, G. M., et all., "Interaction between the joints in the shoulder mechanism: the function of the coracoclavicular, nonoid and trapezoid ligaments", *Proc. Instn. Mech. Engrs.*, Vol 207, pp. 219-229, 1993.
- [Redert 1998]. Redert, P.A., Kaptein, B.L., et all. "Extraction of semantic 3d models of human faces from stereoscopic image sequences" Presented at 7th European Congress for Stereology, Amsterdam. Accepted for publication in *ACTA STEREOLOGICA*, Ljubljana, Slovenia, 1998.
- [Rozendaal 1997]. Rozendaal, L.A., "Stability of the shoulder: Intrinsic muscle properties and reflexive control", doctoral thesis Delft University of Technology, ISBN 90-9010231-0, 1997.
- [Rugg 1990]. Rugg, S.G., Gregor, R.J., Mandelbaum, B.R., and Chiu, L., "In vivo moment arm calculations of the ankle using magnetic resonance imaging (MRI)", *J. Biomechanics* 23, pp. 495-501, 1990.
- [Salter 1987]. Salter, E. G., Nasca, R. J., and Shelly, B. S., "Anatomical observations on the acromioclavicular joint and supporting ligaments", *Am. J. Sports Med.*, 15, pp. 199-206, 1987.

- [Schiemann 1992]. Schiemann, T., Bomans, M, Tide, U., Höhne, K.H., "*Interactive 3D-Segmentation*", Visualization in Biomedical Computing II, Proc. SPIE 1808, Chapel Hill, NC, 1992.
- [Schiemann 1997]. Schiemann, T., Tiede, U., Höhne, K.H., "*Segmentation of the Visible Human for High Quality Volume based Visualization*", Medical Image Analysis, Vol. 1, No. 4, pp. 263-271, 1997.
- [Spoor 1980]. Spoor, C. W., Veldpaus, F. E., "*Rigid body motion calculated from spatial co-ordinates of markers*", J. Biomechanics 13, pp. 391-393, 1980.
- [Spoor 1992]. Spoor, C.W., Leeuwen, J.L. van, "*Knee muscle moment arms from MRI and from tendon travel*", J. Biomechanics 25, pp. 201-206, 1992.
- [Stroeve 1998]. Stroeve, S. H., "*Neuromuscular control of arm movements: A modelling approach*", doctoral thesis Delft University of Technology, ISBN 90-9011423-8, 1998.
- [Terzopoulos 1987]. Terzopoulos, D., Platt, J., Barr, A., Fleischer, K. "*Elastically deformable models*", Comp. Graph. vol. 21(4), pp. 205-214, 1987.
- [Terzopoulos 1991]. Terzopoulos, D., Metaxas, D. "*Dynamic 3D Models with Local and Global Deformations: Deformable Superquadrics*", IEEE Trans. PAMI vol. 13(7), pp. 703-714, 1991.
- [Thedens 1991]. Thedens, D.R., Skorton, D.J., Fleagle, S.R., "*A Three-Dimensional Graph Searching Technique for Cardiac Border Detection in Sequential Images and its Applications to Magnetic Resonance Images*", Proceedings Computers in Cardiology pp. 57-60, 1991.
- [Thedens 1995]. Thedens, D.R., Skorton, D.J., Fleagle, S.R., "*Methods of Graph Searching for Border Detection in Image Sequences with Applications to Cardiac Magnetic Resonance Imaging*", IEEE Trans. Medical Imaging, vol. 14(1), pp. 42-55, 1995.
- [Udupa 1982]. Udupa, J.K., "*Interactive Segmentation and Boundary Surface Formation for 3-D Digital Images*", Computer Graphics and Image Processing 18, pp. 213-235, 1982.
- [Veeger 1991a]. Veeger, H. E. J., Helm, F. C. T. van der, Woude, L. V. H. van der, Pronk, G. M., Rozendal, R. H., "*Inertia and muscle contraction parameters for musculoskeletal modelling of the shoulder mechanism*", J. Biomechanics 24, pp. 615-629, 1991.
- [Veeger 1991b]. Veeger, H.E.J., Woude, L.H.V. van der, Rozendal, R.H., "*Load on the upper extremity in manual wheelchair propulsion*", Journal of Electromyography and Kinesiology, 1, pp. 270-280, 1991.

-
- [Werff 1977]. Werff, K. van der, "*Kinematic and dynamic analysis of mechanisms, a finite element approach*" PhD-thesis, Delft Univ. Techn., Delft 1977.
- [Westen 1993]. Westen, P. "*Elaboration of cadaver morphology to model parameters*", Graduation report A-654., Faculty of Mechanical Engineering and Marine Technology, Delft University of Technology, The Netherlands, (In Dutch), 1993.
- [Windt 1997]. Windt, de D.A.W.M. "*Shoulder disorders in primary care*", PhD. Thesis, Free University of Amsterdam, The Netherlands, 1997.
- [Wuelker 1995]. Wuelker, N., Wirth, C. J., Plitz, W., Roetman, B., "*A dynamic shoulder model: Reliability testing and muscle force study*", J. Biomechanics 28, pp. 489-499, 1995.

Appendix A:

Coordinate systems and definitions of rotations

One of the most annoying things in working with models of the human shoulder, is that each research group uses its own coordinate systems and rotations of these systems. Different attempts for standardization have been done, but a real standard is not accepted yet. We follow most of the definitions from the work of van der Helm [Helm 1995][Helm 1997]. The prefix of vectors or local coordinate systems defines the co-ordinate system in which the vector or local coordinate system is defined, e.g. G_{y_t} defines the y-axis of the thorax with respect to the global coordinate system.

Coordinate systems:

- Global:
 - O_g (origo): connected to the floor;
 - X_g -axis: horizontally to the right;
 - Y_g -axis: vertically upward;
 - Z_g -axis: horizontally backward;
- Thorax:
 - $^G O_t$ (origo): $^G IJ$
 - $^G x_t$ -axis: perpendicular to the plane through the points $^G IJ$, $^G C7$ and $(^G PX + ^G T8)/2$, pointing to the right of the body;
 - $^G y_t$ -axis: $((^G IJ + ^G C7)/2 - (^G PX + ^G T8)/2) / \text{norm}((^G IJ + ^G C7)/2 - (^G PX + ^G T8)/2)$;
 - $^G z_t$ -axis: perpendicular to $^G x_t$ - and $^G y_t$ -axis, calculated using the cross-product.
- clavicle¹
 - $^G O_c$ (origo): $^G SC$;
 - $^G x_c$ -axis: $(^G AC - ^G SC) / \text{norm}(^G AC - ^G SC)$;
 - $^G y_c$ -axis: perpendicular to $^G x_c$ - and $^G z_c$ -axis, calculated using the cross-product;
 - $^G z_c$ -axis: perpendicular to the $^G x_c$ -axis and the global $^G y_g$ -axis (!!), pointing backwards.

1. On the clavicle only two landmarks can be found (SC and AC). Initially, the global y_g -axis is used to define the y_c -axis and z_c -axis. Pronk estimated the axial rotation of the clavicle by minimizing the rotations at the AC-joint. [Pronk 1991a]

- Scapula
 - G_{O_s} (origo): G_{AC} ;
 - G_{x_s} -axis: $(G_{AC}-G_{TS}) / norm(G_{AC}-G_{TS})$;
 - G_{y_s} -axis: perpendicular to G_{x_s} - and G_{z_s} -axis, calculated using the cross-product;
 - G_{z_s} -axis: perpendicular to $(G_{AI}-G_{AC})$ and G_{x_s} , pointing backwards.

- Humerus
 - G_{O_h} (origo): G_{GH} ;
 - G_{x_h} -axis: perpendicular to G_{y_h} - and G_{z_h} -axis;
 - G_{y_h} -axis: $(G_{GH} - (G_{EM}+G_{EL})/2) / norm(G_{GH} - (G_{EM}+G_{EL})/2)$;
 - G_{z_h} -axis: Perpendicular to G_{y_h} and $(G_{EL}-G_{EM})$, pointing backward.

In this definition, G_{IJ} is the vector containing the position coordinates of bony landmarks IJ , etc. Each local coordinate system is described by a 3x3 orientation matrix $([x, y, z])$ describing the orientation of a bone with respect to the thorax coordinate system. (The thorax coordinate system uses the global coordinate system as a reference). In Figure 1 the local coordinate systems for thorax, scapula, clavicle, and humerus are shown.

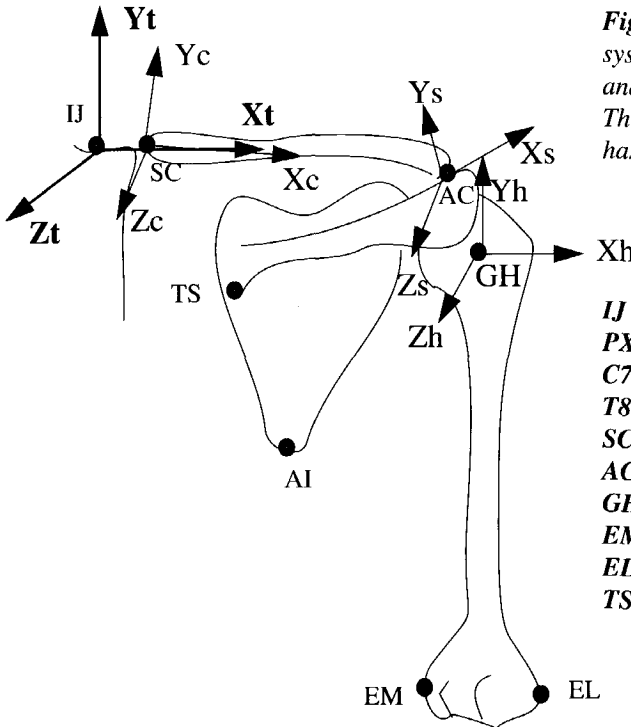


Figure A.1: Local coordinate systems for scapula, clavicle, and humerus. (Dorsal view). The thorax coordinate system has its origin in IJ.

- IJ** Incisura Jugularis
- PX** Processus Xiphoideus
- C7** 7th cervical vertebra
- T8** 8th thoracic vertebra
- SC** sterno-clavicular joint
- AC** acromio-clavicular joint
- GH** gleno-humeral joint
- EM** epicondile medialis
- EL** epicondile lateralis
- TS** trigonum spinae

Orientations:

In this work, bone orientations are defined with respect to a virtual reference position. This is necessary since for the thorax, clavicle and scapula no well-defined anatomical position exists. In the virtual reference position, the local coordinate systems ${}^G T$, ${}^G C$, ${}^G S$, and ${}^G H$, were chosen to be positioned along the axes of the global coordinate system in order to optimise for interpretability. The orientation of the thorax is defined with respect to the global coordinate system. The orientations of the clavicle, scapula and humerus are defined with respect to the thorax coordinate system.

Note that the virtual reference position of the scapula, with the scapular spine along the frontal axis and the scapular plane parallel to the frontal plane, is physically impossible. This also counts for the virtual reference position of the clavicle with its length axis along the frontal axis.

Rotations are described by their rotation axis which is the only way for unambiguously describing 3D rotations. However, it should be noted that only the first rotation is around the axis as defined, the next rotations are around local axes, transformed by prior rotations, denoted by single quote (') and double quote (") for the first and second local rotation, respectively. The following rotations and their interpretation are defined:

- Rt_i : R_x : backward/forward rotation around the frontal (X -)axis;
- R_y : torsion around the vertical (Y' -)axis;
- R_z : lateral flexion around the sagittal (Z'' -)axis;
- Rc_i : R_y : pro/retraction (ventral/dorsal rotation) around the vertical (Y -)axis;
- R_z : elevation/depression (cranial/caudal rotation) around the sagittal (Z' -)axis;
- R_x : rotation around the frontal (X'' -)axis;
- Rs_i : R_y : pro/retraction around the vertical (Y -)axis;
- R_z : lateral/medial rotation around the sagittal (Z' -)axis;
- R_x : tipping forward/backward around the frontal (X'' -)axis;
- Rh_i : R_y : pole angle of the humerus with the frontal plane, rotation around the vertical (Y -)axis;
- R_z : elevation (abduction) angle with respect to the vertical axis, rotation around the (Z' -)axis;
- R_x : axial rotation of the humerus around the (Y'' -)axis.

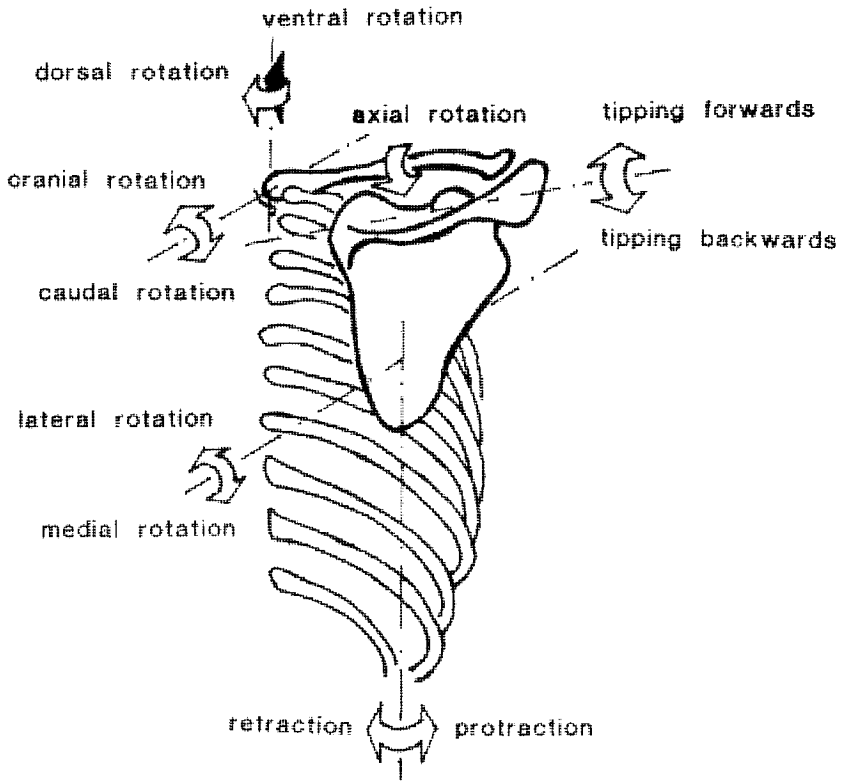
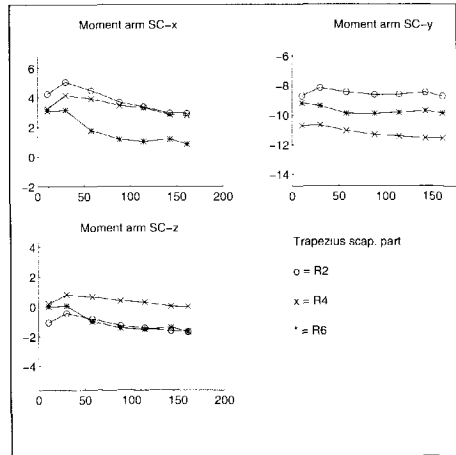
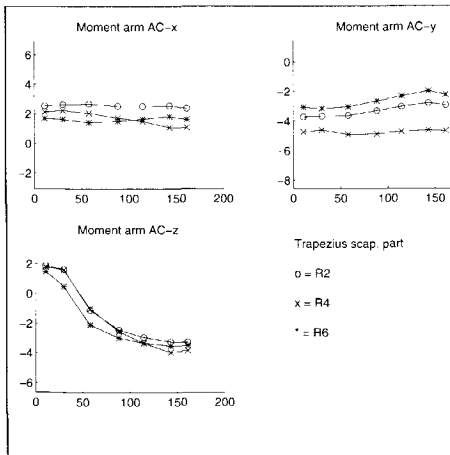


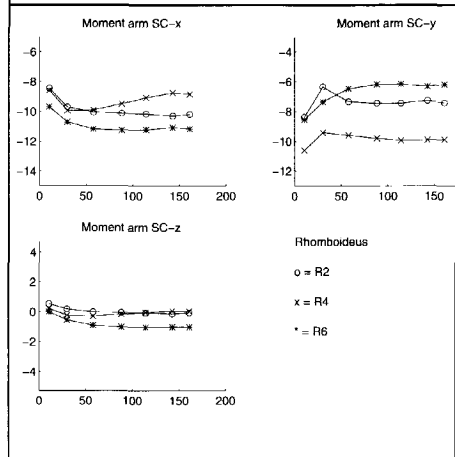
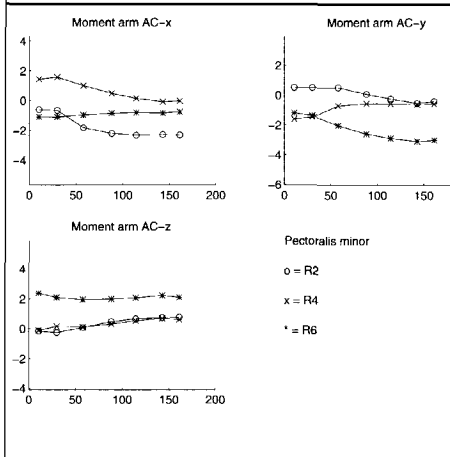
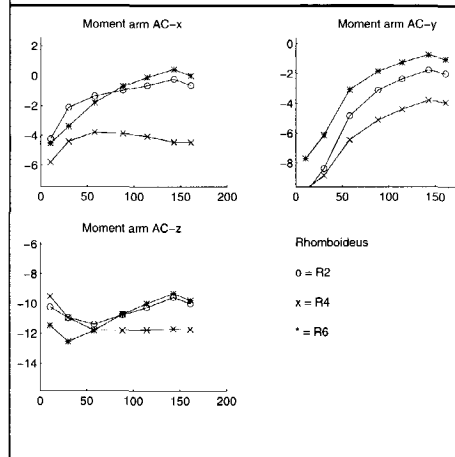
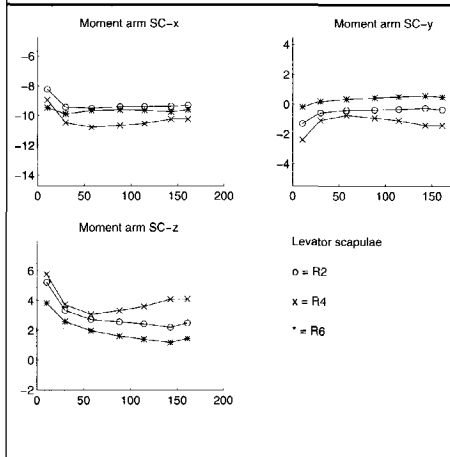
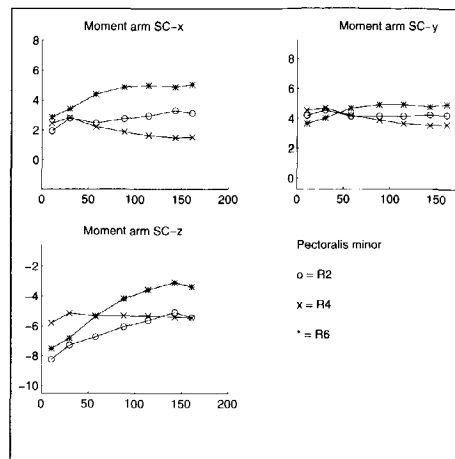
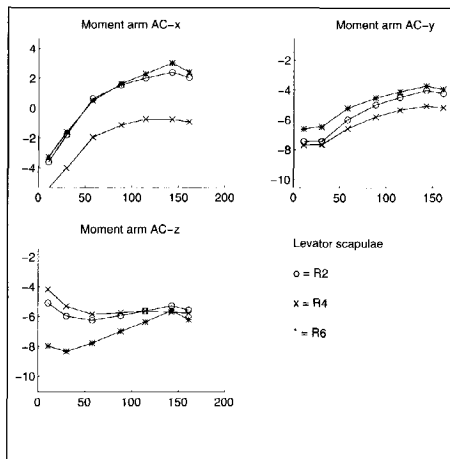
Figure A.2: Rotations of the shoulder girdle.

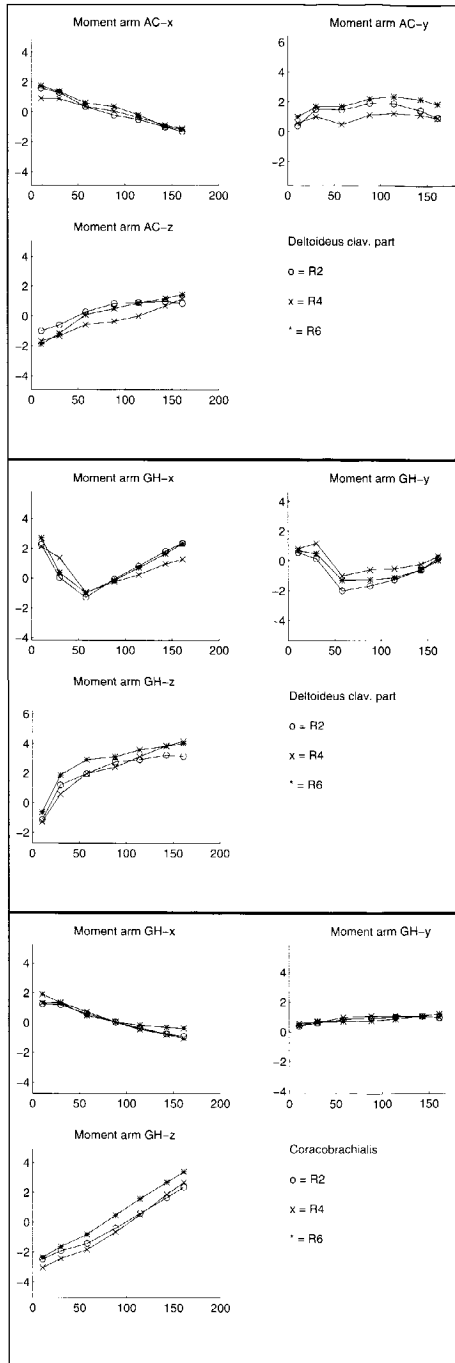
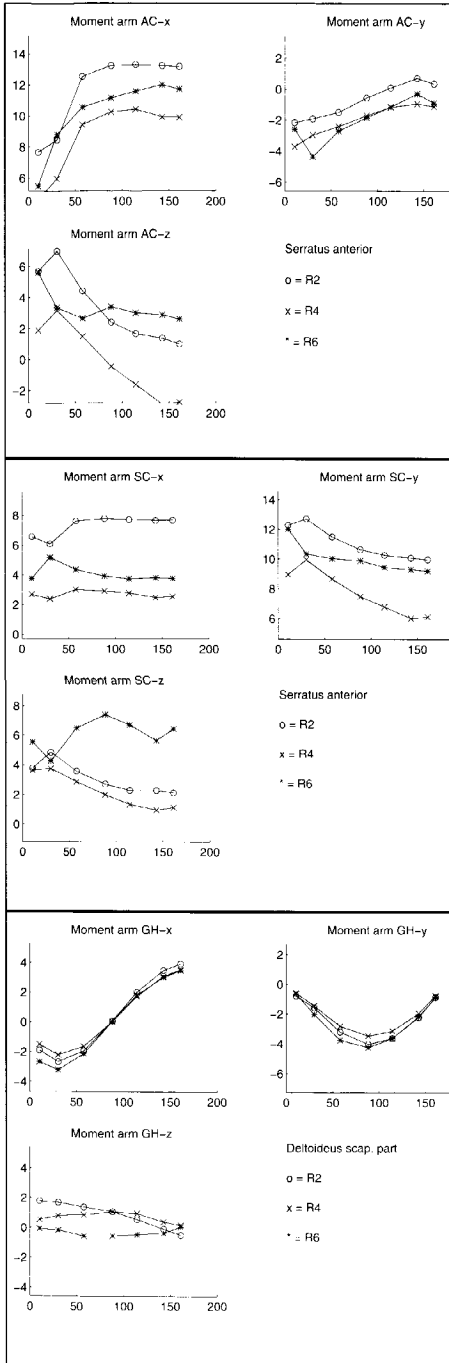
Appendix B: Muscle moment arms

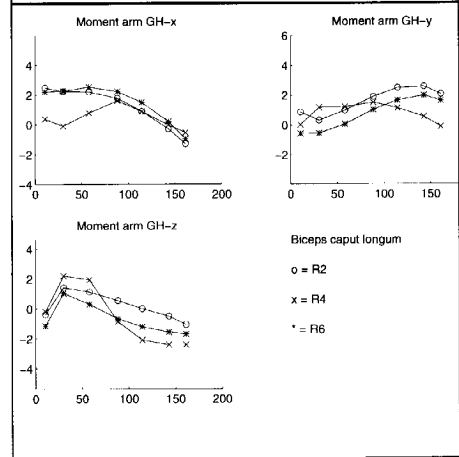
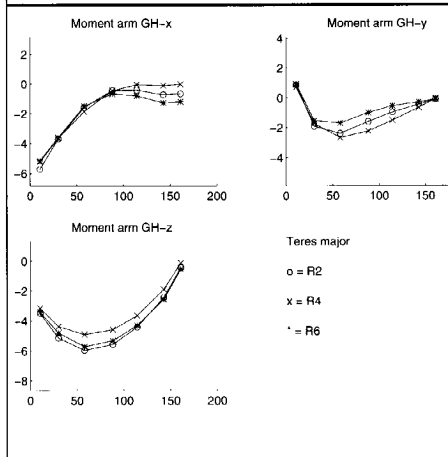
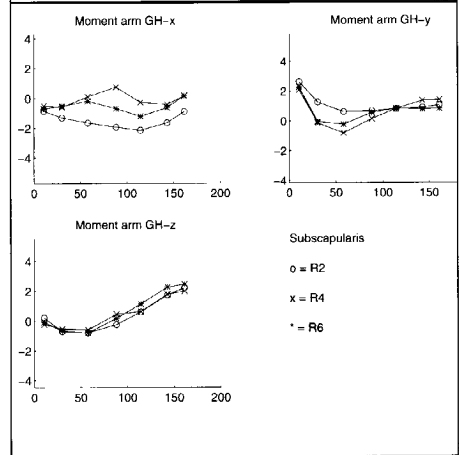
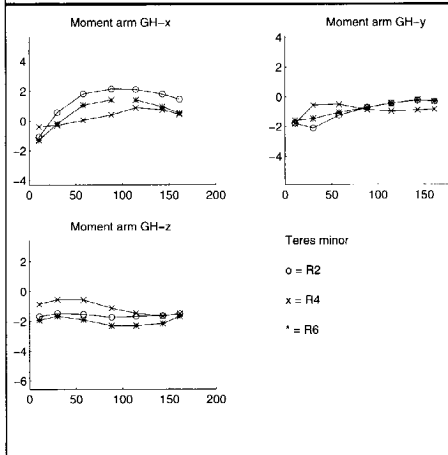
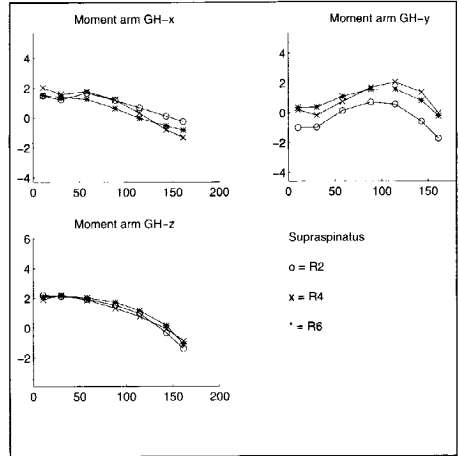
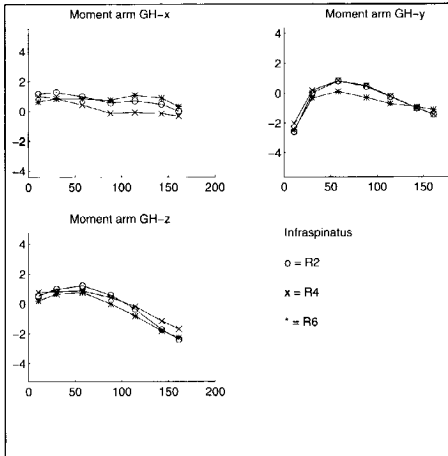
In this appendix, for each muscle the muscle moment arms (cm) are shown as a function of humeral elevation angle (deg) for an abduction movement in seven steps. The abduction movement is the mean abduction movement as has been measured by ten different subjects.

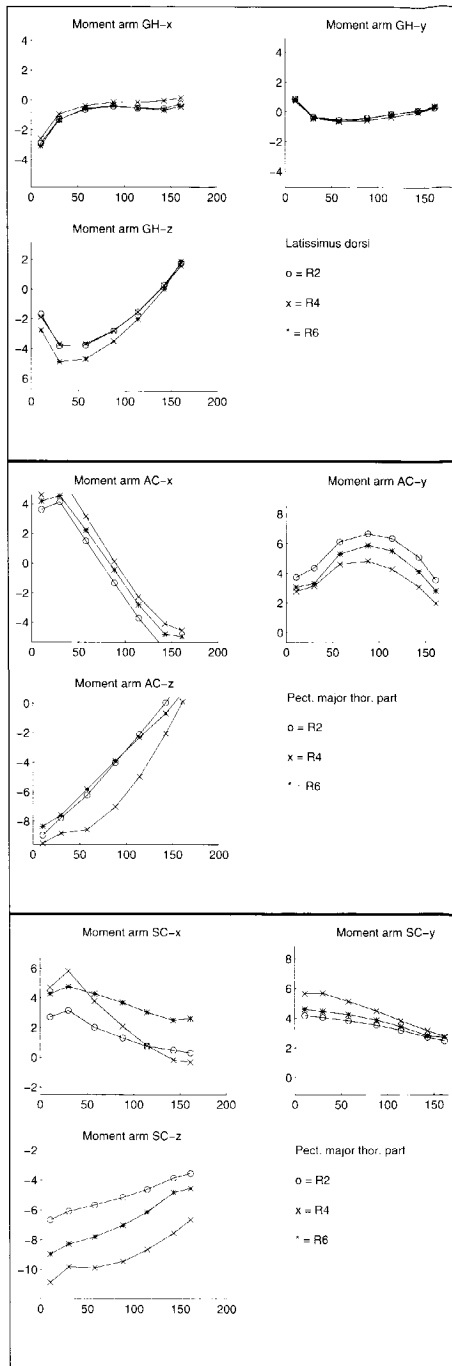
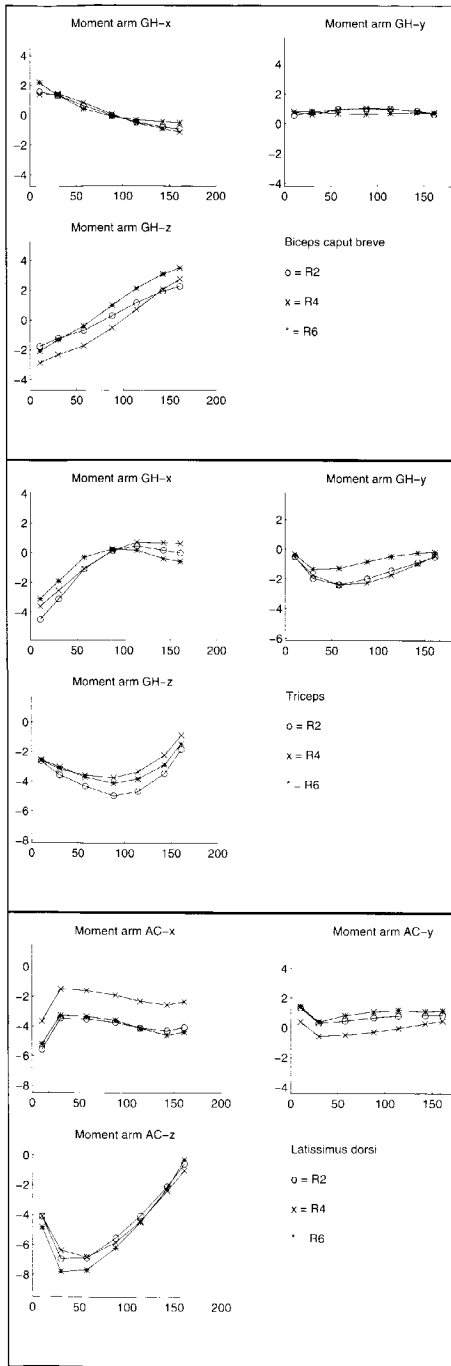
Each figure shows the mean moment arm for the complete muscle decomposed into three directions. The three lines in each graph show the results for the shoulder model based on one of the three different parameter sets. The differences between these three lines are caused by differences in these three parameter sets, as well as by differences in the movements of the model based on these parameter sets.

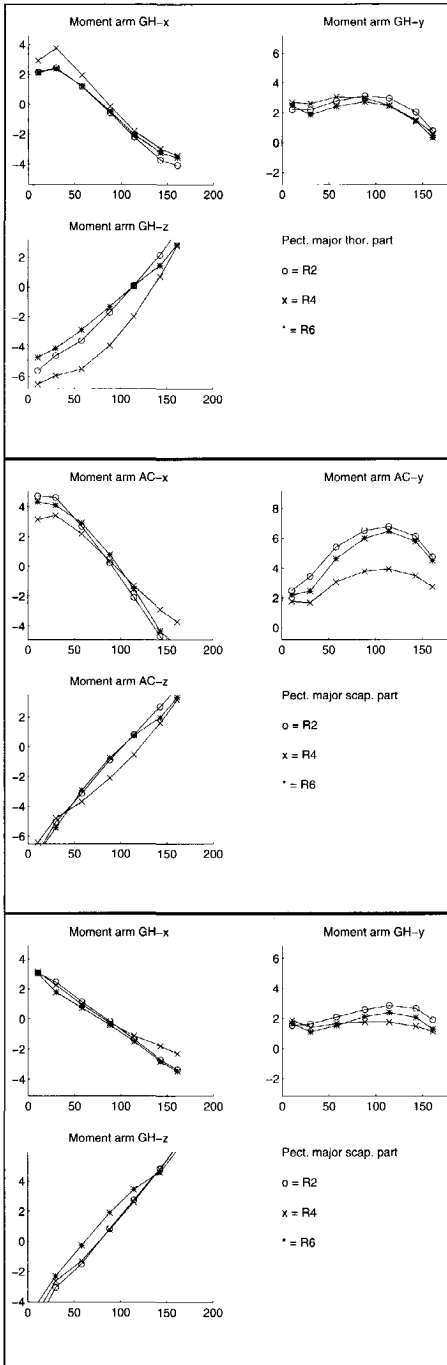












Appendix C: Muscle attachment data

This appendix shows the distances from all palpated muscle attachment contours to their corresponding bone surfaces obtained from MRI images..

Table C.1 Distance between palpated muscle attachment contours and their corresponding bone surface obtained from CT images. (Mean and standard deviation in millimeters.)

	Scapula R2		Scapula R4		Scapula R6	
	mean	std	mean	std	mean	std
biceps caput b.	13.7	0.4	1.9	0.5	2.2	0.3
biceps caput l.	7.3	1.4	8.3	0.2	6.7	0.2
corocobrachialis	11.9	3.5	2.1	1.7	2.9	1.1
deltoid	4.1	1.5	2.0	2.4	2.6	2.7
infraspinatus	2.2	1.1	1.2	0.9	1.7	1.2
levator scapula	3.4	2.6	2.4	1.3	2.4	1.1
pectoralis minor	3.1	3.1	1.9	0.8	2.3	0.9
rhomboideus	2.7	1.1	1.6	1.1	2.0	1.1
serratus anterior	2.3	1.7	3.2	2.1	3.0	2.1
subscapularis	1.9	1.6	1.6	1.0	1.2	0.9
supraspinatus	3.2	2.1	4.2	3.8	2.8	1.3
teres major	3.7	3.1	2.2	1.8	2.1	2.3
teres minor	5.3	2.2	2.7	2.9	2.2	1.9
trapezius	4.1	1.3	1.4	0.8	1.7	0.8
triceps	6.2	1.7	2.2	1.1	2.4	2.0

Table C.2 Distance between palpated muscle attachment contours and their corresponding bone surface obtained from CT images. (Mean and standard deviation in millimeters)

	Clavicle R2		Clavicle R4		Clavicle R6	
	Mean	Std	Mean	Std	Mean	Std
Deltoid	2.3	1.8	1.3	0.5	0.9	0.6
Pectoralis Major	1.6	1.1	4.2	0.9	1.9	0.8
Trapezius	5.4	2.1	0.5	0.4	1.1	0.7

Table C.3 Distance between palpated muscle attachment contours and their corresponding bone surface obtained from CT images. (Mean and standard deviation in millimeters.)

	Humerus R2		Humerus R4		Humerus R6	
	Mean	Std	Mean	Std	Mean	Std
Biceps	23.7	0.5	22.6	0.0	21.1	0.4
Coracobrachialis	3.4	1.5	1.0	1.0	0.8	0.5
Deltoid	4.3	3.4	1.4	1.0	3.1	1.8
Infraspinatus	7.0	1.3	5.5	0.9	3.7	0.9
Latisimus Dorsi	1.5	0.3	0.7	0.6	0.7	0.4
Pectoralis Major	0.7	0.5	1.4	0.9	3.4	0.8
Subscapularis	2.0	1.6	1.8	1.9	2.7	1.4
Supraspinatus	4.5	1.0	5.2	1.2	1.7	0.8
Teres Major	2.4	0.4	0.6	0.6	0.9	0.6
Teres Minor	3.0	0.7	3.5	1.3	1.7	0.8

Appendix D: Muscle attachments.

This appendix shows the muscle attachment data from R4 and R6 transformed to R2. This results in three sets of muscle attachment contours, connected to the geometry of R2. If the assumption that the muscle geometry is attached to the bone geometry is true, there is no difference between these three muscle attachment data sets. In this appendix, the data is checked visually, as well as by checking the distances from the attachment contours of the muscles to each other Table 1, shows the way the data in this appendix is ordered. Table 2 shows the categorization of the muscle attachment contours in five different types..

Table D.1 Typical example of analyzing the results of the Insertion of the Subscapularis muscle. (R24 = Data of R2, transformed from R4)

<i>data set</i>	<i>muscle name</i>	<i>attachment type</i>	<i>distances to bone surface (mm, (standard deviation)</i>		
<i>Insertion</i>	Subscapularis	(line)	<i>conclusion from visual check</i>		
R2	Wrong position		2.0	(1.6)	
R24	Right position		1.8	(1.9)	
R26	Same as R24		2.7	(1.4)	
R2-R24	8.3	11.2	14.6	LARGE	
R2-R26	10.3	12.3	14.3	LARGE	
R24-R26	0.5	4.2	10.7	SMALL	
<i>distance from - to</i>	<i>min dist.</i>	<i>mean dist.</i>	<i>max dist.</i>	<i>type</i>	<i>visual check</i>

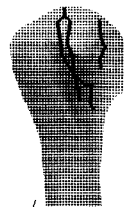


Table D.2 Categorization of muscle attachment contours in 5 different types.**LARGE:**

min.dist > 5 mm
 mean.dist > 7 mm
 max.dist > 12 mm

SMALL:

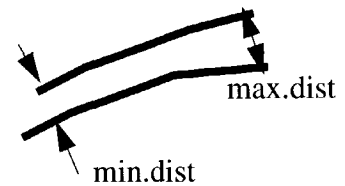
min.dist < 5 mm
 mean.dist < 7 mm
 max.dist < 12 mm

T1: Slide or length difference in direction

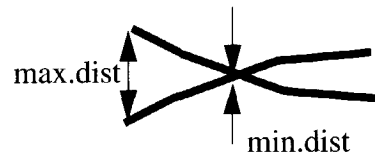
min.dist < 5 mm
 mean.dist < 7 mm
 max.dist > 12 mm

**T2:** Shift perpendicular to direction

min.dist > 0 mm
 mean.dist > 0 mm
 max.dist < 12 mm
 (not small)

**T3:** Cross, or different directions

min.dist < 5 mm
 mean.dist > 7 mm
 max.dist > 12 mm



Scapula

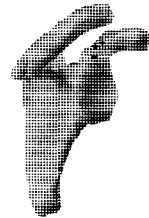
Origo biceps caput breve (point)

R2	Inside humeral head (Wrong)			13.7	(0.4)
R24	Right position			1.9	(0.5)
R26	Right position, same as R24			2.2	(0.3)
SM	Wrong position, same as R2				
R2-R24	12.7	13.2	13.7	LARGE	
R2-R26	13.0	13.5	14.1	LARGE	
R24-R26	0.5	1.1	1.8	SMALL	



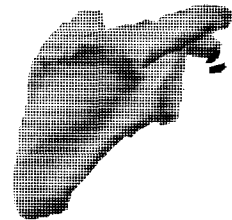
Origo biceps caput longum (point)

R2	Inside humeral head (Wrong)			7.3	(1.4)
R24	Same as R2 (Wrong)			8.3	(0.2)
R26	Same as R2 (Wrong)			6.7	(0.2)
SM	Wrong position, same as R2				
R2-R24	5.0	6.0	7.0	SMALL	
R2-R26	9.5	10.5	11.6	T2	
R24-R26	5.8	5.9	6.1	T2	



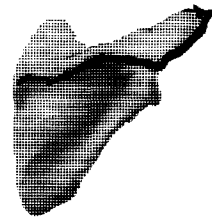
Origo coraco brachialis (point)

R2	Inside humeral head (Wrong)			11.9	(3.5)
R24	Right position			2.1	(1.7)
R26	Right position, same as R24			2.9	(1.1)
SM	Wrong position, same as R2				
R2-R24	7.8	8.9	11.2	T2	
R2-R26	7.9	9.9	12.1	LARGE	
R24-R26	0.1	1.8	4.1	SMALL	



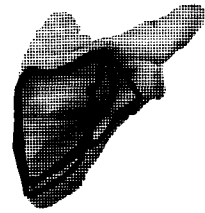
Origo Deltoid (line)

R2	Right position			4.1	(1.5)
R24	Right position, longer than R2			2.0	(2.4)
R26	Right position, same as R24			2.6	(2.7)
SM	On line R2, not covering the whole length				
R2-R24	0.9	3.5	7.2	SMALL	
R2-R26	0.2	5.3	8.7	SMALL	
R24-R26	0.8	3.5	9.2	SMALL	

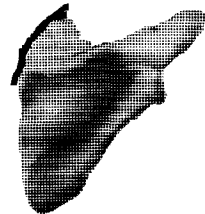


Origo Infraspinatus (plane)

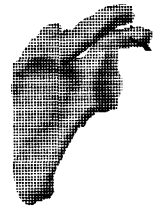
R2	Right position			2.2	(1.1)
R24	Same as R2, closer to ext. border			1.2	(0.9)
R26	Same as R2, further from ext. border			1.7	(1.2)
SM	OK				
R2-R24	0.3	6.3	15.5	T1	
R2-R26	1.7	6.8	14.5	T1	
R24-R26	0.2	8.3	33.6	T3	

**Insertion Levator Scapulae (line)**

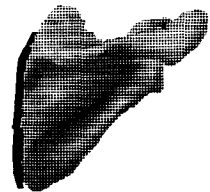
R2	Right position			3.4	(2.6)
R24	Same as R2, only lower			2.4	(1.3)
R26	Same as R2, only much shorter			2.4	(1.1)
SM	OK				
R2-R24	0.1	2.4	11.9	SMALL	
R2-R26	0.7	8.6	29.8	T3	
R24-R26	0.1	11.7	36.9	T3	

**Insertion Pectoralis Minor (line)**

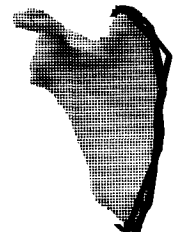
R2	Right position			3.1	(3.1)
R24	Same as R2			1.9	(0.8)
R26	Same as R2			2.3	(0.9)
SM	Wrong (line perpendicular to bone surface)				
R2-R24	3.6	5.4	9.4	SMALL	
R2-R26	6.9	8.4	11.7	T2	
R24-R26	1.9	5.1	10.8	SMALL	

**Insertion Rhomboideus (line)**

R2	Right position			2.7	(1.1)
R24	Same as R2, further from inf. angle			1.6	(1.1)
R26	Same as R2, closer to superior angle			2.0	(1.1)
SM	OK				
R2-R24	1.5	4.3	7.5	SMALL	
R2-R26	0.1	3.8	6.0	SMALL	
R24-R26	1.2	2.2	3.8	SMALL	

**Insertion Serratus Anterior (line)**

R2	Right position			2.3	(1.7)
R24	Right position			3.2	(2.1)
R26	Same as R24			3.0	(2.1)
SM	OK				
R2-R24	0.2	2.9	7.8	SMALL	
R2-R26	0.2	4.8	13.5	T1	
R24-R26	0.1	5.1	17.5	T1	



Origo Subscapularis (plane)

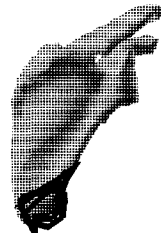
R2	Right position			1.9	(1.6)
R24	Right position, different from R2			1.6	(1.0)
R26	Same as R2			1.2	(0.9)
SM	OK				
R2-R24	0.6	11.3	31.1	T3	
R2-R26	0.4	6.8	30.0	T1	
R24-R26	0.2	7.7	19.0	T3	

**Origo Supraspinatus (plane)**

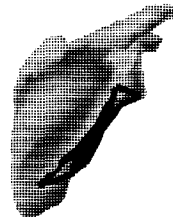
R2	Right position			3.2	(2.1)
R24	Same as R2			4.2	(3.8)
R26	Same as R2			2.8	(1.3)
SM	OK				
R2-R24	0.6	4.6	12.3	T1	
R2-R26	0.4	6.8	17.5	T1	
R24-R26	1.2	7.3	17.8	T3	

**Origo Teres Major (line)**

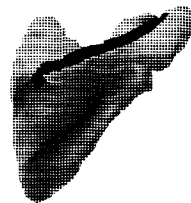
R2	Right position			3.7	(3.1)
R24	Right position, more superior than R2			2.2	(1.8)
R26	Same as R2			2.1	(2.3)
SM	OK				
R2-R24	0.9	5.4	8.3	SMALL	
R2-R26	1.0	5.4	10.3	SMALL	
R24-R26	0.9	7.6	27.3	T3	

**Origo Teres Minor (plane)**

R2	Right position			5.3	(2.2)
R24	Same as R2, closer to glenoid			2.7	(2.9)
R26	Same as R2, closer to inferior angle			2.2	(1.9)
SM	OK				
R2-R24	0.1	5.1	10.8	SMALL	
R2-R26	0.3	3.7	7.1	SMALL	
R24-R26	0.5	6.8	27.7	T1	

**Insertion Trapezius (line)**

R2	Wrong position			4.1	(1.3)
R24	Right position			1.4	(0.8)
R26	Same as R24, further from acromion			1.7	(0.8)
SM	OK				
R2-R24	9.1	19.3	33.7	LARGE	
R2-R26	9.3	19.9	34.0	LARGE	
R24-R26	0.1	2.2	8.0	SMALL	



Origo Triceps (line)

R2	Wrong position			6.2	(1.7)
R24	Right position			2.2	(1.1)
R26	Same as R24			2.4	(2.0)
SM	OK				
R2-R24	3.6	7.4	11.2	T2	
R2-R26	3.9	6.4	8.2	SMALL	
R24-R26	0.2	1.8	2.9	SMALL	

**Humerus****Insertion Biceps (point)**

R2	Right position			23.7	(0.5)
R24	Same as R2			22.6	(0.0)
R26	Same as R2			21.1	(0.4)
SM	OK				
R2-R24	27.2	27.4	27.6	LARGE	
R2-R26	5.6	6.3	7.2	T2	
R24-R26	29.3	29.7	30.2	LARGE	

**Insertion Coracobrachialis (plane)**

R2	Right position			3.4	(1.5)
R24	Same as R2, a but more distal			1.0	(1.0)
R26	Same as R24			0.8	(0.5)
SM	OK				
R2-R24	2.0	7.5	17.2	T3	
R2-R26	2.5	6.2	12.4	T1	
R24-R26	0.1	1.5	3.7	SMALL	

**Insertion Deltoid (plane)**

R2	Right position			4.3	(3.4)
R24	Same as R2			1.4	(1.0)
R26	Same as R2, a line is very proximal			3.1	(1.8)
SM	OK				
R2-R24	0.4	4.3	9.4	SMALL	
R2-R26	0.3	6.7	13.5	T1	
R24-R26	0.6	4.0	10.7	SMALL	



Insertion Infraspinatus (line)

R2	Wrong position			7.0	(1.3)
R24	Wrong position			5.5	(0.9)
R26	Wrong position			3.7	(0.9)
SM	Same as R2, (Wrong)				
R2-R24	1.8	5.6	9.4	SMALL	
R2-R26	3.1	5.1	6.7	SMALL	
R24-R26	0.3	5.3	10.4	SMALL	

**Insertion Latissimus (line)**

R2	Right position			1.5	(0.3)
R24	Same as R2			0.7	(0.6)
R26	Same as R2, a bit more distal			0.7	(0.4)
SM	OK				
R2-R24	0.4	2.2	7.9	SMALL	
R2-R26	1.5	2.4	3.5	SMALL	
R24-R26	0.2	1.5	2.9	SMALL	

**Insertion Pectoralis Major (line)**

R2	Right position			0.7	(0.5)
R24	Same as R2, a bit more proximal			1.4	(0.9)
R26	Same as R2, a bit less distal			3.4	(0.8)
SM	OK				
R2-R24	1.0	9.0	38.0	T3	
R2-R26	3.2	9.8	28.1	T3	
R24-R26	0.4	6.9	26.1	T1	

**Insertion Subscapularis (line)**

R2	Wrong position			2.0	(1.6)
R24	Right position			1.8	(1.9)
R26	Same as R24			2.7	(1.4)
SM	OK				
R2-R24	8.3	11.2	14.6	LARGE	
R2-R26	10.3	12.3	14.3	LARGE	
R24-R26	0.5	4.2	10.7	SMALL	

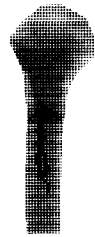
**Insertion Supraspinatus (line)**

R2	Wrong position			4.5	(1.0)
R24	Right position			5.2	(1.2)
R26	Wrong position			1.7	(0.8)
SM	OK (manually corrected)				
R2-R24	19.2	22.6	27.2	LARGE	
R2-R26	10.9	13.9	18.0	LARGE	
R24-R26	8.9	11.0	12.3	LARGE	



Insertion Teres Major (line)

R2	Right position			2.4	(0.4)
R24	Same as R2			0.6	(0.6)
R26	Same as R2, smaller			0.9	(0.6)
SM	OK				
R2-R24	1.0	3.0	5.8	SMALL	
R2-R26	0.1	3.8	12.9	T1	
R24-R26	1.4	6.5	18.1	T1	

**Insertion Teres Minor (line)**

R2	Right position			3.0	(0.7)
R24	Wrong position, too close to glenoid			3.5	(1.3)
R26	Same as R24			1.7	(0.8)
SM	OK				
R2-R24	8.4	9.8	11.6	T2	
R2-R26	7.3	8.6	10.3	T2	
R24-R26	0.2	2.5	5.9	SMALL	

**Clavicle****Origo Deltoid (line)**

R2	Right position			2.3	(1.8)
R24	Same as R2			1.3	(0.5)
R26	Same as R2			0.9	(0.6)
SM	OK				
R2-R24	0.6	2.8	11.0	SMALL	
R2-R26	0.3	2.0	7.2	SMALL	
R24-R26	0.2	1.8	6.6	SMALL	

**Origo Pectoralis Major (line)**

R2	Right position			1.6	(1.1)
R24	Right position, different from R2			4.2	(0.9)
R26	Right position, different from others			1.9	(0.8)
SM	OK				
R2-R24	0.6	3.5	9.7	SMALL	
R2-R26	0.2	3.9	7.9	SMALL	
R24-R26	2.3	5.0	8.2	SMALL	



Insertion Trapezius (line)

R2	Wrong position			5.4	2.1
R24	Right position			0.5	0.4
R26	Right position, different from R24			1.1	0.7
SM	OK				
R2-R24	2.1	6.7	8.7		SMALL
R2-R26	8.6	11.7	16.0		LARGE
R24-R26	3.2	11.0	24.4		T3



Summary

The incidence of shoulder complaints in the total Dutch population is estimated between 70 and 160 per thousand a year. Because the functioning of the human shoulder is very important in labour situations, as well as in performing the Activities of Daily Living (ADL), the development of adequate treatment of shoulder disorders is very important. Despite the importance of treatment of shoulder disorders, and the growing interest in the human shoulder, many questions about the shoulder are still unanswered.

To improve the results of medical intervention on the shoulder and to increase the knowledge about the shoulder, at the Man-Machine Systems and Control Group at the Faculty of Design, Engineering and Production of the Delft University of Technology a musculoskeletal model of the human shoulder has been developed. This multi-body computer model describes the relationships between movements and external forces acting on the arm and the internal forces and movements of the muscles. This model, also known as the Delft Shoulder Model, is based on parameters of a cadaver, but simulations are done using input motions of healthy subjects, or patients. The discrepancy between model and subject parameters decreases the accuracy of the simulation results of the model, which makes correct interpretation and medical intervention on the basis of these simulation results more difficult.

One of the methods to improve the accuracy of the simulation results of the Delft Shoulder Model is to adapt the parameters of the model to the individual subject. Simulation results of such an individualized model can be interpreted better resulting in better medical treatment and better understanding of the functioning of the human shoulder. The goal of the research described in this thesis is to individualize the Delft Shoulder Model in order to obtain simulation results that are more accurate. To reach this goal, different approaches have been developed and tested. Results are described in this thesis.

To measure the inner structures of the human body in vivo in a quantitative way, MRI can be used very well. When one tries to use MRI for measuring a musculoskeletal system, the problem arises that the muscles are difficult to distinguish from each other. All muscles have the same greyvalue and the fascia in between the muscles is very thin and often not detectable.

Therefore automatic segmentation of the muscles of the shoulder is not possible. To measure the musculoskeletal structures from MRI images of the inner body, an interactive contour detection algorithm is developed. This interactive contour detection method is used to segment the MRI images, as well as the CT images necessary for analysis of the images used in the thesis. The method shows to be very useful for semi-automatic segmentation of tomographic images.

To know which parameters of the Delft Shoulder Model have the most influence on the simulation results of the model, three sets of parameters have been obtained from dissection experiments of three cadavers. Analysis of simulation results of the model based on these different parameter sets shows that the model is very sensitive to its parameters. Mean differences between simulated and measured rotations can be as much as 20 degrees. Adapting the model to an individual subject is thus necessary. The simulation results of the model based on one of the parameter sets show strange behaviour. For a specific situation the model shows some instable behaviour. This kind of unpredictable behaviour makes that one should be very careful with adapting the model parameters.

To investigate the possibilities of obtaining model parameters for the Delft Shoulder Model from MRI images, an MRI image dataset has been made of a human cadaver. Because this cadaver is also used in a dissection experiment model parameters obtained using dissection and "MRI dissection" can be compared. This study shows that most parameters can be obtained from MRI images with reasonable accuracy. The study also showed that for some muscle attachments the dissection data might be wrong. It is a problem that a dissection experiment can only be performed once on the same cadaver. The results of this study show that it is advisable always to combine a dissection experiment with an MRI experiment, because the MRI dataset can help to verify the dissection data afterwards.

Because automatic segmentation of the muscles in an MRI image is not possible and because muscle architecture cannot be obtained from MRI, other methods to adapt the Delft Shoulder Model to individual subjects are studied. We hypothesize that the location and shape of muscle attachment sites correlate with the shape of the bones they are attached to. If this hypothesis holds, it is possible to predict the location of muscle attachments when the shape of the bones is known. To validate this hypothesis, geometric models of three sets of shoulder bones were built based on CT scans. These models consist of 3-D surface models of the scapula, clavicle and humerus, with the muscle attachment contours connected to them. Two of these models were transformed to the third model. The muscle attachment contours could be compared. Using these techniques, 45 percent of the muscle attachment contours could be predicted with high accuracy. For 40 percent of the muscle attachment contours it was not possible to distinguish the interindividual differences from the inaccuracies of the method used. Measurement errors were the reason why there was a great divergence between 15 percent of the measured and observed muscle attachments. From this study, we conclude that most muscle attachment contours can be predicted by means of geometric models of the bones. To gain more insight in the interindividual differences, it is necessary to repeat this experiment with a better dissection protocol and a larger dataset.

Adapting the dynamic and static properties of the shoulder model, like muscle volume and muscle attachment locations shows to be very complicated. Especially when adaptation has to take place in a clinical practice.

To adapt the Delft Shoulder Model for the kinematic differences between subject and model, a model transformation technique is developed. The kinematic differences between subject and model cause differences between the measured movements of the subject and the simulated movements of the model. These differences are a result of the closed chain mechanism of the Delft Shoulder Model. It is important to reduce these differences because they have great influence on the kinematic and dynamic simulation results of the model. To reduce the size of these kinematic differences, a parameter optimization technique is developed. Using this technique, based on an optimization the simulation results by means of adapting a few kinematic parameters, the differences in mean scapula orientation are reduced from 7.2 degree to 3.8 degree. The movements necessary for this optimization are measured using standardized protocol.

From this thesis we can conclude that it is very well possible to improve the kinematic simulation results of the Delft Shoulder Model. We believe that improvement of the kinematic results also results in an improvement of the static and dynamic results. Adapting the static and dynamic parameters of the Delft Shoulder Model to the individual subject is still far away. The methods like geometric model transformation and MRI are very time consuming and validation of the simulation results is not possible. This makes it impossible to know whether an adapted shoulder model provides more accurate simulation results. MRI has shown to be a promising method to measure the musculoskeletal structures of the inner body. Difficulties using MRI for obtaining information about the musculoskeletal structures of the human shoulder are that it is often problematic to distinguish between two adjacent muscles, and the muscle fibre direction and the exact locations of the muscle attachments cannot be detected.

Samenvatting

Van de totale nederlandse samenleving wordt geschat dat er per jaar 70 tot 160 van de duizend mensen last van hun schouder hebben. Het ontwikkelen van juiste behandelingsmethoden voor deze schouderproblemen is erg belangrijk omdat het goed functioneren van de schouder van belang is tijdens het werk, maar ook bij de persoonlijke verzorging. Ondanks dit belang en ondanks de groeiende interesse in het functioneren van de schouder zijn er nog steeds vele onbeantwoorde vragen over de menselijke schouder.

Aan de Technische Universiteit Delft bij de Faculteit voor Ontwerp, Constructie en Productie bij de werkgroep voor Mens-Machine Systemen is een spier-skelet model ontwikkeld. Doel van dit model is om meer inzicht te verkrijgen in het functioneren van de schouder en om de resultaten van medisch ingrijpen op de schouder te verbeteren. Dit eindige elementen computermodel beschrijft het verband tussen de inwendige krachten en bewegingen van spieren enerzijds en de externe krachten en bewegingen die op de arm werken anderzijds. Dit model staat bekend als het Delftse Schoudermodel en is gebaseerd op parameters die gemeten zijn aan een menselijk kadaver. Probleem is dat simulaties gedaan worden gebaseerd op metingen van bewegingen en krachten aan proefpersonen of patiënten. Door deze discrepantie tussen modelparameters en de parameters van de proefpersoon worden de resultaten van de modelsimulaties minder nauwkeurig en daardoor moeilijker te interpreteren. Hierdoor wordt ook medisch ingrijpen op basis van modelsimulaties van de patiënt lastig.

Het aanpassen van de modelparameters van het schoudermodel aan de individuele persoon zal de nauwkeurigheid van de simulatieresultaten van het model verbeteren. Hierdoor wordt het interpreteren van simulatieresultaten eenvoudiger waardoor behandelingsmethoden van de schouder verbeterd kunnen worden. Het doel van het onderzoek dat in dit proefschrift beschreven wordt is om het Delftse Schoudermodel te individualiseren waardoor de simulatieresultaten van het model nauwkeuriger zullen zijn. Om dit doel te bereiken zijn verschillende methodes onderzocht. De resultaten van dit onderzoek worden in dit proefschrift beschreven.

Om structuren in het menselijk lichaam kwantitatief te meten is MRI zeer geschikt. Bij het gebruik van MRI om een spier-skelet systeem te meten wordt het lastiger omdat de verschillende spieren niet goed van elkaar te onderscheiden zijn. In het MRI beeld hebben de spieren dezelfde grijswaarden en de spierfacia is zo dun dat het vaak niet te detecteren is.

Om deze redenen is automatisch segmenteren en detecteren van spieren niet mogelijk. Om toch spieren te kunnen meten in MRI beelden is een interactief segmentatie algoritme ontwikkeld. Deze interactieve methode is gebruikt om zowel de MRI al de CT-beelden die gebruikt zijn in dit proefschrift te analyseren. Deze methode blijkt zeer geschikt te zijn voor semi-automatische segmentatie van tomografische beelden.

Om te bepalen welke parameters van het Delftse Schoudermodel de meeste invloed hebben op de simulatieresultaten zijn drie parametersets, verkregen door middel van dissectie experimenten van drie menselijke kadavers, gebruikt in het model. Uit de analyse van de simulatieresultaten van het model gebaseerd op deze drie verschillende parametersets blijkt dat het model zeer gevoelig is voor de modelparameters. Verschillen tussen gesimuleerde en gemeten oriëntaties van het schouderblad lopen op tot 20 graden. Hieruit blijkt dat het nodig is om het model aan te passen aan de individuele persoon. De simulatieresultaten laten ook een vreemd gedrag van het model zien. Voor een van de parametersets raakt het model bij een bepaalde stand in een soort onstabiele toestand. Vanwege dit soort onvoorspelbaar modelgedrag moet men zeer voorzichtig zijn bij het aanpassen van de modelparameters.

Om te onderzoeken wat de mogelijkheden zijn om modelparameters voor het Delftse Schoudermodel uit MRI beelden te verkrijgen is er een MRI dataset gemaakt van een menselijk kadaver. Hetzelfde kadaver is ook gebruikt bij een dissectie experiment waardoor het mogelijk wordt om de modelparameters die verkregen zijn door middel van dissectie te vergelijken met modelparameters die verkregen zijn door middel van "MRI-dissectie". Deze studie toont aan dat de meeste parameters met een aanvaardbare nauwkeurigheid door middel van MRI verkregen kunnen worden. Uit deze studie blijkt tevens dat voor een aantal spieraanhechtingen de dissectie resultaten verkeerd zouden kunnen zijn. Een probleem is dat een dissectie experiment slechts eenmaal uitgevoerd kan worden op hetzelfde kadaver. Het is dus van belang om een dissectie experiment altijd te combineren met een MRI experiment zodat controle van de dissectie resultaten achteraf mogelijk is.

Omdat automatische segmentatie van MRI beelden van de menselijke schouder niet mogelijk is en omdat belangrijke modelparameters zoals spierwerklijnen niet uit MRI verkregen kunnen worden wordt er verder gezocht naar methoden om het Delftse Schoudermodel aan te passen aan de individuele persoon. Als we uitgaan van de hypothese dat de aanhechtingsplaatsen van spieren gerelateerd zijn aan de vorm van het bot waar ze aan hechten, dan zou het mogelijk kunnen zijn om spieraanhechtingen te voorspellen uit de vorm van de botten. Om deze hypothese te valideren zijn er van een drietal datasets geometrische modellen gemaakt van de botten. Deze modellen bestaan uit driedimensionale oppervlaktemodellen van het schouderblad, het sleutelbeen en het bovenarmbot, met daarbij de posities van de spieraanhechtingen. Na geometrische transformatie van deze modellen kunnen de

spieraanhechtingen met elkaar vergeleken worden. Door middel van deze techniek kunnen 45 procent van de spieraanhechtingen nauwkeurig voorspeld worden. Voor 40 procent van de spieraanhechtingen was het niet mogelijk om te bepalen of de voorspellingsfout een gevolg was van inter-individuele verschillen of onnauwkeurigheden die het gevolg zijn van de gebruikte methodieken. Voor 15 procent van de spieraanhechtingen is een aantoonbare meetfout de oorzaak van een verkeerde voorspelling. Uit dit experiment concluderen we dat de positie van de meeste spieraanhechtingen voorspeld kan worden door middel van geometrische modellen van de botten. Om meer inzicht te verkrijgen in de inter-individuele verschillen zou dit experiment herhaald moeten worden met een grotere dataset en een verbeterd dissectie protocol.

Uit voorgaande experimenten blijkt dat het aanpassen van dynamische en statische parameters van het Delftse Schoudermodel zeer gecompliceerd is. Vooral als de aanpassingen in de medische praktijk toegepast dienen te worden.

Om de kinematica van het Delftse Schoudermodel aan te passen aan de individuele persoon is een modeltransformatietechniek ontwikkeld. De verschillen in kinematica tussen het model en de individuele persoon veroorzaken verschillen tussen de bewegingen die aan een persoon gemeten zijn en de bewegingen die het model maakt. Deze verschillen worden veroorzaakt door de gesloten keten structuur van het Delftse Schoudermodel. Het verkleinen van deze verschillen is belangrijk omdat ze grote invloed hebben op de dynamische en statische simulatieresultaten van het model. Om de verschillen in kinematica te verkleinen is een parameter optimalisatie techniek ontwikkeld. Met behulp van deze techniek, die gebaseerd is op de optimalisatie van simulatie resultaten door het aanpassen van een beperkt aantal modelparameters, is het verschil in de gemiddelde afwijking van de oriëntatie van het schouderblad verkleind van 7,2 graden naar 3,8 graden. De bewegingen die gemeten moeten worden om deze optimalisatie uit te voeren bestaan uit standaard meetprotocollen.

De eindconclusies van dit proefschrift zijn dat het mogelijk is om de kinematische resultaten van het Delftse Schoudermodel te verbeteren. We nemen aan dat verbetering van de kinematische resultaten tot gevolg heeft dat de statische en dynamische resultaten van het model ook verbeteren. Aanpassingen van de statische en dynamische modelparameters is nog steeds een grote stap. De methodes zoals modeltransformatie en MRI zijn zeer tijdrovend en validatie van de modelresultaten is niet mogelijk. Hierdoor is het niet mogelijk om te bepalen of een aangepast schoudermodel nauwkeuriger simulatieresultaten geeft dan een standaard model. Het blijkt dat MRI een veelbelovende techniek is om spierskelet systemen te meten. De problemen met MRI zijn dat het vaak lastig is om aangrenzende spieren van elkaar te onderscheiden en het is niet mogelijk om spierwerklijnen te bepalen met behulp van MRI.

Acknowledgements

It is a pleasure to be able to thank those that have contributed to the work in this thesis.

First of all, I would like to express my thanks to my promotor Henk Stassen for giving me the opportunity to start, but especially to finish this research. During the writing of this thesis we had fruitful discussions about the project, but also about other subjects. I also want to thank my other promotor Frans van der Helm for his contributions to my work during many discussions and for his work on the shouldermodel. A lot of cadaver data that I used for my research are the results of his work. I wish to thank my copromotor Jan Gerbrands for introducing me to the Information Theory Group and for learning me the art of image analysis. My fourth supervisor is dr. ir. Ton van Lunteren to whom I also feel gratitude for reading and commenting on my manuscript. This team of supervisors helped me through some difficult periods and for that I wish to thank them especially.

There were also other people who contributed to my work. I want to mention Boudewijn Lielieveldt, who made sure that MRI images were made of the cadaver while I was on holiday in New Zealand. Dissecting this cadaver has been done by Cees Spoor and Merie Klein Breteler who provided me with fine data. I want to thank the department of Radiology at the Academic Hospital in Leiden for providing me with the necessary MRI and CT images. I also want to thank Mirjam Nieman for proofreading the manuscript.

Apart from these people, I want to thank my colleagues. Those are the people that you work with every day, and I am grateful that we also spent time after work. From the Man-Machine Systems group, I would like to mention the colleagues of the shoulder research group: Jurriaan de Groot, Leonard Rozendaal, Sybert Stroeve, Guido Brouwn and Sanjay Gupta. I felt like part of a team when I was at mechanical engineering, but also during our cycling trips, and other activities apart from work.

At the Information Theory Group I spent most of my time. I felt very much at home there. My special position in this group made that I was transferred from one room to the other every year, so I have had a lot of roommates: Erica van de Stadt, Jan van Lieshout, Yaonan Zhang, Marcel Reinders, John Schavemaker, Cor Veenman, Stefan Westen, Cees Kamminga, Erik Mouw, Danillo Tromp, and Sorin Jacobs. From the other colleagues I want to mention Gerhard Langelaar, Ernst Bovenkamp, Andre Redert, Allan Hanjalic, Lodewijk Wessels and Peter van Roosmalen. I remember some nice parties and a lot of tasteful meals.

I also want to thank the supporting staff of both the Information Theory Group and the Man-Machine Systems Group. I want to mention the names of Ben van den Boom, Annet Bosch and Jaap van Dieten.

Last but not least I want to thank the people that took my mind away from my work. My friends from “Wortelgros”, Korvezeeimperium, SWG, volleyball, and “Digitale Stad Delft”.

Finally I want to thank my family and my mother for giving me a home and many fine hours away from Delft.

Curriculum Vitae

Bart Kaptein was born on 28 november 1969 in Breezand (Noord Holland). He got his VWO diploma at "Het Johannes College" in Den Helder in 1988. In the same year he started his study Mechanical Engineering at the technical university of Delft. He did his MSc. project at the laboratory for information theory at the faculty of electrical engineering in Delft under the supervision of dr. ir. J.J. Gerbrands, dr. ir. G. Pronk, dr. F.C.T. van der Helm and prof. dr. ir. H.G. Stassen. The title of his MSc. thesis is: "Model based image analysis of NMR images of the human shoulder". He got his MSc. diploma in 1993 at the laboratory for measurement and control in the Man Machine Systems Group. He started his PhD. study at the first of januar 1994.

